

**SPACECRAFT'S ATTITUDE DYNAMICS AND
VARIABLE STRUCTURE CONTROLLERS DESIGN**

**M.Sc. Thesis by
Erkan ABDULHAMİTBİLAL, B.Sc.**

Department : Aeronautical and Astronautical Eng.

Programme: Aeronautical and Astronautical Eng.

FEBRUARY 2005

**SPACECRAFT'S ATTITUDE DYNAMICS AND
VARIABLE STRUCTURE CONTROLLERS DESIGN**

**M.Sc. Thesis by
Erkan ABDULHAMITBILAL, B.Sc.
(511021023)**

Date of submission: 23 December 2004

Date of defense examination: 25 January 2005

Supervisor (Chairman): Prof.Dr. Elbrus CAFEROV

Members of the Examining Committee: Prof.Dr. Umur DAYBELGE

Prof.Dr. Levent GÜVENÇ

FEBRUARY 2005

**UZAY ARACININ YÖNELME DİNAMIĞI
VE DEĞİŞKEN YAPILI DENETLEYİCİLER TASARIMI**

**Yüksek Lisans Tezi
Müh. Erkan ABDULHAMİTBİLAL
(511021023)**

**Tezin Enstitüye Verildiği Tarih: 23 Aralık 2004
Tezin Savunulduğu Tarih: 25 Ocak 2005**

**Tez Danışmanı: Prof.Dr. Elbrus CAFEROV
Diğer Jüri Üyeleri: Prof.Dr. Umur DAYBELGE
Prof.Dr. Levent GÜVENÇ**

ŞUBAT 2005

PREFACE

This thesis contains a comparison analysis and design of attitude linear and variable structure controllers for a geosynchronous communication satellite.

This thesis is dedicated to my family. I would like to thank to my thesis supervisor Prof. Dr. Elbrus Caferov and the members of the examining committee, Prof. Dr. Umur Daybelge and Prof. Dr. Levent Güvenç. I also thank Dr. Cuma Yarim for checking of language errors.

January, 2005.

Erkan Abdulhamitbilal

CONTENTS

ABBREVIATIONS	v
LIST OF TABLES	vi
LIST OF FIGURES	vii
NOMENCLATURES	x
SUMMARY	xi
ÖZET	xii
1. INTRODUCTION	1
1.1. Spacecraft Specification	4
1.2. Preliminary Design	4
2. SATELLITE ATTITUDE DYNAMICS AND PROBLEM STATEMENT	7
2.1. Rotational Kinematics	7
2.1.1. Direction cosine matrix	7
2.2. Rigid Body Dynamics	11
2.2.1. Inertia matrix	11
2.2.2. Euler's rotationla equation of motion	12
2.2.3. Rigid body in circular orbit	14
2.2.4. Gyrostat in circular orbit	17
2.2.5. Representation of equation of motion with θ	19
2.3. Linearization of Rigid Body Dynamics	20
2.4. Structural Dynamics	21
2.4.1. Flexible frames	21
3. LINEAR CONTROL SYSTEM DESIGN	23
3.1. System Linearization	23
3.2. Linear Controllers Design	24
3.2.1. Passive linear controller design	24
3.2.2. Active linear controller design	26
3.2.3. Combined linear controller design	28
3.3. Pole Placement	29
3.3.1. Pole placement for passive linear controller	30
3.3.2. Pole placement for active linear controller	30
3.3.3. Pole placement for combined linear controller	31
4. VARIABLE STRUCTURE CONTROL DESIGN	32
4.1. Design of Sliding Surfaces	31
4.2. Sliding Mode Controllers Design	33
4.2.1. Passive slidign mode controller design	33
4.2.2. Active slidign mode controller design	38
4.2.3. Combined slidign mode controller design	40

5. ATTITUDE CONTROL DESIGN EXAMPLES	43
5.1. Spacecraft Sensors and Control Elements	43
5.1.1. Sensors	43
5.1.2. Control elements	43
5.2. Rigid Spacecraft in Circular Orbit	44
5.3. Gyrostat in Circular Orbit	45
5.4. Pole Placed Linear Controllers Design	45
5.5. Sliding Mode Controllers Design	47
6. CONCLUSION	51
REFERANCES	53
APPENDICES	55
Appendix.1. Controllers' Matlab-Simulink Block Diagrams	55
A1.1. Block Diagram of Dynamic System	55
A1.2. Block Diagram of Linear Controllers	55
A1.2. Block Diagram of Sliding Mode Controllers	56
Appendix 2. Time Responses of the System and Designed Controllers	57
A2.1. Spacecraft Dynamics	57
A2.2. Linear Controllers with Pole Placement	59
A2.3. Sliding Mode Controllers	65
Appendix 3. Source Codes for Matlab-Simulink Block Diagrams	78
A3.1. Dyanmic System Initializaiton	78
A3.2. Linear Controllers and System Initializaiton	78
A3.2. Some Linear Controllers Functions	79
A3.4. Sliding Mode Controllers System Initializaiton	79
A3.5. Some Sliding Mode Controllers Functions	80
Appendix 4. Sensors and Control Elements	82
A4.1. Sensors	82
A4.2. Control Elements	86
BIOGRAPHY	88

ABBREVIATIONS

LVLH : Local Vertical Local Horizontal

LIST OF TABLES

	<u>Page</u>
Table 1.1. Intelsat V technical specifications.....	4
Table 1.2. Single solar array flexibility model at 6 a.m.....	5
Table 5.1. Eigenvalues of the system and designed linear controllers.....	46

LIST OF FIGURES

	<u>Page</u>
Figure 1.1 : Communication satellite Intelsat V.....	3
Figure 1.2 : Attitude control elements configuration.....	5
Figure 1.3 : Intelsat V in orbit simulation.....	6
Figure 2.1 : Two reference frames A and B, and attitude angles.....	8
Figure 2.2 : Rigid body in circular orbit.....	14
Figure 2.3 : Gyrostat in circular orbit.....	18
Figure 2.4 : Flexible spacecraft Intelsat V.....	22
Figure 4.1 : Sliding mode boundary layer function $\gamma(s)$	40
Figure 5.1 : Configuration of the attitude thrusters for design example.....	49
Figure A1.1 : Block diagram of the dynamic system.....	55
Figure A1.2 : Block diagram of the combined linear controller.....	55
Figure A1.3 : Block diagram of the sliding mode controller.....	56
Figure A1.4 : Block diagram of the sliding manifold dynamics.....	56
Figure A2.1 : Time responses of small attitude errors $\theta_1, \theta_2, \theta_3$ of dynamic system.....	57
Figure A2.2 : Time responses of angular velocities $\omega_1, \omega_2, \omega_3$ for small attitude errors of dynamic system.....	57
Figure A2.3 : Time responses of large attitude errors $\theta_1, \theta_2, \theta_3$ of dynamic system.....	58
Figure A2.4 : Time responses of angular velocities $\omega_1, \omega_2, \omega_3$ for large attitude errors of dynamic system.....	58
Figure A2.5 : Time responses of attitude errors $\theta_1, \theta_2, \theta_3$ for small attitude angles orientation of passive linear controller.....	59
Figure A2.6 : Time responses of angular velocities $\omega_1, \omega_2, \omega_3$ for small attitude angles orientation of passive linear controller.....	59
Figure A2.7 : Time responses of control functions u_1, u_2, u_3 for small attitude angles orientation of passive linear controller.....	60
Figure A2.8 : Time responses of attitude errors $\theta_1, \theta_2, \theta_3$ for small attitude angles orientation of combined linear controller.....	60
Figure A2.9 : Time responses of angular velocities $\omega_1, \omega_2, \omega_3$ for small attitude angles orientation of combined linear controller.....	61
Figure A2.10 : Time responses of control functions u_1, u_2, u_3 for small attitude angles orientation. Note that, two small inside-plots have same time scale and torque scale as $u(t)$. u_p and u_a , plots represent the passive and active linear control functions, respectively, of combined linear controller.....	61
Figure A2.11 : Time responses of attitude errors $\theta_1, \theta_2, \theta_3$ for large attitude angles orientation of passive linear controller.....	62

Figure A2.12	: Time responses of angular velocities $\omega_1, \omega_2, \omega_3$ for large attitude angles orientation of passive linear controller.....	62
Figure A2.13	: Time responses of control functions u_1, u_2, u_3 for large attitude angles orientation of passive linear controller.....	63
Figure A2.14	: Time responses of attitude errors $\theta_1, \theta_2, \theta_3$ for large attitude angles orientation of combined linear controller.....	63
Figure A2.15	: Time responses of angular velocities $\omega_1, \omega_2, \omega_3$ for large attitude angles orientation of combined linear controller.....	64
Figure A2.16	: Time responses of combined control functions u_1, u_2, u_3 for large attitude angles orientation. Note that, two small inside-plots have same time scale and torque scale as $u(t)$. u_p and u_a , plots represent the passive and active linear control functions, respectively, of combined linear controller.....	64
Figure A2.17	: Time responses of attitude errors $\theta_1, \theta_2, \theta_3$ for small attitude angles orientation of passive sliding mode controller.....	65
Figure A2.18	: Time responses of angular velocities $\omega_1, \omega_2, \omega_3$ for small attitude angles orientation of passive sliding mode controller..	65
Figure A2.19	: Time responses of sliding manifolds s_1, s_2, s_3 for small attitude angles orientation of passive sliding mode controller..	66
Figure A2.20	: Time responses of control functions u_1, u_2, u_3 for small attitude angles orientation of passive sliding mode controller..	66
Figure A2.21	: Three in one plot: gravity-gradient $G_g(t)$, flexible membrane effects $M_q(t)$ and external disturbance effects such as sun pressure $d(t)$ for small attitude angles orientation for passive sliding mode controller.....	67
Figure A2.22	: Time responses of attitude errors $\theta_1, \theta_2, \theta_3$ for small attitude angles orientation of combined sliding mode controller.....	67
Figure A2.23	: Time responses of angular velocities $\omega_1, \omega_2, \omega_3$ for small attitude angles orientation of combined sliding mode controller.....	68
Figure A2.24	: Time responses of sliding manifolds s_1, s_2, s_3 for small attitude angles orientation of combined sliding mode controller.....	68
Figure A2.25	: Time responses of combined control functions u_1, u_2, u_3 for small attitude angles orientation of combined sliding mode controller.....	69
Figure A2.26	: Time responses of active u_{1a}, u_{2a}, u_{3a} and passive u_{1p}, u_{2p}, u_{3p} control functions of combined sliding mode controller.....	69
Figure A2.27	: Three in one plot: gravity-gradient $G_g(t)$, flexible membrane effects $M_q(t)$ and external disturbance effects such as sun pressure $d(t)$ for small attitude angles orientation for combined sliding mode controller.....	70
Figure A2.28	: Time responses of attitude errors $\theta_1, \theta_2, \theta_3$ for large attitude angles orientation of passive sliding mode controller.....	70
Figure A2.29	: Time responses of angular velocities $\omega_1, \omega_2, \omega_3$ for large attitude angles orientation of passive sliding mode controller..	71

Figure A2.30	: Time responses of sliding manifolds s_1, s_2, s_3 for large attitude angles orientation of passive sliding mode controller..	71
Figure A2.31	: Time responses of control functions u_1, u_2, u_3 for large attitude angles orientation of passive sliding mode controller..	72
Figure A2.32	: Three in one plot: gravity-gradient $G_g(t)$, flexible membrane effects $M_q(t)$ and external disturbance effects such as sun pressure $d(t)$ for large attitude angles orientation for passive sliding mode controller.....	72
Figure A2.33	: Time responses of attitude errors $\theta_1, \theta_2, \theta_3$ for large attitude angles orientation of combined sliding mode controller.....	73
Figure A2.34	: Time responses of angular velocities $\omega_1, \omega_2, \omega_3$ for large attitude angles orientation of combined sliding mode controller.....	73
Figure A2.35	: Time responses of sliding manifolds s_1, s_2, s_3 for large attitude angles orientation of combined sliding mode controller.....	74
Figure A2.36	: Time responses of combined control functions u_1, u_2, u_3 for large attitude angles orientation of combined sliding mode controller.....	74
Figure A2.37	: Time responses of active u_{1a}, u_{2a}, u_{3a} and passive u_{1p}, u_{2p}, u_{3p} control functions of combined sliding mode controller.....	75
Figure A2.38	: Three in one plot: gravity-gradient $G_g(t)$, flexible membrane effects $M_q(t)$ and external disturbance effects such as sun pressure $d(t)$ for large attitude angles orientation for combined sliding mode controller.....	76
Figure A2.39	: Time responses of dynamic Equation (4.9) for small attitude angles orientation.....	76
Figure A2.40	: Time responses of dynamic Equation (4.9) for large attitude angles orientation.....	77

NOMENCLATURES

\vec{a}_i, \vec{b}_i	: Orthogonal unit base vector, $i = 1, 2, 3$.
$C_{ij}, C^{B/A}, C^{A/B}, C_i(\theta_i)$: Direction cosine matrix, $i, j = 1, 2, 3$.
C_3	: Direction cosine vector.
θ_i	: Attitude angles for $i = 1, 2, 3$.
ω_i	: Angular velocities for $i = 1, 2, 3$.
\vec{e}	: Eigenvector.
\vec{H}, \vec{h}_0	: Angular velocity momentum vector.
\vec{M}_i	: External moment or torque, $i = 1, 2, 3$.
$\vec{R}, \vec{R}_c, \vec{r}, \vec{\rho}$: Position vector.
m	: Mass.
$\delta_1, \delta_2, \delta_3$: Rigid-elastic coupling scalars of a single solar array.
$\sigma_1, \sigma_2, \sigma_3$: Modal frequencies.
q_1, q_2, q_3	: Modal coordinates.
$I_{ij} (i = j)$: Moments of inertia, $i, j = 1, 2, 3$.
$I_{ij} (i \neq j)$: Products of inertia, $i, j = 1, 2, 3$.
$\Omega, \Gamma, \tilde{\Omega}$: Skew-symmetric matrices.
n	: Orbital rate.
μ	: Gravitational parameter.
$d\vec{f}$: Gravitational force on a small dm .
x, y	: State and output vectors of linear controller.
A, B, C, D	: System, control, output, kontrol output matrices of lin. contr.
u, u_a, u_p, u_c	: Control vector for linear controllers.
ζ, κ, g^T	: Pole placed matrices.
λ_i	: Eigenvalues, $i = 1, 2, \dots, n$
$I_{3 \times 3}$: Identity (3×3) -matrix.
P	: Desirable pole vector.
Ξ, Ψ	: Weighting matrices.
J	: Optimal cost function.
$f(x, t, u)$: Control function of sliding mode controller
s_i	: Sliding manifolds, $i = 1, 2, 3$.
u_{eq}	: Equivalent control term.
u	: Discontinuous control term of sliding mode controller.
$\text{sign}(\cdot), \text{sgn}(\cdot)$: Mathematical function, signum.
V	: Lyapunov function candidate
$\gamma(\cdot)$: Sliding boundary (dead-band) function
s_0^-, s_0^+	: Sliding boundary value
b	: Sliding boundary function
k_i	: Inertia constants, $i = 1, 2, 3$.
λ	: Nutational frequency

SUMMARY

Control problem of a spacecraft is an important topic in automatic control engineering. Many studies about attitude stabilization of satellite applications have been proposed. In this thesis, a three axis stabilized spacecraft –a communication satellite Intelsat V– is selected to investigate attitude dynamics, and to design linear and variable structure controllers. Spacecraft kinematics and dynamics are studied to recognize how the system operates in circular orbit for attitude motions. The satellite's dynamic model is obtained via linearized rigid spacecraft attitude dynamics, gravity gradient torque, dynamic effects of flexible solar panels, a sinusoidal effect as external and internal disturbances. The designed passive pole placed linear controller, which models reaction wheels, stabilizes the satellite well with longer settling time. Additionally, active pole placed linear controller, which models thrust system, stabilizes the satellite precisely with short settling time. However, it operates continuously that is undesirable for the attitude control system due to the limited amount of propellant of the spacecraft. The combined linear controller model of flexible spacecraft is obtained with passive and active controllers, linearized rigid spacecraft attitude dynamics, a sinusoidal effect as a disturbance which consists of flexible solar panels vibration effects, gravity gradient torque, sun pressure and other unmodeled external or internal disturbances. On the other hand, both active and passive sliding mode controllers constitute combined sliding mode controller which stabilizes the system faster than the linear controllers according to selected sliding manifold which needs to be designed. The passive sliding mode controller supplies inner torques with continuous control signal produced by equivalent control term. Beside, the thrust system is used seldom and only a few on-off logic operations are done for precise stabilization of the designed model of the spacecraft. Nonlinear design for thrust system is sufficient model for on-off logic and it depends on the switching functions and selected sliding boundary layer. Although, this is a simple design described via a few blocks, it is a complicated mathematical model to be studied with. Nonlinear controller model includes passive and active controllers with the dynamic model of the satellite. The time responses are obtained from Matlab-Simulink block diagrams of the designed satellite attitude dynamic model, linear and sliding mode controllers which are given to illustrate the considered procedure.

ÖZET

Uzay aracının kontrol problemi otomatik kontrol mühendisliğinin önemli bir başlığıdır. Uzay aracı uygulamalarının yönelme stabilizasyonu hakkında birçok çalışma sunulmuştur. Bu tezde üç eksenle dengelenmiş bir uzay aracı olan haberleşme uydusu Intelsat V'in yönelme dinamiklerini araştırmak, lineer ve kayma kipli kontrolörler tasarlamak için seçilmiştir. Bu amaç ile uzay aracı kinematikleri ve dinamikleri sistemin dairesel yörüngedeki yönelme hareketlerini anlamak için çalışıldı. Uydunun dinamik modeli lineerleştirilmiş rijit uzay aracı yönelme dinamikleri, eğimin yerçekimi torku, güneş panellerin dinamik etkileri, sinüsoidal etki olarak iç ve dış bozucular ile elde edildi. Tasarlanan pasif kutup atanmış lineer kontrolcü, ki hareket tekerciklerini modeller, uyduyu uzun oturma süresi ile iyi denge konumuna getirmektedir. Ek olarak, aktif kutup atanmış doğrusal kontrolcü, ki itki sistemini modeller, uyduyu kısa oturma süresiyle tam olarak denge konumuna getirmektedir. Ancak, sürekli çalışması uzay aracının sınırlı yakıt hacminden dolayı yönelme kontrol sistemi için arzu edilmemektedir. Esnek uzay aracının birleştirilmiş lineer kontrolcü modeli pasif ve aktif kontrolcüler, doğrusallaştırılmış rijit uzay aracı yönelme dinamikleri, bozucu olarak sinüsoidal etkiyi oluşturan esnek panellerin salınım etkileri, eğimin yerçekimi torku, güneş basıncı ve diğer modellenmemiş dış ve iç bozucular ile elde edildi. Diğer yandan, her iki pasif ve aktif kayma kipli kontrolcüler birleştirilmiş kayma kipli kontrolcü oluştururlar ki tasarım gerektiren kayma manifolduna nazaran sistemi doğrusal kontrolcülerden süratli dengeler. Pasif kayma kipli kontrolcü iç torkları eşdeğer kontrol teriminin oluşturduğu sürekli kontrol sinyal ile sağlamaktadır. Yanısıra, itki sistemi nadiren kullanılır ve uzay aracının tasarlanmış modelinin kesin denge konumu için sadece birkaç açma-kapama mantığı işlemleri yapılmaktadır. İtki sisteminin doğrusal olmayan tasarımı açma-kapama mantığı için yeterli bir modeldir ve anahtarlama fonksiyonu ile seçilen kayma sınır tabakasına bağlıdır. Birkaç blok ile ifade edilen basit bir tasarım olmasına rağmen çalışılması karışık bir matematiksel modeldir. Doğrusal olmayan kontrol modeli pasif ve aktif kontrolcüler ile uydunun dinamik modelinin içerir. Tasarlanmış uydunun yönelme dinamiği modelinin, lineer ve kayma kipli kontrolcülerin Matlab-Simulink blok diagramlarından elde edilen zaman yanıtları gözönünde tutulan prosedürü örneklemek için verilmiştir.

1. INTRODUCTION

Control problem of a spacecraft is an important topic in automatic control engineering. A body orbiting the Earth in geosynchronous orbit has instabilities in attitude dynamics and disturbances caused by the Earth, the Moon, the Sun and other bodies in space. These effects force the body to lose initial orbit and attitude. Here the control system takes important part of spacecraft missions where it keeps the body in designed orbit and desired attitude. The control system consists of control elements and control algorithms. The control elements for a spacecraft in a geosynchronous orbit are thrusters, reaction or momentum wheels. The control algorithms are logics developed for the mission by control engineer.

Thrusters and reaction wheels are commonly used spacecraft attitude control devices for geosynchronous orbits. In this thesis, thrusters are controlled via active control algorithms whereas reaction wheels are controlled via passive control algorithms. Thrusters or active controllers are used for rapid large attitude angles motions. On the other hand, reaction wheels or passive controllers are used for small attitude angles motions for precise determination.

In this thesis two studies of control algorithms for the communication satellite Intelsat V are given. First, linear control method with pole placement is used to design both active and passive controllers. Second, sliding mode control method has designed active and passive controllers for better results. The performances and disadvantages are discussed in Section 5 and simulated in Appendices.

The linear control procedure in the thesis is designed in two steps according to modern control theory. First, linearization of the system is given and then linear model is obtained. Next, controls and outputs for the linear system are given. Second step includes pole placement method, which stabilizes the system with desirable poles chosen by designer. In this design, control function is given as a pole placed matrix, thus, less calculations are required. The designed linear controllers for passive and active controls are in same logic and it is simple combination of them. The linear controllers have continuous control signal, but for active controllers that continuous control command may not be wanted since the operations of thrusters as on-off logic.

A study about linear attitude stabilization has been proposed by Franklin *et al.* (2002). A linear attitude control model of a communication spacecraft and a state-variable example are given. According to that example, a similar linear model and control algorithms for yaw, roll and pitch axes are designed in the thesis.

The sliding mode theory has an attention in the aerospace field. The technique permits the use of a lower order systems model for generating control commands. On the other hand, the system is robust with respect to the external disturbances and includes unmodelled dynamics, as well.

The sliding mode control procedure in this thesis is designed in three steps. First, switching surfaces with desired properties are selected according to the spacecraft attitude dynamics. Next, control laws that will guarantee the existence of sliding mode on the switching surface for both active and passive controllers are designed. For passive controller, sliding mode control law is designed as equivalent control method to avoid from chattering problem and to generate continuous control command. On the other hand, for active controller, sliding mode control law is selected with some restrictions on thrusters for limited fuel usage. Finally, it is obtained that state trajectories can be forced toward the sliding manifold from any initial state. The above procedure is applied both to large and small attitude angles orientations for a spacecraft. For the active control algorithms chattering is an undesirable problem. Although a dead-band is included into the system depending on the switching surfaces and thrust magnitude, it may occur along the boundary layer bounded with the dead-band function. Avoiding chattering problem and keeping advantages of sliding mode, for large attitude angles orientations, the control law scheme firstly applies some pulses via thrusters until the state trajectories reach the sliding boundary layer, then reaction wheels that are used as a primary control elements, tune the system for fine attitude stabilization where the system is forced to reach the sliding manifold.

A similar design for variable structure control topic was done by Vadali (1986) with quaternion representation for optimal sliding mode. Automatic controller for active nutation damping in momentum biased stabilized spacecraft is introduced by Sira-Ramirez and Dwyer (1987), where robust feedback stabilization of roll and yaw angular dynamics are achieved successfully with prescribed qualitative characteristics for a spinning satellite. A maneuvering of a flexible spinning spacecraft is treated with variable structure control by Öz (1993) where system is stabilized perfectly in 100 seconds. Slotine and Li (1991) introduced boundary layer for sliding mode controllers. Also, some simple spacecraft thrust control algorithms were given as applied nonlinear control examples.

There are many nonlinear examples of controllers design for spacecrafts, where some of them are cited as follow. Somov *et.al.* (2004) has proposed a controller design for nonlinear model of a spacecraft with weak inner torques produced via reaction wheels which stabilize the system in 20 minutes. Yoon and Tsotras (2002) have developed an algorithm for controlling the spacecraft attitudes in orbit while simultaneously tracking a desired power profile using a cluster of variable-speed single gimbaled control moment gyroscope which stabilizes the small spacecraft in 10 minutes. Zhang and Li (2004) proposed a new Lyapunov based controller which stabilizes the system nearly in one hour.



Figure 1.1 Communication satellite Intelsat V.

Designed nonlinear controllers stabilize the systems well; however, their settling times are very high. The designed sliding mode controllers studied in this thesis stabilize the system in 100 seconds maximum with passive control algorithms, and 40 seconds maximum with combined control algorithms.

The variable structure controller design procedures such as equivalent control term and modeling of second order systems and general form of sliding mode are studied by Utkin (1993), Utkin (1992), Hung (1993), Slotine and Li (1991).

1.1 Spacecraft Specification

The spacecraft in this thesis is chosen to be a communication satellite Intelsat V as shown in Figure 1.1. Three-axis stabilization has been employed for many geosynchronous communication satellites. The bias momentum provides gyroscopic stiffness to the environmental disturbances and primarily to the solar radiation pressure torque.

1.2 Preliminary Design of Spacecraft

Figure 1.2 shows an attitude control system configuration that consists of one reaction/momentum wheel at pitch axis and two reaction wheels on yaw and roll axes, Earth sensor that measures pitch and roll attitude references and thrusters that provide wheel momentum desaturation torques. The satellite also includes star tracker for fine attitude determination, optic gyroscopes that measures attitude angle rates and attitude errors, and sun sensor for solar array pointing operations.

Table 1.1 Intelsat V technical specifications [1]

Principle moments of inertias, I_1, I_2, I_3	3026, 440, 3164 kg.m ²
Main body dimensions, x-y-z.....	1.5 x 1.7 x 2.2 m
Solar arrays.....	20 m (tip-to-tip)
Max. torques supplied via R.W.....	0.10 Nm
Bias momentum.....	91.4 Nms
Liquid bi-propellant thrusters.....	N ₂ O ₄ /MMH
Array power.....	1.5 kW

In Figure 1.2, the direction 1, yaw, is toward to the Earth; direction 2, pitch, is normal to the orbit plane and direction 3, roll, is nominally in flight direction. Roll, yaw and pitch control axes are coincided with the principle axes of the spacecraft.

The increased demand of electrical power for communications and/or direct TV broadcasting leads to large flexible solar panel arrays for three axis stabilized spacecraft as shown in Figure 1.3. Consequently, the structural flexibility of the solar arrays have been one of the primary topics in the design of attitude control systems

for a certain class of the three axis stabilized spacecraft. For most cases, the structural flexibility of the solar arrays does not strongly interact with attitude control

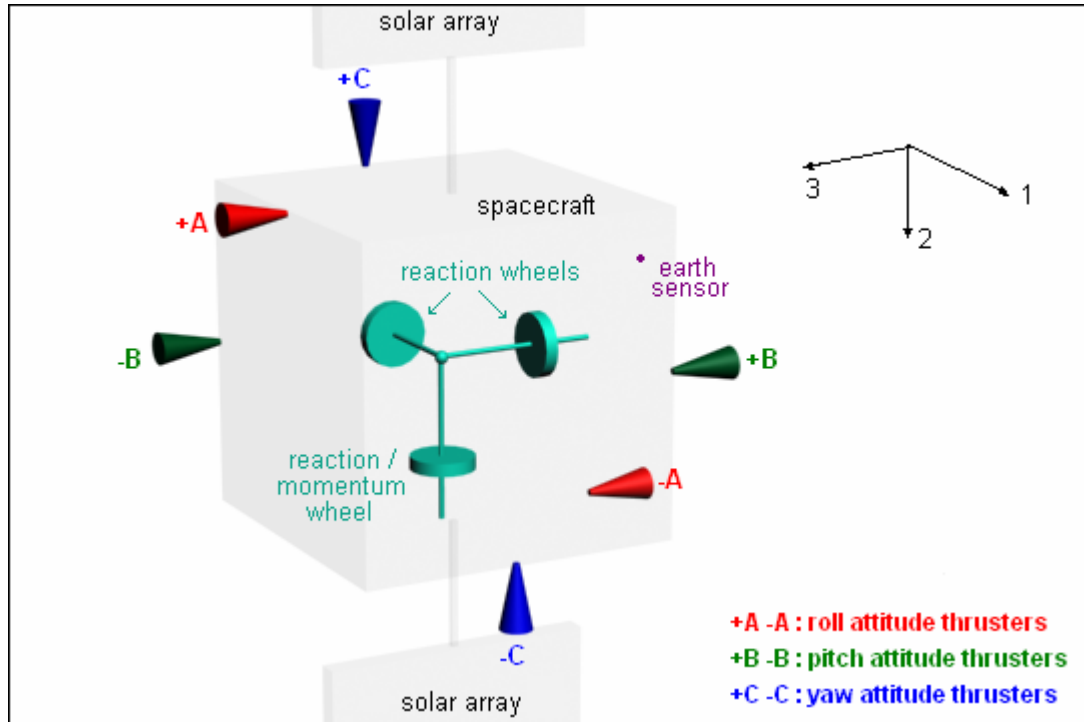


Figure 1.2 Attitude control elements configuration.

systems. Thus, all of structural modes are often gain stabilized by the step rolloff at a frequency well below first structural frequency [1]. In this thesis, a case is selected which does not interact strongly with attitude control system but need to be considered in the control design procedure. For this case, flexibility of solar array is given in Table 1.2.

Table 1.2 Single solar array flexibility model at 6 a.m. [1].

Cantilever mode description ^a	Cantilever frequency σ , rad/s	Coupling scalars, $\sqrt{kg \cdot m^2}$		
		Roll, δ_1	Pitch, δ_2	Yaw, δ_3
OP-1	0.885	0	0	35.372
OP-2	6.852	0	0	4.772
OP-3	16.658	0	0	2.347
OP-4	33.326	0	0	0.548
T-1	5.534	0	2.532	0
T-2	17.668	0	0.864	0
T-3	33.805	0	0.381	0
IP-1	1.112	35.865	0	0
IP-2	36.362	2.768	0	0

^a : OP is out-of plane, T is torsion and IP is in-plane.

Therefore a rigid body with flexible solar arrays may be modeled. In Section 2.4, the dynamic model of the solar arrays will be presented, and more realistic model of a

flexible spacecraft will be obtained. Only performances of sliding mode controllers with flexible solar panels model will be studied. In linear controllers design, flexibility will be assumed as a sinusoidal effect that consists of internal and external disturbances, as well.



Figure 1.3 Intelsat V in orbit simulation.

2. SATELLITE ATTITUDE DYNAMICS AND PROBLEM STATEMENT

This section introduces a three-axis stabilized spacecraft motions in circular orbit to investigate attitude dynamics. The spacecraft attitude dynamics problem will firstly be introduced via rotational kinematics and then via rigid body dynamics. In kinematics, the orientation of a body is described as in rotational motion. This subject is somewhat mathematical in nature because it does not involve any forces associated with motion. The motion of a rigid body in space consists of the translational motion of its center of mass and the rotational motion of the body about its center of mass. Thus, a rigid body in space is a dynamic system with six degrees of freedom. However, this chapter is concerned with rotational motion of a rigid vehicle with or without the influence of gravitational and other external forces. Rotational kinematics include direction cosine matrix of the rigid spacecraft and gyrostator in circular orbit. In this subtopic rigid body dynamics, inertial matrix, Euler's rotational equation of motion, rigid body and gyrostator in circular orbit will be given. Finally, more realistic option of flexibility of solar membranes will be studied.

2.1 Rotational Kinematics

Problem statement of spacecraft attitude dynamics and control includes rotational kinematics. Kinematics describe orientation of a rotating body. In this section, direction cosine matrix is described as rotation matrix between two directions. Also, the dynamic model called as kinematic differential equation for direction cosine is given. Finally, angular velocities are represented with dynamic model of direction cosine.

2.1.1 Direction cosine matrix [1]

Assume a reference frame A with a right-hand set of three orthogonal unit vectors $\{\vec{a}_1, \vec{a}_2, \vec{a}_3\}$ and a reference frame B with another right-hand set of three orthogonal unit vectors $\{\vec{b}_1, \vec{b}_2, \vec{b}_3\}$ as shown in Figure 2.1. Basis vectors of B are expressed in terms of basis vectors of A as following:

$$\vec{b}_1 = C_{11}\vec{a}_1 + C_{12}\vec{a}_2 + C_{13}\vec{a}_3 \quad (2.1.a)$$

$$\vec{b}_2 = C_{21}\vec{a}_1 + C_{22}\vec{a}_2 + C_{23}\vec{a}_3 \quad (2.1.b)$$

$$\vec{b}_3 = C_{31}\vec{a}_1 + C_{32}\vec{a}_2 + C_{33}\vec{a}_3 \quad (2.1.c)$$

where $C_{ij} \equiv \vec{b}_i \cdot \vec{a}_j$ is the cosine of the angle between \vec{b}_i and \vec{a}_j , and C_{ij} is simply called the direction cosine. The matrix form of Equations (2.1) is as below:

$$\begin{bmatrix} \vec{b}_1 \\ \vec{b}_2 \\ \vec{b}_3 \end{bmatrix} = \begin{bmatrix} C_{11} & C_{12} & C_{13} \\ C_{21} & C_{22} & C_{23} \\ C_{31} & C_{32} & C_{33} \end{bmatrix} \begin{bmatrix} \vec{a}_1 \\ \vec{a}_2 \\ \vec{a}_3 \end{bmatrix} = C^{B/A} \begin{bmatrix} \vec{a}_1 \\ \vec{a}_2 \\ \vec{a}_3 \end{bmatrix} \quad (2.2)$$

where $C^{B/A} \equiv [C_{ij}]$ describes the orientation of B relative to A is called direction cosine matrix. It can be rewritten as

$$C^{B/A} = \begin{bmatrix} \vec{b}_1 \cdot \vec{a}_1 & \vec{b}_1 \cdot \vec{a}_2 & \vec{b}_1 \cdot \vec{a}_3 \\ \vec{b}_2 \cdot \vec{a}_1 & \vec{b}_2 \cdot \vec{a}_2 & \vec{b}_2 \cdot \vec{a}_3 \\ \vec{b}_3 \cdot \vec{a}_1 & \vec{b}_3 \cdot \vec{a}_2 & \vec{b}_3 \cdot \vec{a}_3 \end{bmatrix} \equiv \begin{bmatrix} \vec{b}_1 \\ \vec{b}_2 \\ \vec{b}_3 \end{bmatrix} \cdot [\vec{a}_1 \quad \vec{a}_2 \quad \vec{a}_3] \quad (2.3)$$

The direction cosine matrix $C^{B/A}$ is also called the rotation matrix or coordinate transformation matrix to B from A which is shown as, $C^{B/A} : B \leftarrow A$.

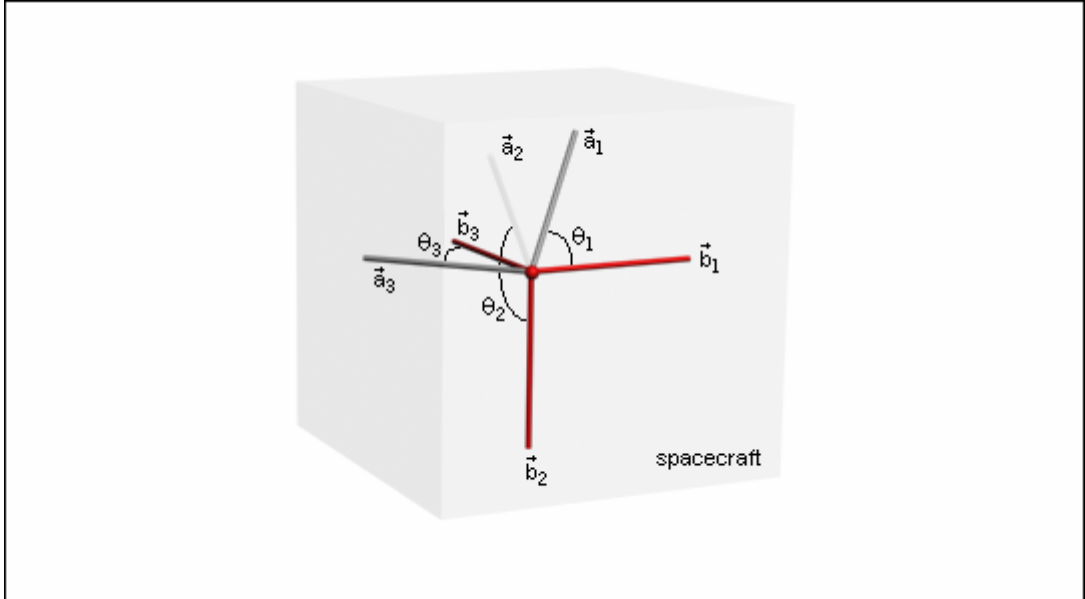


Figure 2.1 Two reference frames A and B, and attitude angles

The transformation matrix to A from B can be written as below,

$$C^{A/B} = \begin{bmatrix} \vec{a}_1 \cdot \vec{b}_1 & \vec{a}_1 \cdot \vec{b}_2 & \vec{a}_1 \cdot \vec{b}_3 \\ \vec{a}_2 \cdot \vec{b}_1 & \vec{a}_2 \cdot \vec{b}_2 & \vec{a}_2 \cdot \vec{b}_3 \\ \vec{a}_3 \cdot \vec{b}_1 & \vec{a}_3 \cdot \vec{b}_2 & \vec{a}_3 \cdot \vec{b}_3 \end{bmatrix} \equiv \begin{bmatrix} \vec{a}_1 \\ \vec{a}_2 \\ \vec{a}_3 \end{bmatrix} \cdot [\vec{b}_1 \quad \vec{b}_2 \quad \vec{b}_3] \quad (2.4)$$

The relation between $C^{B/A}$ and $C^{A/B}$ can be shown as follows:

$$[C^{B/A}]^{-1} = [C^{B/A}]^T = C^{A/B} \quad (2.5)$$

$$[C^{A/B}]^{-1} = [C^{A/B}]^T = C^{B/A} \quad (2.6)$$

In two sets of reference frames A and B consider an arbitrary vector \vec{H} which can be expressed in terms of A and B as follows,

$$\vec{H} = H_1\vec{a}_1 + H_2\vec{a}_2 + H_3\vec{a}_3 = H'_1\vec{b}_1 + H'_2\vec{b}_2 + H'_3\vec{b}_3. \quad (2.7)$$

Thus,

$$H'_1 \equiv \vec{b}_1 \cdot \vec{H} = \vec{b}_1 \cdot (H_1\vec{a}_1 + H_2\vec{a}_2 + H_3\vec{a}_3) \quad (2.8.a)$$

$$H'_2 \equiv \vec{b}_2 \cdot \vec{H} = \vec{b}_2 \cdot (H_1\vec{a}_1 + H_2\vec{a}_2 + H_3\vec{a}_3) \quad (2.8.b)$$

$$H'_3 \equiv \vec{b}_3 \cdot \vec{H} = \vec{b}_3 \cdot (H_1\vec{a}_1 + H_2\vec{a}_2 + H_3\vec{a}_3) \quad (2.8.c)$$

The Equations (2.8) can be rewritten in matrix form as below,

$$\begin{bmatrix} H'_1 \\ H'_2 \\ H'_3 \end{bmatrix} = \begin{bmatrix} \vec{b}_1 \cdot \vec{a}_1 & \vec{b}_1 \cdot \vec{a}_2 & \vec{b}_1 \cdot \vec{a}_3 \\ \vec{b}_2 \cdot \vec{a}_1 & \vec{b}_2 \cdot \vec{a}_2 & \vec{b}_2 \cdot \vec{a}_3 \\ \vec{b}_3 \cdot \vec{a}_1 & \vec{b}_3 \cdot \vec{a}_2 & \vec{b}_3 \cdot \vec{a}_3 \end{bmatrix} \begin{bmatrix} H_1 \\ H_2 \\ H_3 \end{bmatrix} = C^{B/A} \begin{bmatrix} H_1 \\ H_2 \\ H_3 \end{bmatrix} \quad (2.9)$$

Therefore, the components of a vector \vec{H} are transformed to B from A using direction cosine matrix $C^{B/A}$ defined in Equation (2.3) for the transformation of the orthogonal basis vectors.

Three elementary rotational revolution about first, second and third axes of the reference frame A are described by the following rotation matrices, respectively

$$C_1(\theta_1) = \begin{bmatrix} 1 & 0 & 0 \\ 0 & \cos \theta_1 & \sin \theta_1 \\ 0 & -\sin \theta_1 & \cos \theta_1 \end{bmatrix} \quad (2.10.a)$$

$$C_2(\theta_2) = \begin{bmatrix} \cos \theta_2 & 0 & -\sin \theta_2 \\ 0 & 1 & 0 \\ \sin \theta_2 & 0 & \cos \theta_2 \end{bmatrix} \quad (2.10.b)$$

$$C_3(\theta_3) = \begin{bmatrix} \cos \theta_3 & \sin \theta_3 & 0 \\ -\sin \theta_3 & \cos \theta_3 & 0 \\ 0 & 0 & 1 \end{bmatrix} \quad (2.10.c)$$

where $C_i(\theta_i)$ implies the direction cosine matrix C of an elementary rotation about the i^{th} axis of A with attitude angles θ_i , $i=1,2,3$ as shown also in Figure 2.1.

Equation (2.2) can be rewritten as

$$\begin{bmatrix} \vec{a}_1 \\ \vec{a}_2 \\ \vec{a}_3 \end{bmatrix} = C^{-1} \begin{bmatrix} \vec{b}_1 \\ \vec{b}_2 \\ \vec{b}_3 \end{bmatrix} = C^T \begin{bmatrix} \vec{b}_1 \\ \vec{b}_2 \\ \vec{b}_3 \end{bmatrix} \quad (2.11)$$

The direction cosine matrix is a function of time because the two reference frames are rotating according to each other. Taking the time derivative of (2.11) in A and denoting it by over dot, results

$$\begin{aligned} \begin{bmatrix} 0 \\ 0 \\ 0 \end{bmatrix} &= \dot{C}^T \begin{bmatrix} \vec{b}_1 \\ \vec{b}_2 \\ \vec{b}_3 \end{bmatrix} + C^T \begin{bmatrix} \dot{\vec{b}}_1 \\ \dot{\vec{b}}_2 \\ \dot{\vec{b}}_3 \end{bmatrix} = \dot{C}^T \begin{bmatrix} \vec{b}_1 \\ \vec{b}_2 \\ \vec{b}_3 \end{bmatrix} + C^T \begin{bmatrix} \vec{\omega} \times \vec{b}_1 \\ \vec{\omega} \times \vec{b}_2 \\ \vec{\omega} \times \vec{b}_3 \end{bmatrix} \\ &= \dot{C}^T \begin{bmatrix} \vec{b}_1 \\ \vec{b}_2 \\ \vec{b}_3 \end{bmatrix} - C^T \begin{bmatrix} 0 & -\omega_3 & \omega_2 \\ \omega_3 & 0 & -\omega_1 \\ -\omega_2 & \omega_1 & 0 \end{bmatrix} \begin{bmatrix} \vec{b}_1 \\ \vec{b}_2 \\ \vec{b}_3 \end{bmatrix} \end{aligned} \quad (2.12)$$

where ω_i , $i=1,2,3$ are angular velocities of each axes and

$$\dot{C} = \begin{bmatrix} \dot{C}_{11} & \dot{C}_{12} & \dot{C}_{13} \\ \dot{C}_{21} & \dot{C}_{22} & \dot{C}_{23} \\ \dot{C}_{31} & \dot{C}_{32} & \dot{C}_{33} \end{bmatrix} \quad (2.13)$$

and defining a skew-symmetric matrix Ω as

$$\Omega = \begin{bmatrix} 0 & -\omega_3 & \omega_2 \\ \omega_3 & 0 & -\omega_1 \\ -\omega_2 & \omega_1 & 0 \end{bmatrix} \quad (2.14)$$

Therefore,

$$\left[\dot{C}^T - C^T \Omega \right] \begin{bmatrix} \vec{b}_1 \\ \vec{b}_2 \\ \vec{b}_3 \end{bmatrix} = \begin{bmatrix} 0 \\ 0 \\ 0 \end{bmatrix} \quad (2.15)$$

from which it is obtained that

$$\dot{C}^T - C^T \Omega = \dot{C} + \Omega C = 0 \quad (2.16)$$

which is called kinematic differential equation for the directional cosine matrix C . The angular velocities can be manipulated from Equation (2.16) as,

$$\omega_1 = \dot{C}_{21} C_{31} + \dot{C}_{22} C_{32} + \dot{C}_{23} C_{33} \quad (2.17.a)$$

$$\omega_2 = \dot{C}_{31} C_{11} + \dot{C}_{32} C_{12} + \dot{C}_{33} C_{13} \quad (2.17.b)$$

$$\omega_3 = \dot{C}_{11} C_{21} + \dot{C}_{12} C_{22} + \dot{C}_{13} C_{23} \quad (2.17.c)$$

2.2 Rigid-Body Dynamics

The motion of a rigid body in space, which has six degrees of freedom, is defined with translation motion of the center of mass of the body and rotational motion of the body around the center of mass. This subchapter includes rotational motion of a rigid body in according to [1].

2.2.1 Inertia matrix

Let $\vec{\rho}$ (the position vector of small, infinitesimal, mass element dm) be expressed as

$$\vec{\rho} = \rho_1 \vec{b}_1 + \rho_2 \vec{b}_2 + \rho_3 \vec{b}_3 \quad (2.18)$$

The inertia matrix I is defined as

$$I = \begin{bmatrix} I_{11} & I_{12} & I_{13} \\ I_{21} & I_{22} & I_{23} \\ I_{31} & I_{32} & I_{33} \end{bmatrix} \quad (2.19)$$

where I_{ij} ($i = j$) the moments of inertia are defined as

$$I_{11} = \int (\rho_2^2 + \rho_3^2) dm \quad (2.20.a)$$

$$I_{22} = \int (\rho_1^2 + \rho_3^2) dm \quad (2.20.b)$$

$$I_{33} = \int (\rho_1^2 + \rho_2^2) dm \quad (2.20.c)$$

and I_{ij} ($i \neq j$) the products of inertia are defined as

$$I_{12} = I_{21} = -\int \rho_1 \rho_2 dm \quad (2.20.d)$$

$$I_{13} = I_{31} = -\int \rho_1 \rho_3 dm \quad (2.20.e)$$

$$I_{23} = I_{32} = -\int \rho_2 \rho_3 dm \quad (2.20.f)$$

2.2.2 Euler's rotational equation of motion [1]

Angular momentum equation of a rigid body about its center of mass is simply defined as

$$\vec{M} = \dot{\vec{H}} \quad (2.21)$$

where \vec{H} is the angular momentum vector of a rigid body about its mass center, \vec{M} is the external moment acting on the body about its mass center. Thus following equation can be written

$$\dot{\vec{H}} \equiv \left\{ \frac{d\vec{H}}{dt} \right\}_N = \left\{ \frac{d\vec{H}}{dt} \right\}_B + \vec{\omega}^{B/N} \times \vec{H} \quad (2.22)$$

where

$$\vec{H} = I \vec{\omega}^{B/N} \quad (2.23)$$

Then, the rotational equation of motion of a rigid body about its center of mass is written as

$$\vec{M} = \left\{ \frac{d\vec{H}}{dt} \right\}_B + \vec{\omega}^{B/N} \times \vec{H} \quad (2.24)$$

For later use assume $\vec{\omega} \equiv \vec{\omega}^{B/N}$, then Equation (2.24) becomes

$$\vec{M} = \left\{ \frac{d}{dt} (I \cdot \vec{\omega}) \right\}_B + \vec{\omega} \times (I \cdot \vec{\omega}) = \left\{ \frac{dI}{dt} \right\}_B \vec{\omega} + I \left\{ \frac{d\vec{\omega}}{dt} \right\}_B + \vec{\omega} \times I \cdot \vec{\omega} \quad (2.25)$$

where $\{dI/dt\}_B = 0$ and $\{d\vec{\omega}/dt\}_B = \{d\vec{\omega}/dt\}_N = \dot{\vec{\omega}}$. Thus, it results

$$\vec{M} = I \cdot \dot{\vec{\omega}} + \vec{\omega} \times I \cdot \vec{\omega} \quad (2.26)$$

which is called Euler's rotational equation of motion.

Let \vec{M} and $\vec{\omega}$ be expressed in terms of body-fixed basis vectors $\{\vec{b}_1, \vec{b}_2, \vec{b}_3\}$ as follows:

$$\vec{M} = M_1 \vec{b}_1 + M_2 \vec{b}_2 + M_3 \vec{b}_3 \quad (2.27)$$

$$\vec{\omega} = \omega_1 \vec{b}_1 + \omega_2 \vec{b}_2 + \omega_3 \vec{b}_3 \quad (2.28)$$

Substituting Equation (2.27), (2.28) and (2.19) into (2.26) results

$$\begin{bmatrix} M_1 \\ M_2 \\ M_3 \end{bmatrix} = \begin{bmatrix} \dot{H}_1 \\ \dot{H}_2 \\ \dot{H}_3 \end{bmatrix} + \begin{bmatrix} 0 & -\omega_3 & \omega_2 \\ \omega_3 & 0 & -\omega_1 \\ -\omega_2 & \omega_1 & 0 \end{bmatrix} \begin{bmatrix} H_1 \\ H_2 \\ H_3 \end{bmatrix} \quad (2.29)$$

Then, substituting Equation (2.23) into (2.29) results

$$\begin{bmatrix} M_1 \\ M_2 \\ M_3 \end{bmatrix} = \begin{bmatrix} I_{11} & I_{12} & I_{13} \\ I_{21} & I_{22} & I_{23} \\ I_{31} & I_{32} & I_{33} \end{bmatrix} \begin{bmatrix} \dot{\omega}_1 \\ \dot{\omega}_2 \\ \dot{\omega}_3 \end{bmatrix} + \begin{bmatrix} 0 & -\omega_3 & \omega_2 \\ \omega_3 & 0 & -\omega_1 \\ -\omega_2 & \omega_1 & 0 \end{bmatrix} \begin{bmatrix} I_{11} & I_{12} & I_{13} \\ I_{21} & I_{22} & I_{23} \\ I_{31} & I_{32} & I_{33} \end{bmatrix} \begin{bmatrix} \omega_1 \\ \omega_2 \\ \omega_3 \end{bmatrix} \quad (2.30)$$

Thus,

$$I \dot{\omega} + \Omega I \omega = M \quad (2.31)$$

where I and Ω are defined with Equation (2.19) and (2.14), respectively; $\omega = [\omega_1 \ \omega_2 \ \omega_3]^T$ and $M = [M_1 \ M_2 \ M_3]^T$.

For a principle-axis reference frame with a set of basis vector $\{\vec{b}_1, \vec{b}_2, \vec{b}_3\}$, Euler's rotational equation of motion of a rigid body becomes

$$I_1 \dot{\omega}_1 - (I_2 - I_3) \omega_2 \omega_3 = M_1 \quad (2.32.a)$$

$$I_2 \dot{\omega}_2 - (I_3 - I_1) \omega_3 \omega_1 = M_2 \quad (2.32.b)$$

$$I_3 \dot{\omega}_3 - (I_1 - I_2) \omega_1 \omega_2 = M_3 \quad (2.32.c)$$

where I_1, I_2, I_3 are the principle moments of inertia, $M_i = \vec{M} \cdot \vec{b}_i$ and $\omega_i = \vec{\omega} \cdot \vec{b}_i$. There are three coupled, nonlinear ordinary differential equations for state variables $\omega_1, \omega_2, \omega_3$ of a rigid body. These dynamical equations and kinematical differential equations completely describe the rotation motions of a rigid body with three rotational degrees of freedom.

2.2.3 Rigid body in circular orbit

Spacecraft dynamics and control solutions include gravitational forces and moments. Now, consider a rigid body in a circular orbit. A local vertical and local horizontal (LVLH) reference frame with its origin at the center of mass of the spacecraft had a set of unit vector $\{\vec{a}_1, \vec{a}_2, \vec{a}_3\}$; \vec{a}_1 is along orbiting direction, also called as roll direction; \vec{a}_2 is perpendicular to the orbit plane, also called pitch direction; and \vec{a}_3 is towards the Earth, also called yaw direction as shown in Figure 2.2. The angular velocity of A with respect to N is as below:

$$\vec{\omega}^{A/N} = -n\vec{a}_2 \quad (2.33)$$

where n is constant orbital rate. The angular velocity of the body-fixed reference frame B with basis vectors $\{\vec{b}_1, \vec{b}_2, \vec{b}_3\}$ is given by

$$\vec{\omega}^{B/N} = \vec{\omega}^{B/A} + \vec{\omega}^{A/N} = \vec{\omega}^{B/A} - n\vec{a}_2 \quad (2.34)$$

where $\vec{\omega}^{B/A}$ is the angular velocity of B relative A .

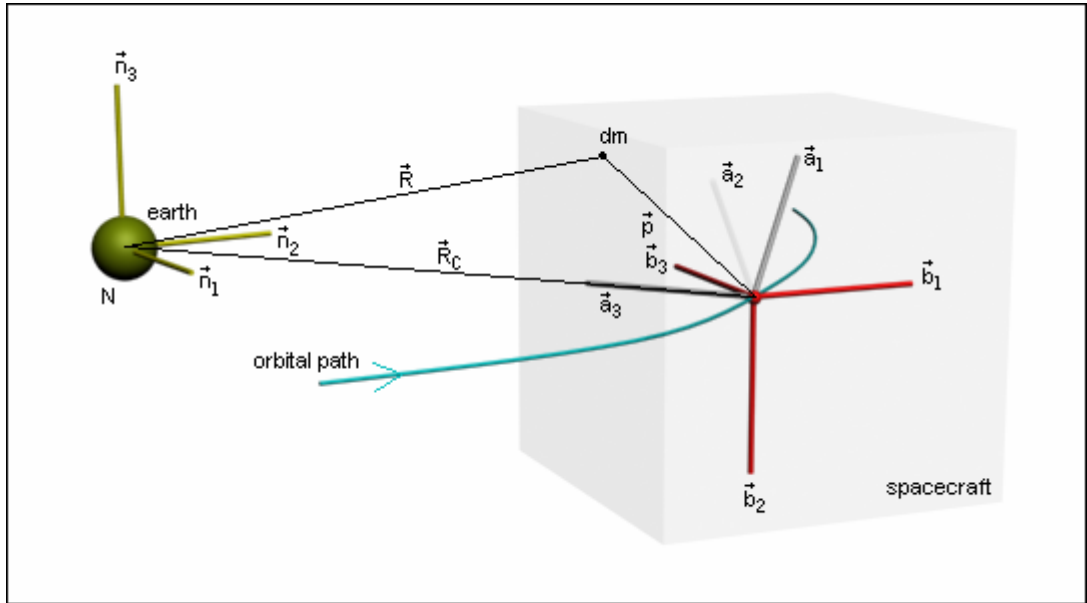


Figure 2.2 Rigid body in circular orbit.

The orientation of the body-fixed reference frame B with the LVLH reference frame A is in general described by the direction cosine matrix $C = C^{B/A}$ by Equation (2.2) or

$$\begin{bmatrix} \vec{a}_1 \\ \vec{a}_2 \\ \vec{a}_3 \end{bmatrix} = \begin{bmatrix} C_{11} & C_{12} & C_{13} \\ C_{21} & C_{22} & C_{23} \\ C_{31} & C_{32} & C_{33} \end{bmatrix}^T \begin{bmatrix} \vec{b}_1 \\ \vec{b}_2 \\ \vec{b}_3 \end{bmatrix} = \begin{bmatrix} C_{11} & C_{21} & C_{31} \\ C_{12} & C_{22} & C_{32} \\ C_{13} & C_{23} & C_{33} \end{bmatrix} \begin{bmatrix} \vec{b}_1 \\ \vec{b}_2 \\ \vec{b}_3 \end{bmatrix} \quad (2.35)$$

$$\text{where} \quad \vec{a}_1 = C_{11}\vec{b}_1 + C_{21}\vec{b}_2 + C_{31}\vec{b}_3 \quad (2.36.a)$$

$$\vec{a}_2 = C_{12}\vec{b}_1 + C_{22}\vec{b}_2 + C_{32}\vec{b}_3 \quad (2.36.b)$$

$$\vec{a}_3 = C_{13}\vec{b}_1 + C_{23}\vec{b}_2 + C_{33}\vec{b}_3 \quad (2.36.c)$$

The gravitational force acting on a small dm element is given by [1]:

$$d\vec{f} = -\frac{\mu\vec{R}dm}{|\vec{R}|^3} = -\frac{\mu(\vec{R}_c + \vec{\rho})dm}{|\vec{R}_c + \vec{\rho}|^3} \quad (2.37)$$

where μ is the gravitational parameter of the Earth, \vec{R} and $\vec{\rho}$ are the position vectors of dm from Earth's center and the spacecraft's mass center, respectively, and \vec{R}_c is the position vector of spacecraft's center from earth's center.

$$\vec{M} = \int \vec{\rho} \times d\vec{f} = -\mu \int \frac{\vec{\rho} \times \vec{R}_c}{|\vec{R}_c + \vec{\rho}|^3} dm \quad (2.38)$$

by some manipulations as in [1] gravity-gradient torque becomes as

$$\vec{M} = \frac{3\mu}{R_c^5} \vec{R}_c \times I \cdot \vec{R}_c = 3n^2 \vec{a}_3 \times I \cdot \vec{a}_3 \quad (2.39)$$

where $n = \sqrt{\mu/R_c^3}$ is orbital rate and $\vec{a}_3 \equiv -\vec{R}_c/R_c$.

The rotational equation of motion of a rigid body with an angular momentum $\vec{H} = I \cdot \vec{\omega}^{B/N}$ ($\vec{\omega}^{B/N} \equiv \vec{\omega}$) in circular orbit above is described with Equation (2.23), which can be rewritten similar to Equation (2.26) as below:

$$I \cdot \dot{\vec{\omega}} + \vec{\omega} \times I \cdot \vec{\omega} = 3n^2 \vec{a}_3 \times I \cdot \vec{a}_3 \quad (2.40)$$

where $\vec{\omega}$ and \vec{a}_3 have expressed in terms of basis vectors of the body-fixed reference frame B by Equation (2.28) and (2.36.c), respectively.

The orientation sequence $C_1(\theta_1) \leftarrow C_2(\theta_2) \leftarrow C_3(\theta_3)$ to B from A of the body-fixed reference frame B with respect to the LVLH reference frame, A in terms of attitude angles θ_i ($i=1,2,3$) becomes as below:

$$\begin{bmatrix} \vec{b}_1 \\ \vec{b}_2 \\ \vec{b}_3 \end{bmatrix} = \begin{bmatrix} C_{11} & C_{12} & C_{13} \\ C_{21} & C_{22} & C_{23} \\ C_{31} & C_{32} & C_{33} \end{bmatrix} \begin{bmatrix} \vec{a}_1 \\ \vec{a}_2 \\ \vec{a}_3 \end{bmatrix} = \begin{bmatrix} c_2 c_3 & c_2 s_3 & -s_2 \\ s_1 s_2 c_3 - c_1 s_3 & s_1 s_2 s_3 + c_1 c_3 & s_1 c_2 \\ c_1 s_2 c_3 + s_1 s_3 & c_1 s_2 s_3 - s_1 c_3 & c_1 c_2 \end{bmatrix} \begin{bmatrix} \vec{a}_1 \\ \vec{a}_2 \\ \vec{a}_3 \end{bmatrix} \quad (2.41)$$

where $c_i \equiv \cos \theta_i$ and $s_i \equiv \sin \theta_i$.

The angular velocity of B relative to A is given as

$$\vec{\omega}^{B/A} = \vec{\omega}_1 \vec{b}_1 + \vec{\omega}_2 \vec{b}_2 + \vec{\omega}_3 \vec{b}_3 \quad (2.42)$$

where

$$\begin{bmatrix} \omega_1 \\ \omega_2 \\ \omega_3 \end{bmatrix} = \begin{bmatrix} 1 & 0 & -s_2 \\ 0 & c_1 & s_1 c_2 \\ 0 & -s_1 & c_1 c_2 \end{bmatrix} \begin{bmatrix} \dot{\theta}_1 \\ \dot{\theta}_2 \\ \dot{\theta}_3 \end{bmatrix} \quad (2.43)$$

Substituting Equation (2.33) and (2.28) into Equation (2.24), $\vec{\omega}^{B/N}$ can be written as

$$\begin{bmatrix} \omega_1 \\ \omega_2 \\ \omega_3 \end{bmatrix} = \begin{bmatrix} 1 & 0 & -s_2 \\ 0 & c_1 & s_1 c_2 \\ 0 & -s_1 & c_1 c_2 \end{bmatrix} \begin{bmatrix} \dot{\theta}_1 \\ \dot{\theta}_2 \\ \dot{\theta}_3 \end{bmatrix} - n \begin{bmatrix} c_2 s_3 \\ s_1 s_2 s_3 + c_1 c_3 \\ c_1 s_2 s_3 - s_1 c_3 \end{bmatrix} \quad (2.44)$$

The linear form of (2.44) is obtained as

$$\begin{bmatrix} \omega_1 \\ \omega_2 \\ \omega_3 \end{bmatrix} = \begin{bmatrix} 1 & 0 & 0 \\ 0 & 1 & 0 \\ 0 & 0 & 1 \end{bmatrix} \begin{bmatrix} \dot{\theta}_1 \\ \dot{\theta}_2 \\ \dot{\theta}_3 \end{bmatrix} + \begin{bmatrix} 0 & 0 & -n \\ 0 & 0 & 0 \\ n & 0 & 0 \end{bmatrix} \begin{bmatrix} \theta_1 \\ \theta_2 \\ \theta_3 \end{bmatrix} + \begin{bmatrix} 0 \\ -n \\ 0 \end{bmatrix} \quad (2.45)$$

where

$$N = \begin{bmatrix} 0 & 0 & -n \\ 0 & 0 & 0 \\ n & 0 & 0 \end{bmatrix} \quad (2.46)$$

$$\tilde{N} = \begin{bmatrix} 0 \\ -n \\ 0 \end{bmatrix} \quad (2.47)$$

The derivative of angular velocity (2.45) is as below

$$\begin{bmatrix} \dot{\omega}_1 \\ \dot{\omega}_2 \\ \dot{\omega}_3 \end{bmatrix} = \begin{bmatrix} 1 & 0 & 0 \\ 0 & 1 & 0 \\ 0 & 0 & 1 \end{bmatrix} \begin{bmatrix} \ddot{\theta}_1 \\ \ddot{\theta}_2 \\ \ddot{\theta}_3 \end{bmatrix} + \begin{bmatrix} 0 & 0 & -n \\ 0 & 0 & 0 \\ n & 0 & 0 \end{bmatrix} \begin{bmatrix} \dot{\theta}_1 \\ \dot{\theta}_2 \\ \dot{\theta}_3 \end{bmatrix} \quad (2.48)$$

Finally, the differential equation of the kinematic (2.44) of an orbiting rigid body can be found as

$$\begin{bmatrix} \dot{\theta}_1 \\ \dot{\theta}_2 \\ \dot{\theta}_3 \end{bmatrix} = \frac{1}{c_2} \begin{bmatrix} c_2 & s_1 s_2 & c_1 s_2 \\ 0 & c_1 c_2 & -s_1 c_2 \\ 0 & s_1 & c_1 \end{bmatrix} \begin{bmatrix} \omega_1 \\ \omega_2 \\ \omega_3 \end{bmatrix} + \frac{n}{c_2} \begin{bmatrix} s_3 \\ c_2 c_3 \\ s_2 s_3 \end{bmatrix} \quad (2.49)$$

The dynamic equation of motion about body-fixed principle axes becomes as shown

$$I_1 \dot{\omega}_1 - (I_2 - I_3) \omega_2 \omega_3 = -3n^2 (I_2 - I_3) C_{23} C_{33} \quad (2.50.a)$$

$$I_2 \dot{\omega}_2 - (I_3 - I_1) \omega_3 \omega_1 = -3n^2 (I_3 - I_1) C_{33} C_{13} \quad (2.50.b)$$

$$I_3 \dot{\omega}_3 - (I_1 - I_2) \omega_1 \omega_2 = -3n^2 (I_1 - I_2) C_{13} C_{23} \quad (2.50.c)$$

and define skew-symmetric direction cosine matrix Γ is defined as

$$\Gamma = \begin{bmatrix} 0 & -C_{33} & C_{23} \\ C_{33} & 0 & -C_{13} \\ -C_{23} & C_{13} & 0 \end{bmatrix} \quad (2.51)$$

The matrix form of Equations (2.50) is as below

$$I \dot{\omega} - \Omega I \omega = -3n^2 \Gamma I C_3 \quad (2.52)$$

where $C_3 = [C_{13} \ C_{23} \ C_{33}]^T$. The compact form of dynamic equation of motion about body-fixed principle axes (2.50) with linear angular velocity (2.45) and linear angular velocity rate (2.48) becomes

$$I(\ddot{\theta} + N\dot{\theta}) - \Omega I(\dot{\theta} + N\theta + \tilde{N}) = -3n^2 \Gamma I C_3 \quad (2.53.a)$$

Simplified mode of Equation (2.52) is as

$$I\ddot{\theta} + (IN - \Omega I)\dot{\theta} - \Omega IN\theta - \Omega I\tilde{N} = -3n^2 \Gamma I C_3 \quad (2.53.b)$$

2.2.4 Gyrostat in circular orbit [1]

This section formulates the equation of motion of an Earth-pointing spacecraft equipped with reaction wheels. A rigid body, consisting of a main platform and spinning wheels, is often referred as a gyrostat.

Assume a model of gyrostat equipped with two reaction wheels aligned along roll and yaw axes and a pitch momentum wheel as shown in Figure 2.3. The pitch momentum wheel is nominally spinning up along negative axis. As shown in the Figure 2.2 a LVLH reference frame A with its origin at the center of mass of a gyrostat has a set of unit vectors $\{\vec{a}_1, \vec{a}_2, \vec{a}_3\}$. Let $\{\vec{b}_1, \vec{b}_2, \vec{b}_3\}$ be a set of a bias vector of a body-fixed reference frame B , which is assumed to be aligned with principle axes of the gyrostat.

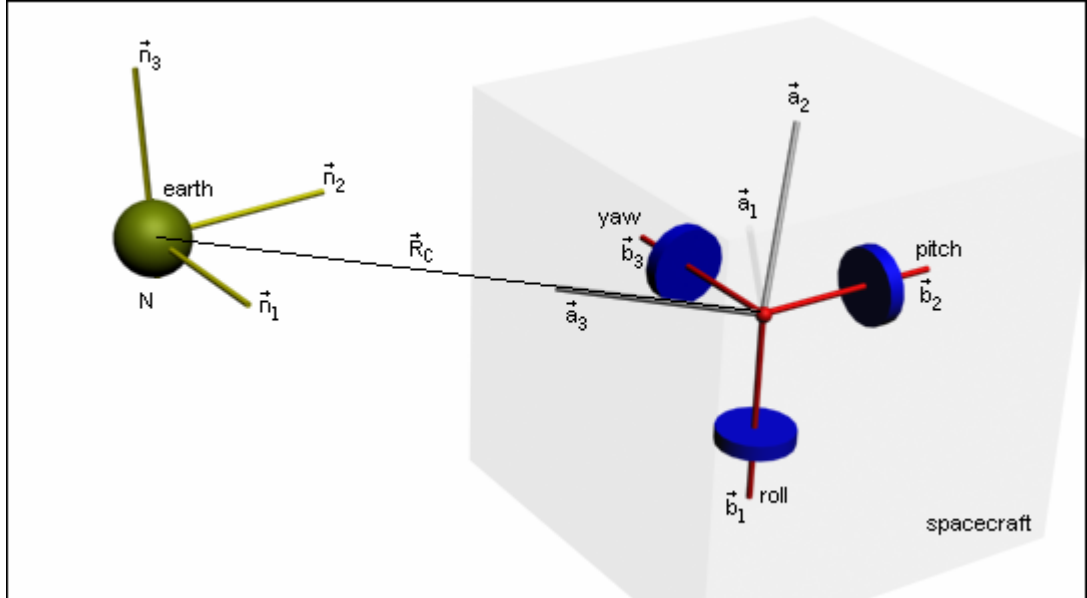


Figure 2.3 Gyrostat in circular orbit.

Then the total angular momentum of a spacecraft is expressed similar to Equation (2.29) as below:

$$\vec{H} = (I_1\omega_1 + h_1)\vec{b}_1 + (I_2\omega_2 + h_2)\vec{b}_2 + (I_3\omega_3 + h_3)\vec{b}_3 \quad (2.54)$$

where I_1, I_2, I_3 are principle moments of inertia of the gyrostat spacecraft; $\omega_1, \omega_2, \omega_3$ are body-fixed components of the angular velocity of the spacecraft; $h_1, -H_0 + h_2, h_3$ are the body-fixed components of the angular momentum of the three wheels; H_0 is the nominal pitch bias momentum along the negative pitch axis.

The rotational equation of motion is expressed before via Equation (2.28), such that

$$\dot{\vec{H}} = \left\{ \frac{d\vec{H}}{dt} \right\}_B + \vec{\omega}^{B/N} \times \vec{H} = \vec{M} \quad (2.55)$$

where \vec{M} is the gravity-gradient torque acting on the vehicle. For the principle-axis frame B the equation of motion can be rewritten as

$$I_1 \dot{\omega}_1 - (I_2 - I_3) \omega_2 \omega_3 + \dot{h}_1 + \omega_2 h_3 - \omega_3 (-H_0 + h_2) = -3n^2 (I_2 - I_3) C_{23} C_{33} \quad (2.56.a)$$

$$I_2 \dot{\omega}_2 - (I_3 - I_1) \omega_3 \omega_1 + \dot{h}_2 + \omega_3 h_1 - \omega_1 h_3 = -3n^2 (I_3 - I_1) C_{33} C_{13} \quad (2.56.b)$$

$$I_3 \dot{\omega}_3 - (I_1 - I_2) \omega_1 \omega_2 + \dot{h}_3 + \omega_1 (-H_0 + h_2) - \omega_2 h_1 = -3n^2 (I_1 - I_2) C_{13} C_{23} \quad (2.56.c)$$

where ω is described by Equation (2.49), and $h_i = J \omega_{rw_i}$.

2.2.5 Representation of Equation of Motion with θ

Equations of motion for a rigid body about body-fixed principle axes with gravity gradient torque and for a gyrostat in circular orbit were derived in Equations (2.50) and (2.56), respectively. Substituting Equation (2.23.a) and (2.52) into (2.56), equation of motion depending on angular velocity, ω , is generated as below:

$$\{I\dot{\omega} + \dot{h}\} - \Omega\{I\omega + h + \vec{H}\} = -3n^2 \Gamma I C_3 \quad (2.57)$$

The matrix form of Equation (2.57) is obtained as below

$$\begin{aligned} & \left\{ \begin{bmatrix} I_{11} & I_{12} & I_{13} \\ I_{21} & I_{22} & I_{23} \\ I_{31} & I_{32} & I_{33} \end{bmatrix} \begin{bmatrix} \dot{\omega}_1 \\ \dot{\omega}_2 \\ \dot{\omega}_3 \end{bmatrix} + \begin{bmatrix} \dot{h}_1 \\ \dot{h}_2 \\ \dot{h}_3 \end{bmatrix} \right\} \\ & - \begin{bmatrix} 0 & -\omega_3 & \omega_2 \\ \omega_3 & 0 & -\omega_1 \\ -\omega_2 & \omega_1 & 0 \end{bmatrix} \left\{ \begin{bmatrix} I_{11} & I_{12} & I_{13} \\ I_{21} & I_{22} & I_{23} \\ I_{31} & I_{32} & I_{33} \end{bmatrix} \begin{bmatrix} \omega_1 \\ \omega_2 \\ \omega_3 \end{bmatrix} + \begin{bmatrix} h_1 \\ h_2 \\ h_3 \end{bmatrix} + \begin{bmatrix} 0 \\ -H_0 \\ 0 \end{bmatrix} \right\} \\ & = -3n^2 \begin{bmatrix} 0 & -C_{33} & C_{23} \\ C_{33} & 0 & -C_{13} \\ -C_{23} & C_{13} & 0 \end{bmatrix} \begin{bmatrix} I_{11} & I_{12} & I_{13} \\ I_{21} & I_{22} & I_{23} \\ I_{31} & I_{32} & I_{33} \end{bmatrix} \begin{bmatrix} C_{13} \\ C_{23} \\ C_{33} \end{bmatrix} \quad (2.58) \end{aligned}$$

Substituting Equation (2.45) and (2.48) into (2.57) results

$$\{I(\ddot{\theta} + N\dot{\theta}) + \dot{h}\} - \Omega\{I(\dot{\theta} + N\theta + \vec{N}) + \vec{h} + \vec{H}\} = -3n^2 \Gamma I C_3 \quad (2.59)$$

Equation (2.59) can be simplified as

$$I\ddot{\theta} + (N + \Omega I)\dot{\theta} - \Omega IN\theta + \Omega(\tilde{H} + I\tilde{N}) + \dot{h} + \Omega\vec{h} = -3n^2\Gamma IC_3 \quad (2.60)$$

Matrix form of the Equation (2.60) is as below

$$\begin{aligned} & \left\{ \begin{bmatrix} I_{11} & I_{12} & I_{13} \\ I_{21} & I_{22} & I_{23} \\ I_{31} & I_{32} & I_{33} \end{bmatrix} \left(\begin{bmatrix} \ddot{\theta}_1 \\ \ddot{\theta}_2 \\ \ddot{\theta}_3 \end{bmatrix} + \begin{bmatrix} 0 & 0 & -n \\ 0 & 0 & 0 \\ n & 0 & 0 \end{bmatrix} \begin{bmatrix} \dot{\theta}_1 \\ \dot{\theta}_2 \\ \dot{\theta}_3 \end{bmatrix} \right) + \begin{bmatrix} \dot{h}_1 \\ \dot{h}_2 \\ \dot{h}_3 \end{bmatrix} \right\} \\ & - \begin{bmatrix} 0 & -\omega_3 & \omega_2 \\ \omega_3 & 0 & -\omega_1 \\ -\omega_2 & \omega_1 & 0 \end{bmatrix} \left\{ \begin{bmatrix} I_{11} & I_{12} & I_{13} \\ I_{21} & I_{22} & I_{23} \\ I_{31} & I_{32} & I_{33} \end{bmatrix} \left(\begin{bmatrix} \dot{\theta}_1 \\ \dot{\theta}_2 \\ \dot{\theta}_3 \end{bmatrix} + \begin{bmatrix} 0 & 0 & -n \\ 0 & 0 & 0 \\ n & 0 & 0 \end{bmatrix} \begin{bmatrix} \theta_1 \\ \theta_2 \\ \theta_3 \end{bmatrix} \right) + \begin{bmatrix} 0 \\ -n \\ 0 \end{bmatrix} \right\} \\ & + \begin{bmatrix} h_1 \\ h_2 \\ h_3 \end{bmatrix} + \begin{bmatrix} 0 \\ -H_0 \\ 0 \end{bmatrix} \left\} = -3n^2 \begin{bmatrix} 0 & -C_{33} & C_{23} \\ C_{33} & 0 & -C_{13} \\ -C_{23} & C_{13} & 0 \end{bmatrix} \begin{bmatrix} I_{11} & I_{12} & I_{13} \\ I_{21} & I_{22} & I_{23} \\ I_{31} & I_{32} & I_{33} \end{bmatrix} \begin{bmatrix} C_{13} \\ C_{23} \\ C_{33} \end{bmatrix} \quad (2.61) \end{aligned}$$

Equation (2.61) is obtained according to the orientation for sequence $C_1(\theta_1) \leftarrow C_2(\theta_2) \leftarrow C_3(\theta_3)$ to B from A of the body-fixed reference frame B with respect to the LVLH reference frame A for a rigid body in circular orbit.

2.3 Matrix of Rigid Body Dynamics

The MATLAB-Simulink model of a spacecraft can be prepared via Equation (2.61) by setting $\ddot{\theta}$ at left side and the other components at right side of the equation. The inertial matrix is assumed to be as $I = \text{diag}[I_1, I_2, I_3]$. Therefore, resulting equation is obtained as

$$\ddot{\theta} = -(N - I^{-1}\Omega I)\dot{\theta} + (I^{-1}\Omega IN)\theta + I^{-1}\Omega I\tilde{N} - 3n^2\Gamma IC_3 - I^{-1}\dot{h} - \Omega(h + \tilde{H}) \quad (2.62)$$

Note that $\Omega(\omega)$ is rewritten as a function of θ . Therefore, simplified form of the Equation (2.62) can be obtained by neglecting \tilde{N} and \tilde{H} as below

$$\ddot{\theta} = [A_1]\dot{\theta} + [A_2]\theta + [A_3]\dot{h} + [A_4]h \quad (2.63)$$

where

$$A_1 = \begin{bmatrix} 0 & 0 & -n(1-k_1) + H_0/I_1 \\ 0 & 0 & 0 \\ -n(k_3+1) + H_0/I_3 & 0 & 0 \end{bmatrix} \quad (2.63)$$

$$A_2 = \begin{bmatrix} -4n^2k_1 - nH_0/I_1 & 0 & 0 \\ 0 & -3n^2k_2 & 0 \\ 0 & 0 & -n2k_3 - nH_0/I_3 \end{bmatrix} \quad (2.64)$$

$$A_3 = \begin{bmatrix} -1/I_1 & 0 & 0 \\ 0 & -1/I_2 & 0 \\ 0 & 0 & -1/I_3 \end{bmatrix} \quad (2.65)$$

$$A_4 = \begin{bmatrix} 0 & 0 & n/I_1 \\ 0 & 0 & 0 \\ -n/I_3 & 0 & 0 \end{bmatrix} \quad (2.66)$$

2.4 Structural Dynamics

This section introduces simple mathematical model for flexible solar panels based on reference [1]. The system is given into matrix form similar to the spacecraft's dynamic model.

2.4.1 Flexible frames

The orientation of the solar arrays with respect to the spacecraft main body depends on orbital position and orbital time. Solar array orientation at 6 a.m. will be considered as a nominal configuration for the subsequent analysis and design. Orbit time of 6 a.m. and 6 p.m. yields out-of-plane bending modes in the yaw axis and in-plane bending modes in the roll axis. Note that, low-frequency characteristics of the first in-plane bending mode is caused by array yoke deformation [1].

During on-orbit normal mode operations, both solar arrays are always pointing towards the sun, whereas the main body is pointing towards the Earth. This results in very slowly changing modal frequencies and modal shapes. For control design purposes, however, the spacecraft model will be treated as a time-invariant system with a known range of modal characteristics. The linearized equation of motion of the three axis stabilized spacecraft with flexible array is given in [1] as below.

Rigid main body:

$$I_1 \dot{\omega}_1 - (I_2 - I_3) \omega_2 \omega_3 + \dot{h}_1 + \omega_2 h_3 - \omega_3 (-H_0 + h_2) + \sqrt{2} \delta_1 \ddot{q}_1 = M_1 \quad (2.67.a)$$

$$I_2 \dot{\omega}_2 - (I_3 - I_1) \omega_3 \omega_1 + \dot{h}_2 + \omega_3 h_1 - \omega_1 h_3 + \sqrt{2} \delta_2 \ddot{q}_2 = M_2 \quad (2.67.b)$$

$$I_3 \dot{\omega}_3 - (I_1 - I_2) \omega_1 \omega_2 + \dot{h}_3 + \omega_1 (-H_0 + h_2) - \omega_2 h_1 + \sqrt{2} \delta_3 \ddot{q}_3 = M_3 \quad (2.67.c)$$

Two solar arrays:

$$\ddot{q}_1 + \sigma_1^2 q_1 + \sqrt{2}\delta_1 \ddot{\theta}_1 = 0 \quad (2.68.a)$$

$$\ddot{q}_2 + \sigma_2^2 q_2 + \sqrt{2}\delta_2 \ddot{\theta}_2 = 0 \quad (2.68.b)$$

$$\ddot{q}_3 + \sigma_3^2 q_3 + \sqrt{2}\delta_3 \ddot{\theta}_3 = 0 \quad (2.68.c)$$

where $\delta_1, \delta_2, \delta_3$ represents rigid-elastic coupling scalars of a single solar array, $\sigma_1, \sigma_2, \sigma_3$ are modal frequencies, and q_1, q_2, q_3 are modal coordinates.

Note that, this model will be included only in designed block diagrams for spacecraft dynamics with sliding mode controllers.

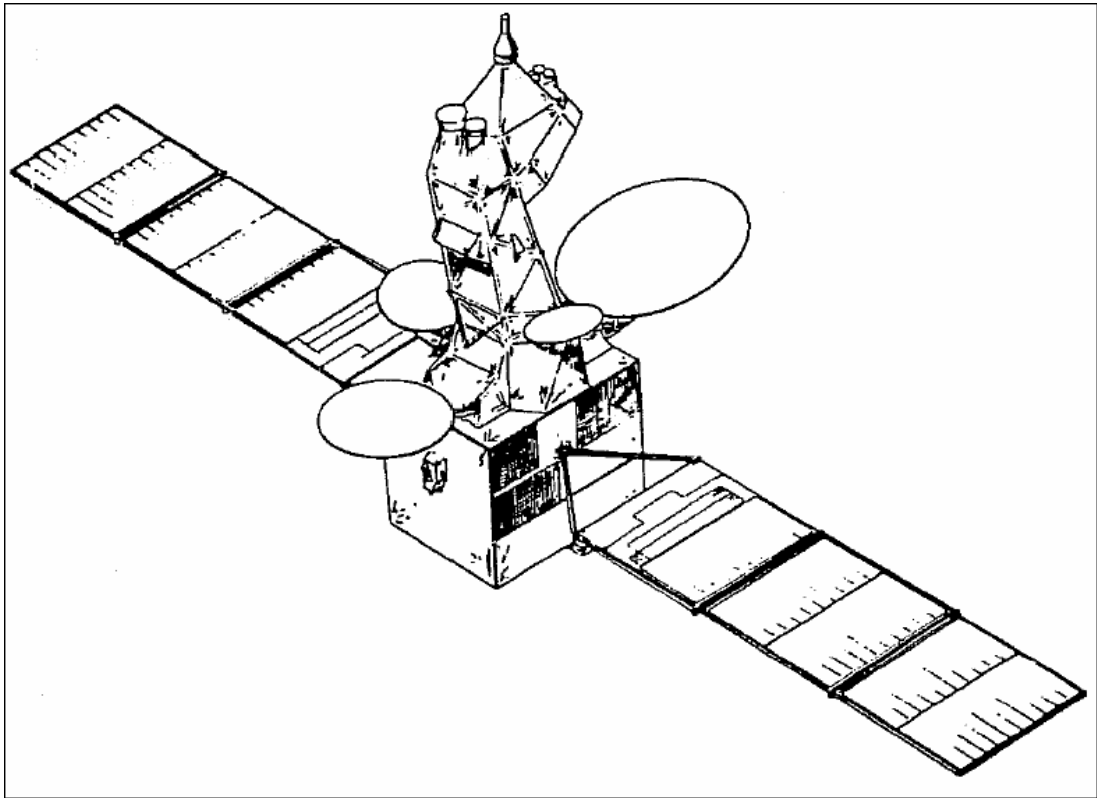


Figure 2.4 Flexible spacecraft Intelsat V [1].

3. LINEAR CONTROL SYSTEM DESIGN

In this section, modern control theory will be used to design linear controllers for active and passive control algorithms of the spacecraft. Passive control is an attitude control application which orients a spacecraft to a reference under small external disturbances or errors. The passive linear control algorithms illustrate the speed control of internal small torquers so-called reaction or momentum wheels. These control elements produce required moment via rotating to stabilize the spacecraft. On the other hand, active linear control algorithms are used for large attitude angles orientations. The signal is applied to the thrust system, so burning the propellant through the nozzle produces the required external torques for an orientation. These torques are large of value than the internal ones, so the active linear control algorithms response fast than passive linear control algorithms. In this section, control signals of the thrust system are considered to be continuous. Therefore, it is assumed that the spacecraft has sufficiently enough propellant for these thrusters. It can be seen that active linear control algorithms are limited with the spacecraft's amount of propellant. Also, passive control elements have a limited operation life due to mechanical failure as active control elements. As a result, when designing a spacecraft the life-time of the control elements should be chosen correctly.

3.1 System Linearization

Consider a system defined with Equations (2.50) with angular velocity (2.45). First step is linearization of attitude angles which are assumed to be as

$$x_1 = \theta \quad (3.1.a)$$

$$\dot{x}_1 = \dot{\theta} = x_2 \quad (3.1.b)$$

$$\dot{x}_2 = \ddot{\theta} \quad (3.1.c)$$

where $\theta = [\theta_1 \quad \theta_2 \quad \theta_3]^T$ describes the attitude angles, and x_i is (3×1) -vector.

Therefore state vector and output vector of the linear system are obtained as

$$x = [\dot{\theta}_1 \quad \theta_1 \quad \dot{\theta}_2 \quad \theta_2 \quad \dot{\theta}_3 \quad \theta_3]^T \quad (3.3)$$

$$y = [\theta_1 \quad \theta_2 \quad \theta_3]^T \quad (3.4)$$

Hence a linear system can be defined with the following equation

$$\dot{x} = Ax + Bu + G \quad (3.7.a)$$

$$y = Cx + Du \quad (3.7.b)$$

where x is (6×1) -state vector, y is (3×1) -output vector of the system, u is (3×1) -control vector, A is (6×6) -system matrix, B is (6×3) -control matrix, C is (3×6) -observer matrix, D is (3×3) -matrix, and G is (6×1) -disturbance vector.

In light of Equation (2.53.b), the system without a control term of linear matrix form is defined as

$$\dot{x} = \begin{bmatrix} A_1 & \vdots & A_2 \\ \cdots & \vdots & \cdots \\ I_{3 \times 3} & \vdots & 0_{3 \times 3} \end{bmatrix} x \quad (3.8.a)$$

$$y = [0_{3 \times 3} \quad \vdots \quad I_{3 \times 3}] x \quad (3.8.b)$$

where A_1 and A_2 are described by Equations (2.63) and (2.64), respectively, and $I_{3 \times 3}$ is (3×3) -identity matrix.

Thus, the linear form of the dynamic equation of motion about body-fixed principle axes is obtained above in Equation (3.8) without a control law. In next three sections passive, active and combined linear control law will be designed, respectively.

3.2 Linear Controllers Design

The linear controller will be design for reaction or momentum wheels as passive linear controller and for thrust mechanism as active linear controller. Finally, these two algorithms will be added to obtain combined linear controller.

3.2.1 Passive linear controller design

Passive linear controller applies continuous small torques to stabilize the attitude angle errors. In linear controllers design the angular momentum, h , of reaction or momentum wheels will be neglected because the angular momentum rate \dot{h} is larger n -times than the angular momentum, where geostationary orbital rate, n , is approximately equal to $7.2921 \times 10^{-5} \text{ sec}^{-1}$. Thus, only effects of the angular momentum rate will be taken into account in passive linear controller which

simulates the speed control algorithm of reaction wheels. The control is assumed to be as

$$u = [\dot{h}_1 \quad \dot{h}_2 \quad \dot{h}_3]^T = [u_1 \quad u_2 \quad u_3]^T \quad (3.9)$$

where u is a (3×1) -control vector.

Consider a system as gyrostat in circular orbit by means of Equation (2.57). The control should supply required internal moment to the system as below:

$$\begin{aligned} \dot{x} - Ax &= Bu \\ \dot{x} - Ax &= \begin{bmatrix} A_3 \\ \dots\dots\dots \\ 0_{3 \times 3} \end{bmatrix} \begin{bmatrix} u_1 \\ u_2 \\ u_3 \end{bmatrix} \end{aligned} \quad (3.10)$$

Then the linear system (3.8) with passive linear control becomes as below

$$[\dot{x}] = \begin{bmatrix} A_1 & \vdots & A_2 \\ \dots\dots & \vdots & \dots\dots \\ I_{3 \times 3} & \vdots & 0_{3 \times 3} \end{bmatrix} [x] + \begin{bmatrix} A_3 \\ \dots\dots\dots \\ 0_{3 \times 3} \end{bmatrix} \begin{bmatrix} u_1 \\ u_2 \\ u_3 \end{bmatrix}_p \quad (3.11.a)$$

$$[y] = [0_{3 \times 3} \quad \vdots \quad I_{3 \times 3}] [x] + [0_{3 \times 3}] \begin{bmatrix} u_1 \\ u_2 \\ u_3 \end{bmatrix}_p \quad (3.11.b)$$

where A_3 is defined by Equation (2.65).

Consider a control law as $u = \zeta_1 \omega + \zeta_2 \theta$ [1], where θ is attitude angles vector, ω is angular velocities vector and ζ_1 and ζ_2 are constants. Note that, the relation between angular velocities and attitude angles according to Equation (2.44) is not linear. Beside, Equation (2.45) is a linear, so control function is linear according to feedback of the system (3.11). Therefore, linear control feedback can be chosen as

$$u_p = -\zeta_1 \omega - \zeta_2 \theta = -\zeta x \quad (3.12)$$

where, x is the state vector and ζ is a constant matrix as

$$\zeta = \begin{bmatrix} \zeta_{11} & \zeta_{21} & 0 & 0 & 0 & -\zeta_{11}n \\ 0 & 0 & \zeta_{12} & \zeta_{22} & 0 & 0 \\ 0 & \zeta_{13}n & 0 & 0 & \zeta_{13} & \zeta_{23} \end{bmatrix} \quad (3.13)$$

The matrix form of Equation (3.12) becomes as

$$\begin{bmatrix} u_1 \\ u_2 \\ u_3 \end{bmatrix}_p = - \begin{bmatrix} \varsigma_{11} & \varsigma_{21} & 0 & 0 & 0 & -\varsigma_{11}n \\ 0 & 0 & \varsigma_{12} & \varsigma_{22} & 0 & 0 \\ 0 & \varsigma_{13}n & 0 & 0 & \varsigma_{13} & \varsigma_{23} \end{bmatrix} [x] \quad (3.14)$$

where ς_{ij} , $i=1,2$ and $j=1,2,3$, are constants to be selected.

Therefore, the linear system (3.11) of a dynamic equation of motion about body-fixed principle axis of a spacecraft is controlled with passive linear control signal defined in Equation (3.14). Note that, the designed control is a simulation of speed control of reaction or momentum wheels.

The stability of control can be analyzed by substituting control law (3.12) into the system (3.7.a) without disturbance vector G as following

$$\dot{x} = Ax + Bu = Ax - B\zeta x = (A - B\zeta)x \quad (3.15)$$

The system (3.15) is said asymptotically stable if matrix $A - B\zeta$ is Hurwitz-stable or the eigenvalues of the matrix have negative sign. Thus, the eigenvalues can be found by using the following relation

$$|sI - A + B\zeta| = 0 \quad (3.16)$$

For each s_i an eigenvalue can be found, and eigenvalue $\lambda_i \equiv s_i$.

3.2.2 Active linear controller design

Active linear controller algorithms are designed for large attitude angles orientations. The active linear controllers apply continuous torques via thrusters to stabilize the spacecraft. Therefore, thrusters should burn the propellant flow rate variably through nozzle. This method is not preferred because of limited amount of propellant during infinite burning at low flow rates caused by disturbances and unmodelled dynamics of attitude motions. However, let design an active linear controller as below.

Assume the control to be as

$$u = [u_1 \quad u_2 \quad u_3]^T \quad (3.17)$$

where u is (3×1) -vector.

Control is applied as a force to the system via thrusters. Therefore to obtain external moment, the distance between center of gravity of the spacecraft and the thruster position should be known. Assume that for principle axes, the distances are d_1, d_2, d_3 for axes 1,2,3, respectively [2].

Then the linear system (3.8) with active linear control takes the following form [2]

$$[\dot{x}] = \begin{bmatrix} A_1 & \vdots & A_2 \\ \cdots & \vdots & \cdots \\ I_{3 \times 3} & \vdots & 0_{3 \times 3} \end{bmatrix} [x] + \begin{bmatrix} I^{-1} \text{diag}(d1, d2, d3) \\ \cdots \\ 0_{3 \times 3} \end{bmatrix} \begin{bmatrix} u_1 \\ u_2 \\ u_3 \end{bmatrix}_a \quad (3.18.a)$$

$$[y] = [0_{3 \times 3} \quad \vdots \quad I_{3 \times 3}] \begin{bmatrix} x_2 \\ x_1 \end{bmatrix} + [0_{3 \times 3}] \begin{bmatrix} u_1 \\ u_2 \\ u_3 \end{bmatrix} \quad (3.18.b)$$

Linear control feedback can be chosen similar to (3.12) as

$$u_a = -\kappa x \quad (3.19)$$

where, x is the state vector and κ is a constant matrix defined as

$$\kappa = \begin{bmatrix} \kappa_{11} & \kappa_{21} & 0 & 0 & 0 & -\kappa_{11}n \\ 0 & 0 & \kappa_{12} & \kappa_{22} & 0 & 0 \\ 0 & \kappa_{13}n & 0 & 0 & \kappa_{13} & \kappa_{23} \end{bmatrix} \quad (3.20)$$

The matrix form of Equation (3.19) becomes as

$$\begin{bmatrix} u_1 \\ u_2 \\ u_3 \end{bmatrix}_a = - \begin{bmatrix} \kappa_{11} & \kappa_{21} & 0 & 0 & 0 & -\kappa_{11}n \\ 0 & 0 & \kappa_{12} & \kappa_{22} & 0 & 0 \\ 0 & \kappa_{13}n & 0 & 0 & \kappa_{13} & \kappa_{23} \end{bmatrix} [x] \quad (3.21)$$

where κ_{ij} , $i = 1, 2$ and $j = 1, 2, 3$, are constants to be selected.

The active linear controller is designed for system (3.18) as above. Note that, this active linear controller design is a continuous control during attitude orientations.

The stability of active linear control can be analyzed similar to the previous controller design by substituting control law (3.19) into system (3.7.a) without disturbance vector G as

$$\dot{x} = Ax + Bu = Ax - B\zeta x = (A - B\kappa)x \quad (3.22)$$

The system (3.22) is said asymptotically stable if matrix $A - B\kappa$ is Hurwitz-stable or the eigenvalues of the matrix have negative sign. Thus, the eigenvalues can be found as below:

$$|sI - A + B\kappa| = 0 \quad (3.23)$$

for each s_i an eigenvalue can be found, and eigenvalue $\lambda_i \equiv s_i$.

3.2.3 Combined linear controller design

The active and passive linear controllers are used together for global stability for large attitude angles orientations or small attitude errors. Passive (3.14) and active (3.21) linear control laws were designed above. In this part, these two controllers will be combined to work together. Then, combined linear control law is applied to the linear system as below:

$$\dot{x} = Ax + B_p u_p + B_a u_a + G \quad (3.24.a)$$

$$y = Cx + Du \quad (3.24.b)$$

Then the matrix form of Equation (3.24) becomes

$$\begin{aligned} [\dot{x}] = & \begin{bmatrix} A_1 & \vdots & A_2 \\ \cdots & \vdots & \cdots \\ I_{3 \times 3} & \vdots & 0_{3 \times 3} \end{bmatrix} [x] \\ & + \begin{bmatrix} A_3 \\ \cdots \\ 0_{3 \times 3} \end{bmatrix} \begin{bmatrix} u_1 \\ u_2 \\ u_3 \end{bmatrix}_p + \begin{bmatrix} I^{-1} \text{diag}(d1, d2, d3) \\ \cdots \\ 0_{3 \times 3} \end{bmatrix} \begin{bmatrix} u_1 \\ u_2 \\ u_3 \end{bmatrix}_a + G \end{aligned} \quad (3.25.a)$$

$$[y] = [0_{3 \times 3} \quad \vdots \quad I_{3 \times 3}] [x] + [0_{3 \times 3}] \begin{bmatrix} u_1 \\ u_2 \\ u_3 \end{bmatrix}_p + [0_{3 \times 3}] \begin{bmatrix} u_1 \\ u_2 \\ u_3 \end{bmatrix}_a \quad (3.25.b)$$

where u_p and u_a are control signals defined above with Equations (3.14) and (3.21), respectively, and G is disturbance vector.

The stability of combined linear controller can be analyzed by substituting control laws (3.12) and (3.19) into system (3.7.a) without disturbance vector G as

$$\dot{x} = Ax + Bu = (A - B\zeta - B\kappa)x = (A - B(\zeta + \kappa))x \quad (3.26)$$

The system (3.26) is said asymptotically stable if matrix $A - B\zeta - B\kappa$ is Hurwitz-stable or the eigenvalues of the matrix have negative sign. Thus, the eigenvalues can be found as below:

$$|sI - A + B(\zeta + \kappa)| = 0 \quad (3.27)$$

for each s_i an eigenvalue can be found, and eigenvalue $\lambda_i \equiv s_i$.

3.3 Pole Placement

This method brings an easiness to control designers to stabilize the linear system at desired type and time. The method is placing system poles at desired values. Therefore, the linear system behaves in order of the chosen poles and characteristics. Linear controller law can be constructed as:

$$u = -g^T x \quad (3.28)$$

So, primary system (3.10) without disturbance vector, G , becomes as:

$$\dot{x}(t) = Ax(t) - Bg^T x(t) = (A - Bg^T)x(t) \quad (3.29)$$

The characteristic equation of open-loop system (3.29) is given by

$$|sI - A| = 0 \quad \Rightarrow \quad s^n + a_1 s^{n-1} + \dots + a_{n-1} s + a_n = 0 \quad (3.30)$$

where a_1, \dots, a_n are constant coefficients. Then, let define a $(n \times n)$ -matrix \bar{A} as:

$$\bar{A} = \begin{bmatrix} -a_1 & \cdots & -a_{n-1} & -a_n \\ 1 & \cdots & 0 & 0 \\ \vdots & \ddots & \vdots & \vdots \\ 0 & \cdots & 1 & 0 \end{bmatrix} \quad (3.31)$$

Therefore, $(n \times n)$ -matrix Bg^T can be defined as:

$$Bg^T = \begin{bmatrix} g_1 & \cdots & g_n \\ 0 & \cdots & 0 \\ \vdots & \ddots & \vdots \\ 0 & \cdots & 0 \end{bmatrix} \quad (3.32)$$

Subtracting (3.31) from (3.32), $(n \times n)$ -canonical matrix is obtained as

$$A^* = \bar{A} - Bg^T = \begin{bmatrix} -(a_1 + g) & \cdots & -(a_{n-1} + g_{n-1}) & -(a_n + g_n) \\ 1 & \cdots & 0 & 0 \\ \vdots & \ddots & \vdots & \vdots \\ 0 & \cdots & 1 & 0 \end{bmatrix} \quad (3.33)$$

For each s_i an eigenvalue can be found, and eigenvalue $\lambda_i \equiv s_i$. According to the these eigenvalues desired pole vector is selected as

$$P = [\lambda_1 \quad \cdots \quad \lambda_n] \quad (3.34)$$

Then characteristic equation is represented in control canonical form as:

$$|sI - A^*| = 0 \Rightarrow s^n + a_1^* s^{n-1} + \dots + a_{n-1}^* s + a_n^* = 0 \quad (3.35)$$

comparing equation (3.33) and (3.35) get the following:

$$\left. \begin{array}{l} g_1 = a_1^* - a_1 \\ \vdots \\ g_n = a_n^* - a_n \end{array} \right\} \quad (3.36)$$

3.3.1 Pole placement for passive linear controller

The linear system (3.8) with passive pole placed linear control method becomes as

$$[\dot{x}] = \begin{bmatrix} A_1 & \vdots & A_2 \\ \cdots & \vdots & \cdots \\ I_{3 \times 3} & \vdots & 0_{3 \times 3} \end{bmatrix} [x] - [Bg^T]_p [x] \quad (3.37.a)$$

$$[y] = [0_{3 \times 3} \quad \vdots \quad I_{3 \times 3}] [x] \quad (3.37.b)$$

The stability of passive pole placed linear controller can be analyzed by substituting control law (3.28) for passive linear controller into system (3.7.a) without disturbance vector G as

$$\dot{x}(t) = Ax(t) - [Bg^T]_p x(t) = \left(A - [Bg^T]_p \right) x(t) \quad (3.38)$$

The system (3.38) is said asymptotically stable if matrix $A - [Bg^T]_p$ is Hurwitz-stable or the eigenvalues of the matrix have negative sign. Thus, the eigenvalues can be found as below:

$$|sI - A + [Bg^T]_p| = 0 \quad (3.39)$$

for each s_i an eigenvalue can be found, and eigenvalue $\lambda_i \equiv s_i$.

3.3.2 Pole placement for active linear controller

The linear system (3.8) with active pole placed linear control method becomes as

$$[\dot{x}] = \begin{bmatrix} A_1 & \vdots & A_2 \\ \cdots & \vdots & \cdots \\ I_{3 \times 3} & \vdots & 0_{3 \times 3} \end{bmatrix} [x] - [Bg^T]_a [x] \quad (3.40.a)$$

$$[y] = [0_{3 \times 3} \quad \vdots \quad I_{3 \times 3}] [x] \quad (3.41.b)$$

The stability of active pole placed linear controller can be analyzed by substituting control law (3.28) for active linear controller into system (3.7.a) without disturbance vector G as

$$\dot{x}(t) = Ax(t) - [Bg^T]_a x(t) = \left(A - [Bg^T]_a \right) x(t) \quad (3.42)$$

The system (3.42) is said asymptotically stable if matrix $A - [Bg^T]_a$ is Hurwitz-stable or the eigenvalues of the matrix have negative sign. Thus, the eigenvalues can be found as below:

$$\left| sI - A + [Bg^T]_a \right| = 0 \quad (3.43)$$

for each s_i an eigenvalue can be found, and eigenvalue $\lambda_i \equiv s_i$.

3.3.3 Pole placement of combined linear controller

The linear system (3.8) with combined pole placed linear control method becomes as

$$[\dot{x}] = \begin{bmatrix} A_1 & \vdots & A_2 \\ \cdots & \vdots & \cdots \\ I_{3 \times 3} & \vdots & 0_{3 \times 3} \end{bmatrix} [x] - \left([Bg^T]_p + [Bg^T]_a \right) [x] \quad (3.44.a)$$

$$[y] = [0_{3 \times 3} \quad \vdots \quad I_{3 \times 3}] [x] \quad (3.44.b)$$

The stability of combined pole placed linear controller can be analyzed by substituting control law (3.28) for both active and passive linear controllers into system (3.7.a) without disturbance vector G as

$$\begin{aligned} \dot{x}(t) &= Ax(t) - \left([Bg^T]_p + [Bg^T]_a \right) x(t) \\ &= \left(A - \left([Bg^T]_p + [Bg^T]_a \right) \right) x(t) \end{aligned} \quad (3.45)$$

The system (3.45) is said asymptotically stable if matrix $A - \left([Bg^T]_p + [Bg^T]_a \right)$ is Hurwitz-stable or the eigenvalues of the matrix have negative sign. Thus, the eigenvalues can be found as below:

$$\left| sI - A + \left([Bg^T]_p + [Bg^T]_a \right) \right| = 0 \quad (3.46)$$

for each s_i an eigenvalue can be found, and eigenvalue $\lambda_i \equiv s_i$.

4. VARIABLE STRUCTURE CONTROL DESIGN

Sliding modes as a phenomenon may appear in a dynamic system governed by ordinary differential equations with discontinuous right-hand sides. Control as a function of the system state switched at high (theoretically infinite) frequency is called sliding mode, which is governed by a differential equation with order less than the order of the original system. If the control is a vector valued quantity and each component undergoes discontinuities in its own switching surface the sliding modes may appear in intersection of several surfaces, also called as multidimensional sliding modes. In general, sliding mode controls high-order nonlinear dynamic plants operating under uncertain conditions, such as spacecrafts defined in [5-9, 13].

$$\dot{x} = f(x, t, u) \quad (4.1)$$

where $x \in \mathfrak{R}^n$, $f \in \mathfrak{R}^n$, $u \in \mathfrak{R}^m$ and t denotes the time.

The control is selected as discontinuous function of the state as

$$u_i = \begin{cases} u_i^+(x, t) & \text{if } s_i(x) > 0 \\ u_i^-(x, t) & \text{if } s_i(x) < 0 \end{cases} \quad (i = 1, \dots, m) \quad (4.2)$$

where $u_i^+(x, t)$ and $u_i^-(x, t)$ are continuous state function with $u_i^+(x, t) \neq u_i^-(x, t)$ and $s_i(x)$ are continuous state functions.

Giving a brief introduction about sliding mode, let first design the sliding surface for the sliding mode controllers.

4.1 Design of Sliding Surfaces

The equation of motion of a rigid spacecraft was described in Chapter 2 with Equations (2.50) and the evolution of spacecraft orientation in terms of attitude angles was given via Equation (2.49). Such that, attitude angles vector is sufficient to describe the motion if the spacecraft's angular velocities are described via a function of the spacecraft's attitudes. A control law subject to the constrained system given by Equation (2.49), $\omega = \omega(\theta)$ should be found to minimize the performance index [6, 7] as

$$J = \frac{1}{2} \int_{t_s}^{\infty} [\theta^T \Xi \theta + \omega^T \Psi \omega] dt \quad (4.3)$$

Note that, the trajectory may arrive at different switching surfaces at different times, but t_s is the time of arrival at the sliding manifold. Ξ and Ψ are weighting matrices described as below:

$$\Xi = \text{diag}[\rho, \rho, \rho] \quad (4.4)$$

$$\Psi(\theta) = \begin{bmatrix} 1 & -\theta_3 & \theta_2 \\ \theta_3 & 1 & -\theta_1 \\ -\theta_2 & \theta_1 & 1 \end{bmatrix} \quad (4.5)$$

After some assumptions and eliminations similar as in [7], the optimal switching surfaces are given as below

$$s_i = \omega_i + k_i \theta_i \quad (4.6)$$

where $k_i = +\sqrt{\rho}$, $i=1,2,3$. For this special case, it can also be shown that the optimal cost of regulation (the value of integral given in Equation (4.3)) is given as

$$J^* = 2k \quad (4.7)$$

The dynamics of the attitude angles may be obtained first via linearization and then via modifying Equation (2.49) as follows

$$\begin{bmatrix} \dot{\theta}_1 \\ \dot{\theta}_2 \\ \dot{\theta}_3 \end{bmatrix} = \begin{bmatrix} 1 & 0 & \theta_2 \\ 0 & 1 & -\theta_1 \\ 0 & \theta_1 & 1 \end{bmatrix} \begin{bmatrix} \omega_1 \\ \omega_2 \\ \omega_3 \end{bmatrix} + n \begin{bmatrix} \theta_3 \\ 1 \\ 0 \end{bmatrix} = \begin{bmatrix} 0 & \omega_3 & n \\ -\omega_3 & 0 & 0 \\ \omega_2 & 0 & 0 \end{bmatrix} \begin{bmatrix} \theta_1 \\ \theta_2 \\ \theta_3 \end{bmatrix} + \begin{bmatrix} \omega_1 \\ \omega_2 + n \\ \omega_3 \end{bmatrix} \quad (4.8)$$

From sliding manifold (4.6), angular velocity becomes $\omega_i = -k\theta_i$ for $s_i = 0$. Therefore, substituting the angular velocity into dynamic equation of attitudes into (4.8) results

$$\begin{bmatrix} \dot{\theta}_1 \\ \dot{\theta}_2 \\ \dot{\theta}_3 \end{bmatrix} = \begin{bmatrix} 0 & \omega_3 & n \\ -\omega_3 & 0 & 0 \\ \omega_2 & 0 & 0 \end{bmatrix} \begin{bmatrix} \theta_1 \\ \theta_2 \\ \theta_3 \end{bmatrix} + \begin{bmatrix} \omega_1 \\ \omega_2 + n \\ \omega_3 \end{bmatrix} = \begin{bmatrix} 0 & -k\theta_3 & n \\ k\theta_3 & 0 & 0 \\ -k\theta_2 & 0 & 0 \end{bmatrix} \begin{bmatrix} \theta_1 \\ \theta_2 \\ \theta_3 \end{bmatrix} + \begin{bmatrix} -k\theta_1 \\ -k\theta_2 + n \\ -k\theta_3 \end{bmatrix}$$

$$\begin{bmatrix} \dot{\theta}_1 \\ \dot{\theta}_2 \\ \dot{\theta}_3 \end{bmatrix} = \begin{bmatrix} -k\theta_3\theta_2 + n\theta_3 - k\theta_1 \\ k\theta_3\theta_1 - k\theta_2 + n \\ -k\theta_2\theta_1 - k\theta_3 \end{bmatrix}$$

$$\begin{bmatrix} \dot{\theta}_1 \\ \dot{\theta}_2 \\ \dot{\theta}_3 \end{bmatrix} = - \begin{bmatrix} k & 0 & 0 \\ 0 & k & 0 \\ 0 & 0 & k \end{bmatrix} \begin{bmatrix} \theta_1 \\ \theta_2 \\ \theta_3 \end{bmatrix} + \begin{bmatrix} 0 & -\theta_3 & \theta_2 \\ \theta_3 & 0 & -\theta_1 \\ -\theta_2 & \theta_1 & 0 \end{bmatrix} \begin{bmatrix} \ell_1 & 0 & 0 \\ 0 & \ell_2 & 0 \\ 0 & 0 & \ell_3 \end{bmatrix} \begin{bmatrix} \theta_1 \\ \theta_2 \\ \theta_3 \end{bmatrix} + \begin{bmatrix} n\theta_3 \\ n \\ 0 \end{bmatrix} \quad (4.9)$$

where

$$\tilde{\theta} = \begin{bmatrix} 0 & -\theta_3 & \theta_2 \\ \theta_3 & 0 & -\theta_1 \\ -\theta_2 & \theta_1 & 0 \end{bmatrix} \begin{bmatrix} \ell_1 & 0 & 0 \\ 0 & \ell_2 & 0 \\ 0 & 0 & \ell_3 \end{bmatrix} \begin{bmatrix} \theta_1 \\ \theta_2 \\ \theta_3 \end{bmatrix} \quad (4.10.a)$$

$$\tilde{\Omega} = \begin{bmatrix} 0 & -\theta_3 & \theta_2 \\ \theta_3 & 0 & -\theta_1 \\ -\theta_2 & \theta_1 & 0 \end{bmatrix} \quad (4.10.b)$$

$$\begin{bmatrix} \ell_1 \\ \ell_2 \\ \ell_3 \end{bmatrix} = \frac{1}{2} \begin{bmatrix} -1 & 1 & -1 \\ -1 & 1 & 1 \\ 1 & 1 & 1 \end{bmatrix} \begin{bmatrix} -k \\ k \\ -k \end{bmatrix} \quad (4.10.c)$$

4.2 Sliding Mode Controllers Design

In control system design of the satellite, continuous and discontinuous sliding mode controllers are used for passive and active control algorithms, respectively. Passive sliding mode controller applies a continuous control signal to the reaction wheels via equivalent control method which is idealization of chattering problem that keeps the state trajectory in the neighborhood of the sliding manifold. On the other hand, the discontinuous sliding mode control is used for active controller to burn out the propellant via thrusters in finite time. This control method may include switching at high gains during on-off logic operations. So, chattering problem may occur. To avoid this problem, discontinuous control is applied outside of the sliding boundary (s_0^-, s_0^+) .

4.2.1 Passive sliding mode controller design

Passive sliding mode controller is designed to stabilize the spacecraft for small attitude errors and as a main control algorithm for geosynchronous communication satellites. The controller applies continuous small torques via reaction or momentum wheels for stabilization. Thus, spacecraft is forced to have desired attitudes in finite time. After giving brief information about passive sliding mode controller let design the control algorithm as follows.

Assume that the initial state vector of system (4.1) is in the intersection of all discontinuous surfaces in the manifold $s(x)=0$, and sliding mode occurs with the state trajectories confined to this manifold for $t > 0$. Also assume that $ds/dt = \dot{s} = 0$ since motion implies $s = 0$ for $t > 0$. Therefore, in addition to $s(x)=0$, $\dot{s}(x)=0$ may be used to characterize the state trajectories during sliding mode. The time derivative of the vector on the state trajectories of system (4.1) is equal to zero [4, 5, 7]:

$$\dot{s} = G \cdot f(x, u) = 0 \quad (4.11)$$

where $G = \partial s / \partial x$ is a $m \times n$ matrix with gradients of functions $s(x)$ as rows. Let a solution to the algebraic Equation (4.11) exists. The solution $u_{eq}(x)$ is called as equivalent control. The continuous function is substituted for the discontinuous control u into the system (4.1). Thus, system becomes

$$\dot{x} = f(x, u_{eq}) \quad (4.12)$$

Equation (4.11) of the equivalent control method for system (4.1) is following

$$\dot{s} = Gf + GBu_{eq} = 0 \quad (4.13)$$

where B is a $n \times m$ matrix. Assuming GB matrix as nonsingular for any x , the equivalent control term becomes as

$$u_{eq}(x) = (-G(x)B(x))^{-1} G(x)f(x) \quad (4.14)$$

Substituting Equation (4.14) into (4.1), the sliding mode equation is formulated as

$$\dot{x} = f(x) - B(x)(G(x)B(x))^{-1} G(x)f(x) \quad (4.15)$$

The real control does not satisfy Equation (4.13), and it may be found as

$$u = u_{eq} + (GB)^{-1} \dot{s} \quad (4.16)$$

Therefore, the motion equation becomes

$$\dot{x} = f + Bu_{eq} + (GB)^{-1} \dot{s} \quad (4.17)$$

For the physical meaning of equivalent control consider a n -equations system with m -controls defined as

$$a_3 \ddot{x} + a_2 \dot{x} + a_1 x = u + d(t) \quad (4.18)$$

where $d(t)$ is bounded disturbance and assume $a_3^{-1}u \rightarrow u$. Note that, in Equation (2.61), \dot{h} (angular momentum rate) and h (angular momentum) are obtained from gyros. From Equations (2.50) for rigid body a_1 , a_2 and a_3 parameters are found as

$$a_3 = I \quad (4.19.a)$$

$$a_2 = \Omega I \quad (4.19.b)$$

$$a_1 = 3n^2 I \Gamma, \quad [C_3 \rightarrow \theta (3 \times 1 \text{ vector})] \quad (4.19.c)$$

Let s represent the sliding manifold as

$$s = [s_1 \quad s_2 \quad \cdots \quad s_m]^T = \dot{x} + cx = 0 \quad (4.20)$$

and assume that the discontinuous control is

$$u = -M \text{sign}(s) \quad (4.21)$$

where M is a constant parameter to be selected.

Taking the derivative of Equation (4.20) results

$$\dot{s} = \ddot{x} + c\dot{x} \quad (4.22)$$

Substituting system (4.19) into sliding motion (4.22) results

$$\dot{s} = -a_2 a_3^{-1} \dot{x} - a_1 a_3^{-1} x + u + a_3^{-1} d(t) = 0 \quad (4.23.a)$$

According to the reaching law, sliding motion is as $\dot{s} = -\eta_1 \text{sgn}(s) - \eta_2 h(s)$, where any of $h(s)$ elements are $s_i h_i(s_i) > 0$ and $\eta_1 = \text{diag}(\eta_{1i})$, $\eta_2 = \text{diag}(\eta_{2i})$. Also, reaching law is Lyapunov stable and it is proved below in Equation (4.34). Thus, using Equation (4.13) and reaching law, the sliding motion is obtained as

$$\dot{s} = GB(-\eta_2 s - \eta_1 \text{sgn}(s)) \quad (4.23.b)$$

Therefore, equivalent control is the solution to equation $\dot{s} = 0$ in terms of u under condition $s = 0$. Substituting $\dot{x} = -cx$ into Equation (4.23.a), equivalent control is obtained as

$$u_{eq} = (-a_2 c + a_1) a_3^{-1} x - a_3^{-1} d(t) \quad (4.24)$$

As seen from Equation (4.24) equivalent control depends on a_1, a_2 and disturbance $d(t)$. Extracting equivalent control by a low-pass filter may be used for improvement of feedback system.

Existence of sliding motion depends on the deviations from sliding surface s and its time derivative should have opposite sign in the neighborhood of switching surface $s = 0$ as [6, 7, 13]

$$\lim_{s \rightarrow +0} \dot{s} < 0 \quad \text{and} \quad \lim_{s \rightarrow -0} \dot{s} > 0 \quad (4.25)$$

The domain of sliding mode via substituting $\dot{x} = -cx$ and $\ddot{x} = c^2x$ into Equation (4.18) and setting it to zero, sliding motion is obtained analytically as below:

$$\dot{s} = (-c^2a_3 + a_2c - a_1)x - M\text{sign}(s) + d(t) \quad (4.26)$$

The domain of sliding mode for bounded disturbance $|d(t)| < d_0$ is given as

$$|x| = \left(|-c^2a_3 + ca_2 - a_1| \right)^{-1} (M - d_0) \quad (4.27)$$

Therefore, sliding mode exists with relation given in Equation (4.27).

Extending Equation (4.18), setting $x \equiv \theta$ and substituting Equation (4.16) the dynamic equation of motion about fixed principle of axes becomes

$$I\dot{\omega} - \Omega I\omega + 3n^2 I\Gamma\theta = -u_{eq} + (GB)^{-1}\dot{s} + d(t) \quad (4.28)$$

Substituting Equation (2.23b) into (4.28) the equivalent control is obtained as below

$$u_{eq} = -I\dot{\omega} + \Omega I\omega - 3n^2 I\Gamma C_3 + (-\eta_2 s - \eta_1 \text{sgn}(s)) \quad (4.29.a)$$

where η_1, η_2 are positive coefficients such that $d_0 < \eta_1$ and $|d_{\text{unmodeled dynamics}}| < \eta_2 |s|$. Assume that $d(t)$ is a disturbance and includes unmodelled dynamics. Then, substituting Equation (4.8) and (4.10) into (4.29.a) the equivalent control term becomes

$$\begin{aligned} u_{eq} &= -I\dot{\omega} + \Omega I\omega - 3n^2 I\Gamma C_3 + (GB)^{-1}\dot{s} \\ &= -I(-k\dot{\theta}) + \Omega I\omega - 3n^2 I\Gamma C_3 + (-\eta_2 s - \eta_1 \text{sgn}(s)) \\ &= -I(-k^2\theta + k\tilde{\theta}) + \Omega I\omega - 3n^2 I\Gamma C_3 + (-\eta_2 s - \eta_1 \text{sgn}(s)) \\ &= -I(-k^2\theta + k\tilde{\Omega}\ell_i\theta) + \Omega I\omega - 3n^2 I\Gamma C_3 + (-\eta_2 s - \eta_1 \text{sgn}(s)) \\ &= -I(k\omega + \tilde{\Omega}\ell_i(-k)^{-1}(-k)\theta) + \Omega I\omega - 3n^2 I\Gamma C_3 + (-\eta_2 s - \eta_1 \text{sgn}(s)) \\ &= -Ik\omega + I\Omega\ell_i k^{-1}\omega + \Omega I\omega - 3n^2 I\Gamma C_3 + (-\eta_2 s - \eta_1 \text{sgn}(s)) \\ &= I(-k + \Omega\ell_i k^{-1} + I^{-1}\Omega I)\omega - 3n^2 I\Gamma C_3 + (-\eta_2 s - \eta_1 \text{sgn}(s)) \end{aligned} \quad (4.29.b)$$

where k is a constant matrix to be selected during sliding manifold design. Finally, ℓ_i can be determined by Equation (4.10.c).

To analyze the stability, consider a positive definite Lyapunov function candidate, $V > 0$, for closed loop system as below:

$$V = \frac{1}{2} s^T s \quad (4.30)$$

The time derivative of a positive definite Lyapunov function candidate along system trajectories via substituting Equation (4.8) for sliding motion, \dot{s} , is as below:

$$\dot{V} = s^T \dot{s} = s^T (\dot{\omega} + k\dot{\theta}) \quad (4.31)$$

If the system trajectories are far from sliding manifold, Equation (2.49) is used instead of (4.9). Substituting $\dot{\omega}$ and $\dot{\theta}$ from Equation (4.28) and (4.9), respectively, into (4.31) and including unmodelled dynamics and disturbances torques, time derivative of positive definite Lyapunov candidate becomes as:

$$\begin{aligned} \dot{V} &= s^T \left(I^{-1}(u + d(t)) - I^{-1}\Omega I \omega + k\dot{\theta} \right) \\ &= s^T \left(I^{-1}(u + d(t)) - I^{-1}\Omega I \omega - k^2\theta + k\tilde{\theta} \right) \\ &= s^T \left(I^{-1}(u_{eq} + (GB)^{-1}\dot{s} + d(t)) + I^{-1}\Omega I \omega + k\omega + k\tilde{\theta} \right) \\ &= s^T \left(I^{-1}(u_{eq} + (GB)^{-1}\dot{s} + d(t)) - I^{-1}\Omega I \omega + k\omega + k\tilde{\Omega}\ell_i\theta \right) \\ &= s^T \left(I^{-1}(u_{eq} + (GB)^{-1}\dot{s} + d(t)) - I^{-1}\Omega I \omega + k\omega + k\tilde{\Omega}\ell_i(-k)^{-1}(-k)\theta \right) \\ &= s^T \left(I^{-1}(u_{eq} + (GB)^{-1}\dot{s} + d(t)) - I^{-1}\Omega I \omega + k\omega + \Omega\ell_i(-k)^{-1}\omega \right) \\ &= s^T \left(\left(I^{-1}I(-k - \Omega\ell_i(-k)^{-1} + I^{-1}\Omega I) \omega + 3n^2\Gamma IC_3 \right) \right. \\ &\quad \left. + (-\eta_2 s - \eta_1 \operatorname{sgn}(s)) + d_d + d_u \right) + \left(-I^{-1}\Omega I + k + \Omega\ell_i(-k)^{-1} \right) \omega \\ &= s^T \left(\left(-k - \Omega\ell_i(-k)^{-1} + I^{-1}\Omega I \right) \omega + 3n^2\Gamma IC_3 \right. \\ &\quad \left. + (-\eta_2 s - \eta_1 \operatorname{sgn}(s)) + d_d + d_u \right) + \left(-I^{-1}\Omega I + k + \Omega\ell_i(-k)^{-1} \right) \omega \\ &= s^T \left((-\eta_2 s - \eta_1 \operatorname{sgn}(s)) + d_d \right) \\ &= -\eta_2 s^T s - \eta_1 s^T \operatorname{sgn}(s) \\ &= -\eta_2 s^T s - \eta_1 |s| \end{aligned} \quad (4.32)$$

From Equation (4.30) it can be seen that η_1 and η_2 are positive constants and $s^T s$ is always positive. Therefore, time derivative of positive definite Lyapunov candidate becomes negative defined as shown below

$$\dot{V} = -\eta_2 s^T s - \eta_1 |s| < 0 \quad (4.33)$$

Hence, the passive sliding mode controller forces the system trajectories toward the sliding manifold asymptotically. In another words, it can be said that system is asymptotically stable in the domain with bounded disturbance specified via Equation (4.27) because of the existence conditions of equivalent control. The reaching law stability can be prove with any of $h(s)$ elements which are $s_i h_i(s_i) > 0$ via a positive definite Lyapunov function candidate $V = 1/2 s^T s$ as

$$\begin{aligned} \dot{V} &= s^T \dot{s} = s^T (-\eta_1 \text{sgn}(s) - \eta_2 h(s)) = -\eta_1 s^T \text{sgn}(s) - \eta_2 s^T h(s) \\ &= -\sum_{i=1}^m (\eta_{1i} s_i \text{sgn}(s_i) + \eta_{2i} s_i h(s_i)) = -\sum_{i=1}^m (\eta_{1i} |s_i| + \eta_{2i} s_i h(s_i)) < 0 \end{aligned} \quad (4.34)$$

where η_{1i} and η_{2i} are positive scalars. Thus, it can be seen that reaching condition holds and system is asymptotically stable.

4.2.2 Active sliding mode controller design

Active sliding mode controller is designed for large attitude angles orientations and faster stabilization of any attitude errors for desaturation of passive sliding mode algorithms for communication satellites. The controller applies discontinuous external torques via thrusters for stabilization. So, spacecraft is forced to have a desired attitude position in finite time of limited thrust. After giving brief information about active sliding mode controller let design the control algorithm as follows.

Control algorithm can be proposed as below

$$u = -N\gamma(s)\text{sign}(s) \quad (4.35)$$

where N is a positive defined scalar to be select and $\gamma(s)$ is a function defined as

$$\gamma(s) = \begin{cases} s - s_0, & s > s_0 \\ 0, & -s_0 < s < s_0 \\ s + s_0, & s < -s_0 \end{cases} \quad (4.36)$$

Sliding mode boundary layer is graphically shown in Figure 4.1.

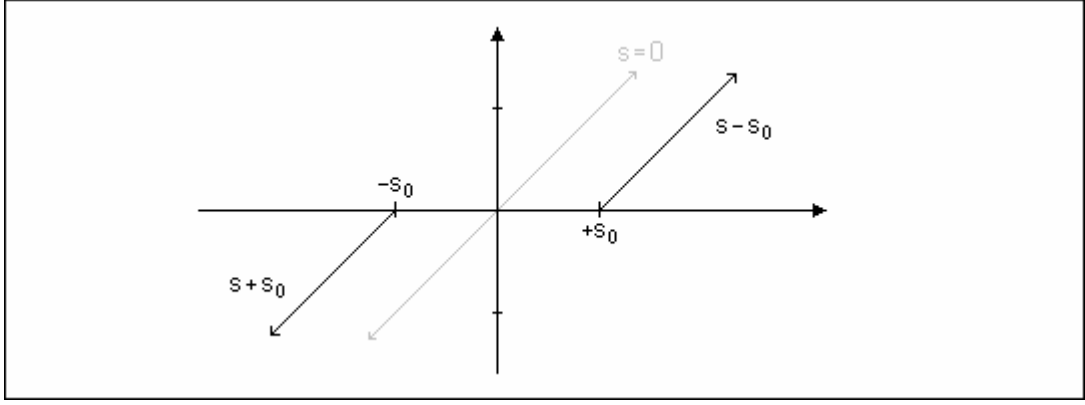


Figure 4.1 Sliding mode boundary layer function $\gamma(s)$.

The function in Equation (4.36) and shown in Figure 4.1 is so-called dead-band function. Therefore, control function (4.35) forces system to sliding manifold and keeps it on sliding manifold boundary $-s_0 < s < s_0$ as described in [13].

Consider a positive definite Lyapunov function candidate for closed loop system specified in Equation (4.30). The time derivative is obtained similar to (4.32) for active sliding mode controller (4.35) as below:

$$\begin{aligned}
\dot{V} &= s^T \left(I^{-1}(u + d(t)) - I^{-1}\Omega I \omega + k\dot{\theta} \right) \\
&= s^T \left(I^{-1}(u + d(t)) - I^{-1}\Omega I \omega - k^2\theta + k\tilde{\theta} \right) \\
&= s^T \left(I^{-1}(u + d(t)) + I^{-1}\Omega I \omega + k\omega + kk\tilde{\Omega}\ell_i\theta \right) \\
&= s^T \left(I^{-1}(u + d(t)) - I^{-1}\Omega I \omega + k\omega + k\tilde{\Omega}\ell_i(-k)^{-1}(-k)\theta \right) \\
&= s^T \left(I^{-1}(u + d(t)) - I^{-1}\Omega I \omega + k\omega + \Omega\ell_i(-k)^{-1}\omega \right) \\
&= s^T \left(\left(I^{-1}I(-k - \Omega\ell_i(-k)^{-1} + I^{-1}\Omega I) \omega + 3n^2\Gamma IC_3 \right) \right. \\
&\quad \left. + (-N\gamma(s)\text{sign}(s)) + d_d + d_u \right) + \left(-I^{-1}\Omega I + k + \Omega\ell_i(-k)^{-1} \right) \omega \\
&= s^T \left(\left(-k - \Omega\ell_i(-k)^{-1} + I^{-1}\Omega I \right) \omega + 3n^2\Gamma IC_3 \right. \\
&\quad \left. + (-N\gamma(s)\text{sign}(s)) + d_d + d_u \right) + \left(-I^{-1}\Omega I + k + \Omega\ell_i(-k)^{-1} \right) \omega \\
&= s^T \left(N\gamma(s)\text{sgn}(s) \right) \tag{4.37}
\end{aligned}$$

for $s > s_0 > 0$ the time derivative of positive definite Lyapunov function candidate becomes

$$\dot{V} = s^T \left(-N\gamma(s)\text{sgn}(s) \right) = s^T \left(-N(s - s_0)\text{sgn}(s) \right) = -Ns^T s + s_0 |s| \tag{4.38.a}$$

and for $s < s_0 < 0$ the time derivative of positive definite Lyapunov function candidate becomes

$$\dot{V} = s^T (-N\gamma(s)\text{sgn}(s)) = s^T (-N(s + s_0)\text{sgn}(s)) = -Ns^T s - s_0 |s| \quad (4.38.b)$$

Design of sliding manifold boundary in respect to asymptotical stability is given in Equations (4.38). Therefore, setting $\dot{V} < 0$, asymptotic stability is forced with relation as below:

$$s_0 |s| < Ns^T s \quad \text{and} \quad -Ns^T s < s_0 |s| \quad (4.39)$$

Thus, sliding manifold boundary is obtained as

$$\gamma(s) = \begin{cases} s_0 < \frac{1}{|s|} Ns^T s, & \text{for } s > s_0 \\ 0, & \text{for } -s_0 < s < s_0 \\ -\frac{1}{|s|} Ns^T s < s_0, & \text{for } s < -s_0 \end{cases} \quad (4.40)$$

where s_0 is a scalar to be select in according to inequality (4.40).

Under sliding manifold boundary conditions (4.40), derivative of positive definite Lyapunov function candidate in Equation (4.38) becomes as

$$\dot{V} = -Ns^T s + s_0 |s| < 0 \quad (\text{for } s > s_0 > 0, N > s_0) \quad (4.41.a)$$

$$\dot{V} = -Ns^T s - s_0 |s| < 0 \quad (\text{for } s < s_0 < 0, N > s_0) \quad (4.41.b)$$

$$\dot{V} = 0 \quad (\text{for } -s_0 < s < s_0) \quad (4.41.c)$$

where (4.41.c) is off period of the active sliding mode controller and do not produce any external control torques. Thus, the system is asymptotically stable and the discontinuous controller forces the system for operational period to reach sliding boundary layer.

4.2.3 Combined sliding mode controller design

In spacecraft attitude orientations, such as communication satellites in geosynchronous orbits, the active and the passive sliding mode controllers are used together for global stability. Combined sliding mode controller consists of active and passive sliding mode controllers which are combined to work together. Now, combined sliding mode control law can be presented as follows:

$$\begin{aligned}
u &= u_{passive} + u_{active} = (u_{eq} + (GB)^{-1}\dot{s}) + (-N\gamma(s)\text{sgn}(s)) \\
&= u_{eq} + (GB)^{-1}\dot{s} - N\gamma(s)\text{sgn}(s)
\end{aligned} \tag{4.42}$$

Therefore for stability analysis, consider a positive definite Lyapunov function candidate for closed loop system specified as in Equation (4.30). The time derivative is obtained similar to (4.32) and (3.37) for controller (4.42) as below:

$$\begin{aligned}
\dot{V} &= s^T (I^{-1}(u + d(t)) - I^{-1}\Omega I\omega + k\dot{\theta}) \\
&= s^T (I^{-1}(u + d(t)) - I^{-1}\Omega I\omega - k^2\theta + k\tilde{\theta}) \\
&= s^T (I^{-1}(u + d(t)) + I^{-1}\Omega I\omega + k\omega + kk\tilde{\Omega}\ell_i\theta) \\
&= s^T (I^{-1}(u + d(t)) - I^{-1}\Omega I\omega + k\omega + k\tilde{\Omega}\ell_i(-k)^{-1}(-k)\theta) \\
&= s^T (I^{-1}(u_{eq} + (GB)^{-1}\dot{s} - N\gamma(s)\text{sgn}(s) + d(t)) \\
&\quad - I^{-1}\Omega I\omega + k\omega + \Omega\ell_i(-k)^{-1}\omega) \\
&= s^T (I^{-1}(I(-k - \Omega\ell_i(-k)^{-1} + I^{-1}\Omega I)\omega + 3n^2\Gamma IC_3 + (-\eta_2s - \eta_1\text{sgn}(s)) \\
&\quad - N\gamma(s)\text{sgn}(s) + d(t)) - I^{-1}\Omega I\omega + k\omega + \Omega\ell_i(-k)^{-1}\omega) \\
&= s^T (I^{-1}I(-k - \Omega\ell_i(-k)^{-1} + I^{-1}\Omega I)\omega + 3n^2\Gamma IC_3 + (-\eta_2s - \eta_1\text{sgn}(s)) \\
&\quad - N\gamma(s)\text{sgn}(s) + d_d + d_u + (-I^{-1}\Omega I + k + \Omega\ell_i(-k)^{-1})\omega) \\
&= s^T ((-\eta_2s - \eta_1\text{sgn}(s)) - N\gamma(s)\text{sgn}(s)) \\
&= -\eta_2s^T s - \eta_1s^T \text{sgn}(s) - N\gamma(s)s^T \text{sgn}(s)
\end{aligned} \tag{4.43}$$

For positive scalars η_1 and η_2 , and sliding manifold boundary (4.41) conditions, Equation (4.43) becomes as

$$\dot{V} = -\eta_2s^T s - \eta_1s^T \text{sgn}(s) - N\gamma(s)s^T \text{sgn}(s) = \dot{V}_{passive} + \dot{V}_{active} \tag{4.44}$$

For passive and active sliding mode controllers, from Equation (4.33) and (4.41), respectively, the time derivative of each positive defined Lyapunov function candidate is negative in sign. Therefore,

$$\dot{V} = \dot{V}_{passive} + \dot{V}_{active} < 0 \tag{4.45}$$

The combined sliding mode controller forces the system trajectories asymptotically to reach the sliding manifold with continuous controller and the sliding boundary with discontinuous controller.

5. ATTITUDE CONTROL DESIGN EXAMPLES

In this chapter, firstly, the spacecraft sensors and control elements for attitude determination will be introduced. Then, spacecraft dynamics presented in Chapter 2 will be applied on selected satellite in Chapter 1. Next, satellite attitude dynamics instability without controllers will be presented and necessity of attitude controllers design will be introduced. A linear model of the spacecraft will be obtained according to the given rules in Chapter 3. The active, passive and combined pole placed linear controllers will be applied for small and large attitude angles orientations, respectively. Moreover, non linear controller law will be introduced, separately, for active, passive and combined sliding mode controllers. Finally, small and large attitude angles orientations will be performed by the designed sliding mode controllers.

5.1 Spacecraft Sensors and Control Elements

5.1.1 Sensors

For attitude determination of the chosen geosynchronous communication satellite, Intelsat V, the measurement elements are assumed to be Earth sensors, optic gyros and star trackers. Earth sensors measure the roll and pitch attitude errors of the satellite. Earth sensors are used for precise attitudes to the center of the Earth. Optic gyros measure the attitude angle rates and attitude errors. Star trackers measure attitude errors according to selected stars initialized during design procedure. Star trackers give precise attitudes for roll, yaw, and pitch axes and they are primary measurement devices for attitude determinations. On the other hand, Sun sensors are used for solar panel pointing, where the satellite supplies the required power for communication payload equipments and other devices. The solar panels are forced to follow the calculated Sun trajectory via sun sensors. Some sensors specifications and pictures are given in Appendix A4.1.

5.1.2 Control elements

Reaction wheels or momentum wheels are main inner torque supplier control elements for satellites. The supplied torque is continuous, but very small of value. These control elements are used for precise attitude orientations. On the other hand, thrusters are external torque suppliers which operate with nonlinear dynamics in real

procedures as described in [13]. For the satellite, bipropellant thrusters are chosen for large angle attitude orientations. Control elements specifications and figures are given in Appendix A4.2.

5.2 Rigid Spacecraft in Circular Orbit

Rigid spacecraft in circular orbit was described in Chapter 2 via Equations (2.50) and matrix form dependent on attitude angles θ is given in Equation (2.53.b). The Inertia matrix is obtained from Table 1.1 for chosen satellite as below:

$$I = \begin{bmatrix} I_1 & 0 & 0 \\ 0 & I_2 & 0 \\ 0 & 0 & I_3 \end{bmatrix} = \begin{bmatrix} 3026 & 0 & 0 \\ 0 & 440 & 0 \\ 0 & 0 & 3164 \end{bmatrix} \text{kgm}^2 \quad (5.1)$$

and inertia constants are calculated as

$$k_1 = \frac{I_2 - I_3}{I_1} = -0.9002 \quad (5.2.a)$$

$$k_2 = \frac{I_1 - I_3}{I_2} = -0.3136 \quad (5.2.b)$$

$$k_3 = \frac{I_1 - I_2}{I_3} = 0.8173 \quad (5.2.c)$$

The orbital rate is calculated for one real day of the spacecraft to orbit the Earth with same angular velocity as

$$n = \frac{2\pi}{(23h + 56m + 4.09054s)} = \frac{2\pi}{(23 \times 3600 + 56 \times 60 + 4.09054s)} \quad (5.3)$$

$$= 7.2921 \times 10^{-5} \text{sec}^{-1}$$

Therefore, required parameters are obtained for rigid body in circular orbit. A Matlab-Simulink model is given in Appendix 1.1 with Figure A1.1. The time responses of the spacecraft are given in Appendix 2.1. Figure A2.1 shows the small attitude errors motion as $\theta_1 = -5 \text{deg}$, $\theta_2 = 7 \text{deg}$, $\theta_3 = -10 \text{deg}$ and angular velocity of this motion is given in Figure A2.2. Figure A2.3 shows the large attitude errors motion as $\theta_1 = -45 \text{deg}$, $\theta_2 = -70 \text{deg}$, $\theta_3 = -50 \text{deg}$ and Figure A2.4 represents the angular velocity of that motion. Note that, these motions are not stable. At least one or more eigenvalues of the system have a positive sign as shown in the first column of Figure 5.1. These four figures show how the attitude angles and angular velocities get larger values in 4000 seconds of time period. If the chosen satellite is not

controlled, main goal will not be able to reach which is earth-satellite-earth communication or to broadcast the television and radio signals to designated area on Earth. As a result, a control algorithm is a must for such a body designed for this mission.

5.3 Gyrostat in Circular Orbit

The nutational frequency of the chosen spacecraft is $\lambda = 0.02 \text{ rad/s}$ [1] where $\lambda \equiv H_0 / \sqrt{I_{11}I_{33}}$. Therefore, necessary momentum for momentum wheels is calculated as

$$H_0 = \lambda \sqrt{I_{11}I_{33}} = 0.02 \sqrt{3026 \times 3164} = 61.8846 \text{ Nms} \quad (5.4)$$

Thus, all rigid spacecraft parameters were obtained.

5.4 Pole Placed Linear Controllers Design

Firstly, linear model of the spacecraft have to be obtained via Equations (3.1) and (3.4) according to modern control theory as in Equation (3.8). The required system matrix, A , is obtained via Equation (2.63) and (2.64), and parameters were calculated in Equations (5.1), (5.2), (5.3) and (5.4). Then, a linear model as $\dot{x} = Ax$ is obtained. The control term may be designed with pole placement method where Equation (3.14) and (3.21) become equal to $\begin{bmatrix} g^T \end{bmatrix}_p$ and $\begin{bmatrix} g^T \end{bmatrix}_a$ matrices specified in Equation (3.28), for passive and active linear control algorithm, respectively. The system matrix, A , control matrices $\begin{bmatrix} g^T \end{bmatrix}_a$ and $\begin{bmatrix} g^T \end{bmatrix}_p$, and controllability matrices B for passive and active linear controllers are given in Appendix A3.2.

Pole placed control term (3.14) and (3.21) for passive and active linear controllers with orbital rate $7.2921 \times 10^{-5} \text{ sec}^{-1}$ are obtained, respectively, as below:

$$\begin{bmatrix} u_1 \\ u_2 \\ u_3 \end{bmatrix}_p = - \begin{bmatrix} g^T \end{bmatrix}_p [x] = - \begin{bmatrix} \varsigma_{11} & \varsigma_{21} & 0 & 0 & 0 & 0 \\ 0 & 0 & \varsigma_{12} & \varsigma_{22} & 0 & 0 \\ 0 & 0 & 0 & 0 & \varsigma_{13} & \varsigma_{23} \end{bmatrix} [x] \quad (5.5.a)$$

$$\begin{bmatrix} u_1 \\ u_2 \\ u_3 \end{bmatrix}_a = - \begin{bmatrix} g^T \end{bmatrix}_a [x] = - \begin{bmatrix} \kappa_{11} & \kappa_{21} & 0 & 0 & 0 & 0 \\ 0 & 0 & \kappa_{12} & \kappa_{22} & 0 & 0 \\ 0 & 0 & 0 & 0 & \kappa_{13} & \kappa_{23} \end{bmatrix} [x] \quad (5.5.b)$$

where ς_{1j} and κ_{1j} , $j=1,2,3$, are feedback gains of attitude angles rates for yaw, pitch, and roll axes measured by optic gyro. ς_{2j} and κ_{2j} , $j=1,2,3$, are feedback gains of attitude errors for yaw, pitch and roll axes measured by star tracker, Earth

sensor and optic gyro. Then, control design matrices ζ and κ are selected as follows:

$$\zeta = \begin{bmatrix} 1 & 60 & 0 & 0 & 0 & 0 \\ 0 & 0 & 1 & 30 & 0 & 0 \\ 0 & 0 & 0 & 0 & 1 & 60 \end{bmatrix} \quad (5.6.a)$$

$$\kappa = \begin{bmatrix} 0.5 & 20 & 0 & 0 & 0 & 0 \\ 0 & 0 & .4 & 10 & 0 & 0 \\ 0 & 0 & 0 & 0 & 0.5 & 20 \end{bmatrix} \quad (5.6.b)$$

These matrices are Hurwitz stable because eigenvalues of the matrices $B_p g_p^T$ and $B_a g_a^T$ have negative sign. Note that, selected matrices also stabilize system as described below because the systems $A - B_p g_p^T$, $A - B_a g_a^T$ and $A - B_p g_p^T - B_a g_a^T$ are Hurwitz stable since eigenvalues have negative sign calculated via source code given in Appendix A3.3.1. The output of the program is shown in Table 5.1.

The time responses of attitude errors, angular velocities and control functions of the system with passive linear controller for small attitude angles orientation as $\theta_1 = -5 \text{ deg}$, $\theta_2 = 7 \text{ deg}$, $\theta_3 = -10 \text{ deg}$ are obtained in Figure A2.5, A2.6 and A2.7, respectively.

Table 5.1 Eigenvalues of the system and designed linear controllers.

Eigenvalues of linear satellite model	Eigenvalues active linear controller	Eigenvalues passive linear controller	Eigenvalues combined linear controller
lamdaA =	lamda_a =	lamda_p =	lamda_c =
0.0026	-0.0037 + 0.0127i	-0.0251 + 0.0149i	-0.0284 + 0.0146i
-0.0013 + 0.0023i	-0.0037 - 0.0127i	-0.0251 - 0.0149i	-0.0284 - 0.0146i
-0.0013 - 0.0023i	-0.0027 + 0.0119i	-0.0234 + 0.0148i	-0.0266 + 0.0148i
-0.0000	-0.0027 - 0.0119i	-0.0234 - 0.0148i	-0.0266 - 0.0148i
0.0001	-0.0114 + 0.0279i	-0.0783	-0.1091
-0.0001	-0.0114 - 0.0279i	-0.0580	-0.0500

The system is stabilized in long period of time (more than 2000 seconds), which shows that passive linear controller takes so much time to stabilize the system precisely. On the other hand, if combined linear control method is applied the spacecraft is stabilized in 300 seconds. The Figure A2.8, A2.9 and A2.10 show the combined linear controller performances of attitude angles, angular velocities, and applied control functions to the system. The mixture of active and passive linear controllers is combined linear controller which is summation of each control algorithms. In combined linear controller case, both passive, main control algorithm, and active, desaturation of main control algorithm, linear controllers force the inner

and external torquers to stabilize the satellite. In Figure A2.10 combined applied torque is given with separated small plots of passive and active linear controllers. Thus, it can be seen that the performances of combined linear algorithms are ten times better than the performances of passive control algorithms for small attitude angles orientations of the linear spacecraft model.

For large attitude errors as $\theta_1 = -45 \text{ deg}$, $\theta_2 = -70 \text{ deg}$, $\theta_3 = -50 \text{ deg}$, the system is stabilized after 2000 seconds relatively, which means that very small disturbances cause the system to be stabilized precisely near 4000 seconds. The performances of large attitude angles orientations of the passive linear controller are given in Figure A2.11, A2.12 and A2.13 as attitude angles, angular velocities and control functions, respectively. Thus, the thrust system is introduced for fastest attitude orientations. The performances of large attitude angles orientations of the combiner linear controller are given in Figure A2.14, A2.15 and A2.16 as attitude angles, angular velocities and control functions, respectively. Figure A2.16 shows the applied inner and external torques separately into combined control functions torque plot. The combined linear controller stabilizes successfully the system with required torques in 250 seconds.

However, active linear control algorithms, which is a part of combined linear controller, generates continuous control signal where propellant is used continuously even for very small attitude errors. During design procedure of satellites, amount of the propellant is optimized for conjectural attitude orientations and orbital maneuvers. As a result, active linear control algorithms may not be useful for such thrust system without any additions. The limits of the reaction wheels caused to use small control gain matrices for passive linear algorithms, so the control functions stabilized the system more slowly. However, matrices with high gains are required for passive linear controllers for faster orientations.

5.5 Sliding Mode Controllers Design

Sliding mode control system design is performed firstly by determining proper switching functions where the system trajectories will be caused to follow the sliding manifold, $s = 0$. Then equivalent control term will be used to model passive sliding mode control algorithms. Active sliding mode controller will be used to force satellite's attitudes to reach determined boundary layer of the sliding manifold. Control system performances will be investigated for small and large attitude angles orientations.

Sliding manifold design is performed via optimization of cost function (4.3). Physical sliding surface consists of input signals from Earth sensor for yaw and pitch

attitude angles, from star tracker for yaw, roll and pitch attitude angles, and from optic gyro for attitude angle rates and attitude errors. Selected sliding functions (4.6) stabilize the dynamic equation of attitude angles presented via Equation (4.9) in Figure A2.39 for small attitude angle errors as $\theta_1 = -5 \text{ deg}$, $\theta_2 = 7 \text{ deg}$, $\theta_3 = -10 \text{ deg}$; and in Figure A2.40 for large attitude angle errors $\theta_1 = -45 \text{ deg}$, $\theta_2 = -70 \text{ deg}$, $\theta_3 = -50 \text{ deg}$. The parameters k_i , $i=1,2,3$, are selected to minimize the cost function (4.3) for $k_i = +\sqrt{\rho}$ obtained as $k = 0.3$. Therefore, Equation (4.9) is optimized dynamic equation for sliding mode controllers. Associated design variables l_i , $i=1,2,3$, are obtained via Equation (4.10.c) with source code given in Appendix A3.5.2 as

$$[l_1 \quad l_2 \quad l_3] = [-0.15 \quad 0.15 \quad 0.45] \quad (5.7)$$

Passive sliding mode controller may be modeled with general representation of equivalent control term selected in Equation (4.14). Therefore, three equations with three controls are considered for each pitch, roll and yaw axes of dynamic system (2.50) for physical meaning of equivalent control. Final form of equivalent control for the spacecraft is given in Equation (4.29). The positive parameters η_1 and η_2 are selected according to the following criteria (5.8):

$$d_0 < \eta_1 \Rightarrow d_0 = 0.0005 \sin(\omega t) \quad (5.8.a)$$

$$|d_{\text{unmodeled dynamics}}| < \eta_2 |s| \Rightarrow \max |d_{\text{unmodeled dynamics}}| < 0.005 \quad (5.8.b)$$

Equations (5.8) become for small angles orientations as $\theta_i < 5 \text{ deg}$, $i=1,2,3$, as

$$\eta_1 > d_0 = 0.0005 \sin(\omega t) = 0.0005 \Rightarrow \eta_1 > 0.0005 \quad (5.9.a)$$

$$\eta_2 |s| > |d_{\text{unmodeled dynamics}}| = 1 \times 10^{-5} \Rightarrow \eta_2 |k\theta_0| = \eta_2 |0.3 \times 0.0873| > 1 \times 10^{-5} \quad (5.9.b)$$

where $\eta_1 = 0.01 > 5 \times 10^{-4}$ and $\eta_2 = 0.1 > 2.62 \times 10^{-2}$ model the nominal moment and maximum torque, respectively, produced by a reaction wheel.

Thus passive sliding mode control term (4.16) becomes as

$$u = u_{eq} + (GB)^{-1} \dot{s} = u_{eq} + (\eta_2 s + \eta_1 \text{sign}(s)) = u_{eq} + (0.1s + 0.01 \text{sign}(s)) \quad (5.10)$$

Control function (5.8) describes the passive sliding mode control algorithm which simulates speed control of reaction wheels for designed non linear controller. The performance of passive sliding mode controller for small attitude errors as $\theta_1 = -5 \text{ deg}$, $\theta_2 = 7 \text{ deg}$, $\theta_3 = -10 \text{ deg}$ are shown in Figures A2.17, A2.18, A2.19, A2.20 and A2.21 for attitude angle errors, angular velocities, switching functions, control functions and disturbances, respectively. The chosen spacecraft is stabilized

in 50 seconds precisely by passive sliding mode controller with 0.03 Nm maximum of inner torque. This is really excellent performance for spacecraft stabilization by variable structure control method according to the all possible modeled dynamics and bounded disturbances.

The performance of large attitude errors of the passive sliding mode controller as $\theta_1 = -45 \text{ deg}$, $\theta_2 = -70 \text{ deg}$, $\theta_3 = -50 \text{ deg}$ are shown in Figures A2.28, A2.29, A2.30 and A2.31 for attitude angle errors, angular velocities, switching functions, control functions and disturbances, respectively. For that case, the satellite is stabilized in 100 seconds by passive sliding mode controller with 0.15 Nm maximum of inner torque. The orientation is performed perfectly; however, required high torque may be produced from the second and/or third stand by inner torquers, where 0.075 Nm is shared by each reaction wheels. Then, the orientation is physically possible, which shows the power of the sliding mode control according to modeled dynamics and bounded disturbances with inner torquers for less time of period.

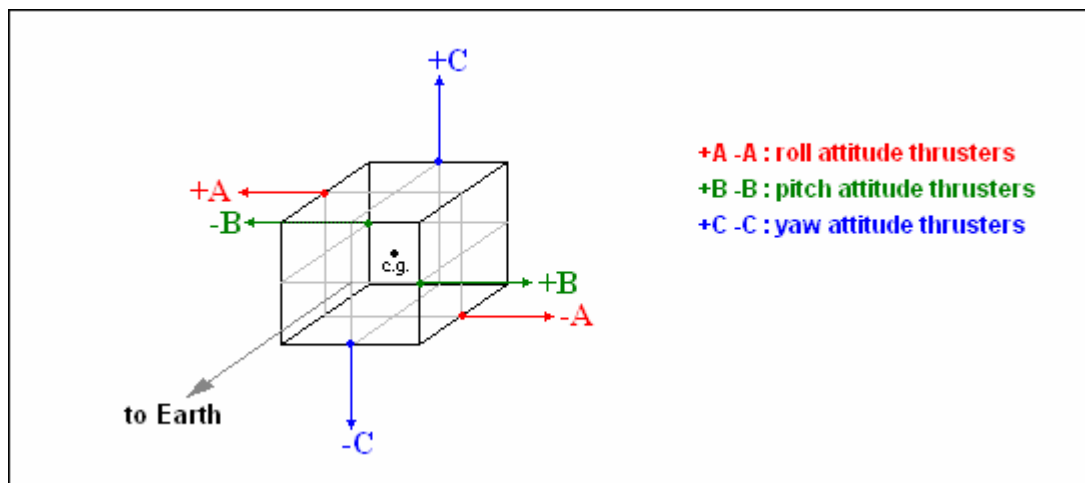


Figure 5.1 Configuration of the attitude thrusters for design example.

Next, the active sliding mode control algorithm is described with a sliding boundary layer where system trajectory is forced to arrive from any arbitrary point via thrusters mounted on the spacecraft as shown in Figure 5.1.

The sliding boundary is selected for stability of the sliding mode controller by Equation (4.39). Therefore, sliding manifold boundary layer (4.40) could be calculated via source code given in Appendix A3.5.1. It is selected to be approximately at $\pm 4 \text{ deg}$ of attitude angles for precise stabilization via passive sliding mode controller after system is forced to reach the sliding boundary. Thus, sliding boundary is calculated by the program code as

$$\max(s_0) = [0.0209 \quad 0.0209 \quad 0.0209] \quad (5.11)$$

This means that maximum value of s_0 is 0.0209 rad/s. In design case, boundary layer is selected at $s_0 = 0.02$ rad/s. Therefore, the thrust system will perform on logic with 1 Nm thrust moment for initial conditions of angular velocity, $\omega = 0$, and attitude errors, $\theta > 3.8197$ deg. The applied torque will be equal to, thrust vector value times perpendicular distance of the thrust vector to the center of gravity, which is assumed to be unit length of 1 m for assumed configuration of mounted thrusters. The thrust system operates with on-off logic and constant thrust value. On-off algorithms are designed with variable structure control via setting a dead-band function as (4.36).

Finally, the scenario of combined controller may be explained as follow. At any initial attitude and angular velocity errors with initial value of switching function $s > 0.02$, thrusters operate on logic until system reaches the sliding boundary layer. When system reaches the sliding boundary $s = \pm s_0$, passive sliding mode control algorithms force the system trajectories to reach sliding manifold $s = 0$ with very small inner torques in short time of period. The performances of small attitude angles orientations of the combined sliding mode controller as $\theta_1 = -5$ deg, $\theta_2 = 7$ deg, $\theta_3 = -10$ deg are shown in Figure A2.22, A2.23, A2.24, A2.25, A2.26 and A2.27 for attitude angle errors, angular velocities, switching functions, combined control functions, control functions of active and passive controllers and disturbances, respectively. It can be seen that the system is stabilized into 30 seconds precisely with 0.025 Nm maximum of applied inner torque and only a few thrust via thrusters as shown in upper part of Figure A2.26 Note that, the system trajectories are forced to reach the sliding boundary in 5 seconds by combined sliding mode controller. After stabilization on sliding boundary layer, system trajectories are forced to achieve the sliding manifold $s = 0$ in 25 seconds of time period.

Orientation of large attitude errors as $\theta_1 = -45$ deg, $\theta_2 = -70$ deg, $\theta_3 = -50$ deg with combined sliding mode controller are shown in Figures A2.33, A2.34, A2.35, A2.36, A2.37 and A2.38 for attitude angles errors, angular velocities, switching functions, combined control functions, control functions of active and passive sliding mode controllers and disturbances, respectively. The spacecraft is precisely stabilized in 30 seconds by combined sliding mode controller. While a thruster operates, it keeps system trajectory and forces them in less than a second on the sliding boundary. During on logic of active sliding mode controller, equivalent control term tries to affect the system possibly with high control commands larger than that reaction wheels may produce. So, gains of equivalent control term should be selected carefully. Performances of the thrusters are given in related plots with pulses less than 10 seconds. Hence limited propellant is used and precise orientation is done in very short time by using combined sliding mode controller.

6. CONCLUSION

Control problem of a spacecraft is an important topic in automatic control engineering. Many studies about attitude stabilization of satellite applications have been proposed. In this thesis, a three axis stabilized spacecraft –a communication satellite Intelsat V– is selected to investigate attitude dynamics, and to design linear and variable structure controllers. Spacecraft kinematics and dynamics are studied to recognize how the system operates in circular orbit for attitude motions. The satellite's dynamic model is obtained via linearized rigid spacecraft attitude dynamics, gravity gradient torque, dynamic effects of flexible solar panels, a sinusoidal effect as external and internal disturbances. The designed passive pole placed linear controller, which models reaction wheels, stabilizes the satellite well with longer settling time. Additionally, active pole placed linear controller, which models thrust system, stabilizes the satellite precisely with short settling time. However, it operates continuously that is undesirable for the attitude control system due to the limited amount of propellant of the spacecraft. The combined linear controller model of flexible spacecraft is obtained with passive and active controllers, linearized rigid spacecraft attitude dynamics, a sinusoidal effect as a disturbance which consists of flexible solar panels vibration effects, gravity gradient torque, sun pressure and other unmodeled external or internal disturbances. On the other hand, both active and passive sliding mode controllers constitute combined sliding mode controller which stabilizes the system faster than the linear controllers according to selected sliding manifold which needs to be designed. The passive sliding mode controller supplies inner torques with continuous control signal produced by equivalent control term. Beside, the thrust system is used seldom and only a few on-off logic operations are done for precise stabilization of the designed model of the spacecraft. Nonlinear design for thrust system is sufficient model for on-off logic and it depends on the switching functions and selected sliding boundary layer. Although, this is a simple design described via a few blocks, it is a complicated mathematical model to be studied with. Nonlinear controller model includes passive and active controllers with the dynamic model of the satellite. The time responses are obtained from Matlab-Simulink block diagrams of the designed satellite attitude dynamic model, linear and sliding mode controllers which are given to illustrate the considered procedure.

Note that, the communication satellite Intelsat V is not operational anymore. However, it is similar to the communication satellites used in nowadays. In this thesis, the design of variable structure controllers are given as suggested main control algorithms for a three axis stabilized spacecraft. Linear controllers are designed to show effectiveness of the sliding mode controllers with performances shown in Appendices.

In conclusion, variable structure controllers stabilize the spacecraft precisely in short time for considered spacecraft model with selected reaction wheels, thrusters and measurement elements such as earth sensors, star trackers, optic gyros and sun sensors. Moreover, variable structure controllers include unmodelled dynamics and disturbances as described under sliding mode controllers design. Hence, sliding mode controllers model the satellite sufficiently enough that makes them useful than linear control algorithms in attitude stabilization control of geosynchronous satellites.

REFERENCES

- [1] **Wie, B.**, 1998. Space Vehicle Dynamics and Control, AIAA, Virginia.
- [2] **Franklin, G.F., Powell, J.D, Emami-Naeini, A.**, 2002. Feedback Control of Dynamic Systems, 4th Edition, Prentice Hall, New Jersey.
- [3] **Somov, Ye.I., Titov, G.P., Butyrin, S.A., Rayevsky V.A., Kozlov, A.G.**, 2004. Nonlinear dynamics of a spacecraft respinup by a weak internal control, *16th IFAC Symposium on Automatic Control in Aerospace*, St. Petersburg, Russia, 14-18 June.
- [4] **Hung. J.Y.**, 1993. Variable structure control: a survey. IEEE Transactions on Industrial Electronics, **40**, 2-22.
- [5] **Utkin, V.I.**, 1993. Sliding mode control design principles and applications to electric drives, IEEE Transactions on Industrial Electronics, **40**, 2-22.
- [6] **Vadali, S.R.**, 1986. Variable-structure control of spacecraft large-angle maneuvers, *Journal of Guidance*, **9**, 235-239.
- [7] **Utkin, V.I.**, 1992. Sliding Modes in Control Optimization, Springer-Verlag, Berlin.
- [8] **Sira-Ramirez, H. and Dwyer, T.A.W.**, 1987. Variable structure controller design for a spacecraft nutation damping, IEEE Transactions on Automatic Control, **32**, 435-438
- [9] **Öz, H.**, 1993. Variable structure control of flexible spacecraft, *Variable Structure Control for Robotics and Aerospace Applications*, K.K.D.Young (Edt.), Elsevier, Amsterdam.
- [10] **Sira-Ramirez, H.**, 1993. Nonlinear pulse width modulation controller design, *Variable Structure Control for Robotics and Aerospace applications*, K.K.D.Young (Edt.), Elsevier, Amsterdam.
- [11] **Zhang, J.R., and Li, J.F.**, 2004. A Lyapunov-typed nonlinear attitude controller for spacecraft, *16th IFAC Symposium on Automatic Control in Aerospace*, St. Petersburg, Russia, 14-18 June.
- [12] **Yoon, H, and Tsiotras, P.**, 2002. Spacecraft adaptive attitude and power tracking with variable speed control moment gyroscopes, *Journal of Guidance, Control and Dynamics*, **25**, 1081-1090.

- [13] **Slotine, J-J.E., and Li, W.**, 1991. Applied Nonlinear Control, Prentice Hall, New Jersey.

APPENDICES

Appendix 1. Controllers' Matlab-Simulink Block Diagrams

A1.1 Block diagram of the dynamics system

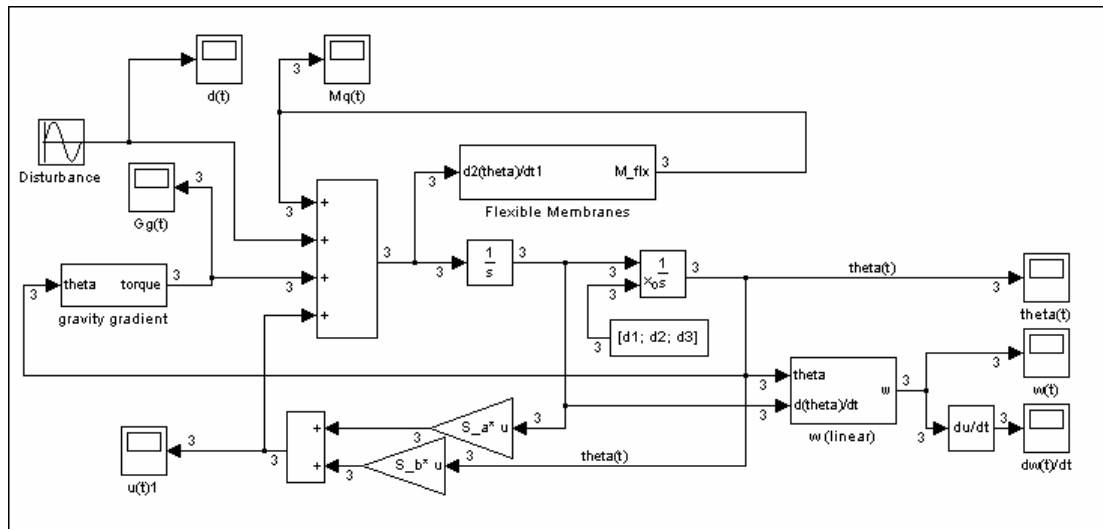


Figure A1.1 Block diagram of the dynamic system [file name: *dynamic_system.mdl*].

A1.2 Block diagram of the linear controllers

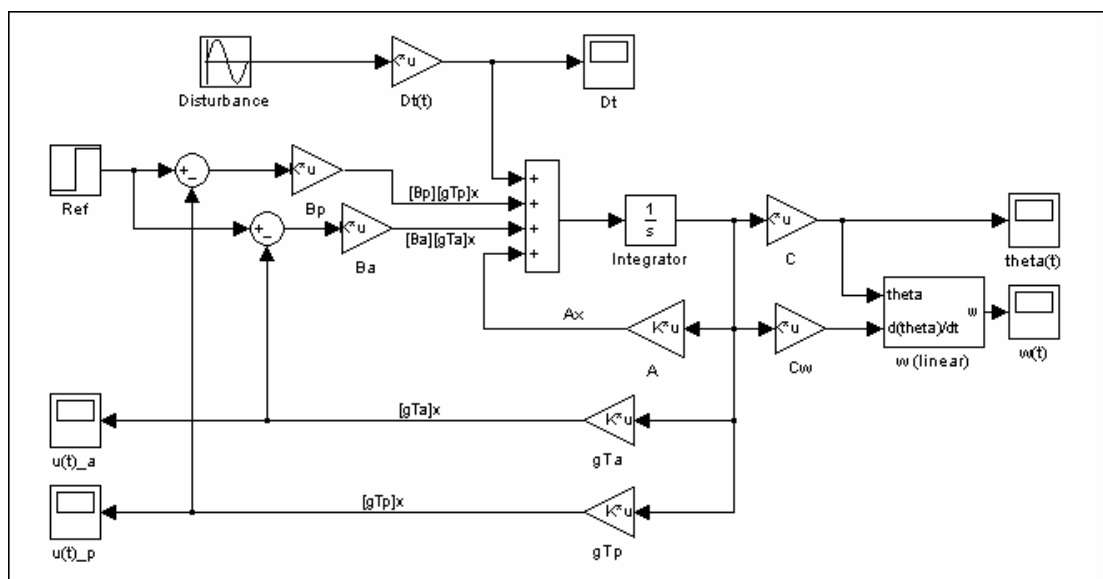


Figure A1.2 Block diagram of the combined linear controller [f.n.: *linear_control.mdl*].

A1.3 Block diagram of the sliding mode controllers

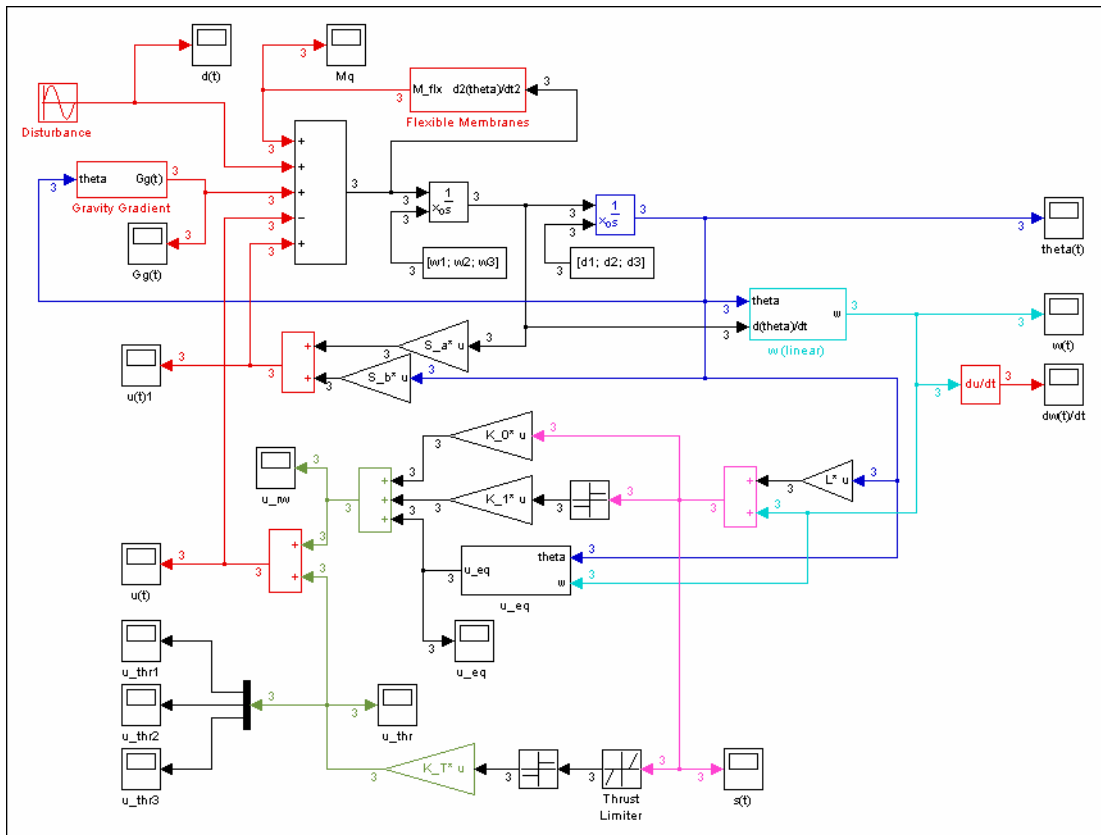


Figure A1.3 Block diagram of the sliding mode controller [file name: sliding_mode.mdl].

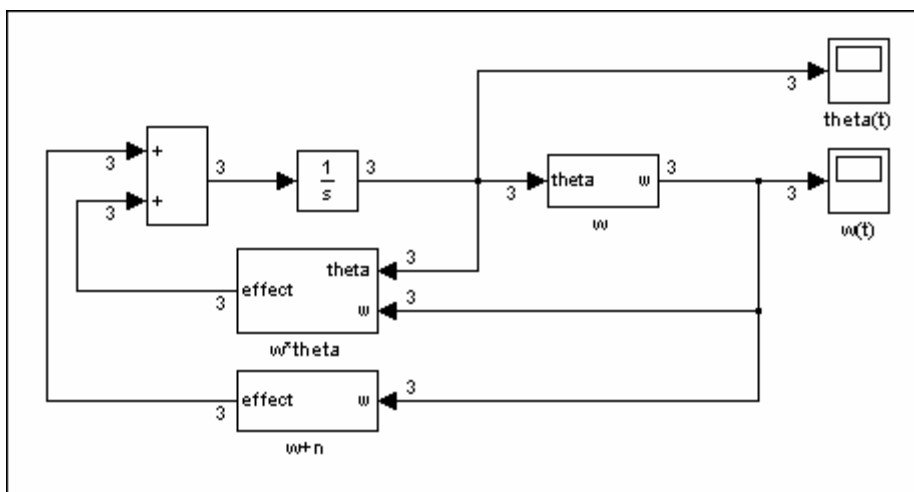


Figure A1.4 Block diagram of the sliding manifold dynamics [f.n.: sliding_manifold.mdl].

Appendix 2. Time Responses of the System and Designed Controllers

A2.1 Spacecraft Dynamics

A2.1.1 Small attitude angles simulations for rigid spacecraft

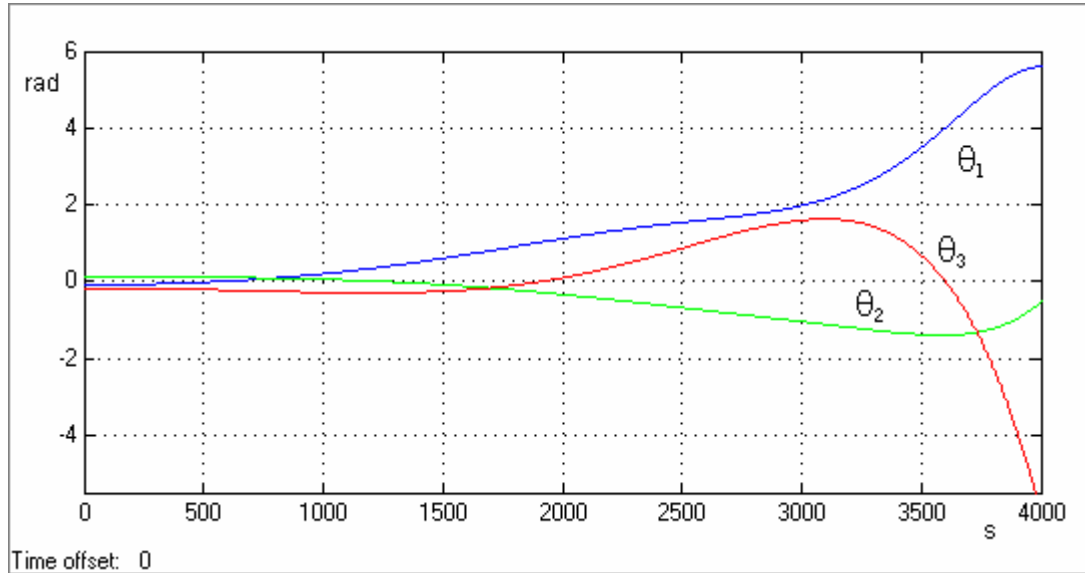


Figure A2.1. Time responses of small attitude errors $\theta_1, \theta_2, \theta_3$ of dynamic system.

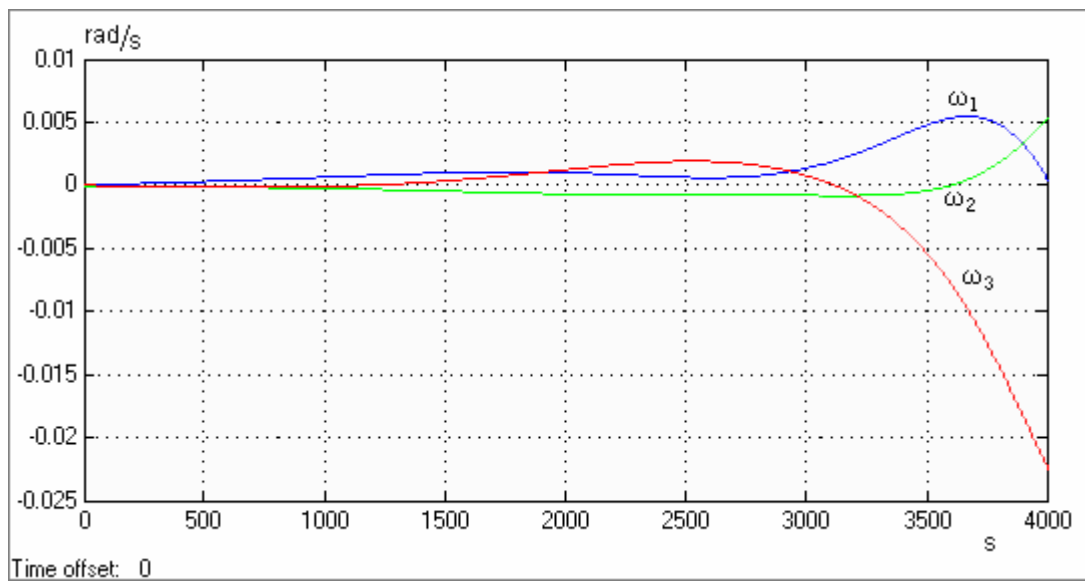


Figure A2.2 Time responses of angular velocities $\omega_1, \omega_2, \omega_3$ for small attitude errors of dynamic system.

A2.1.2 Large attitude angles simulations for rigid spacecraft

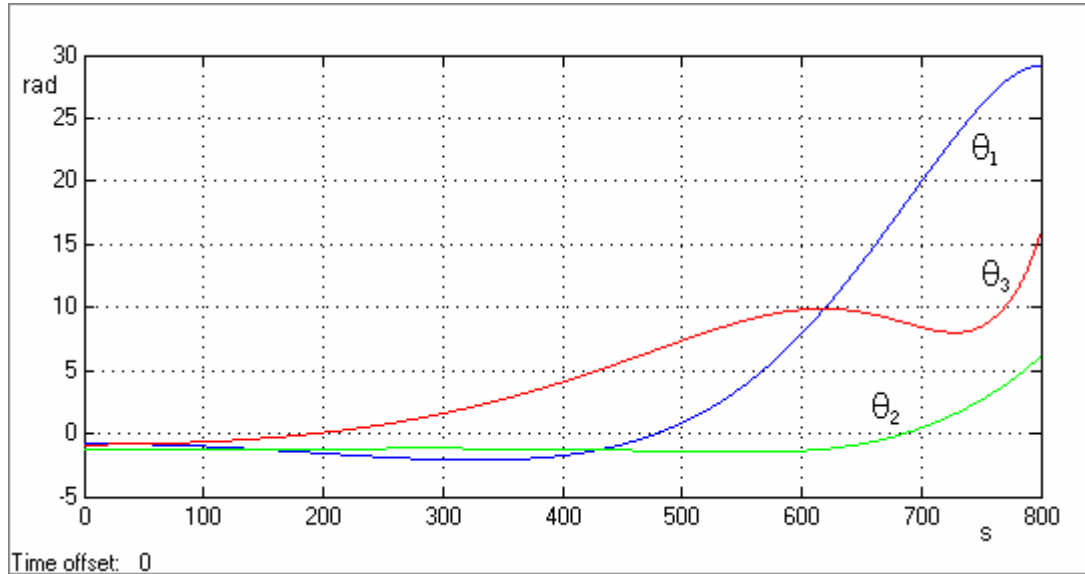


Figure A2.3. Time responses of large attitude errors $\theta_1, \theta_2, \theta_3$ of dynamic system.

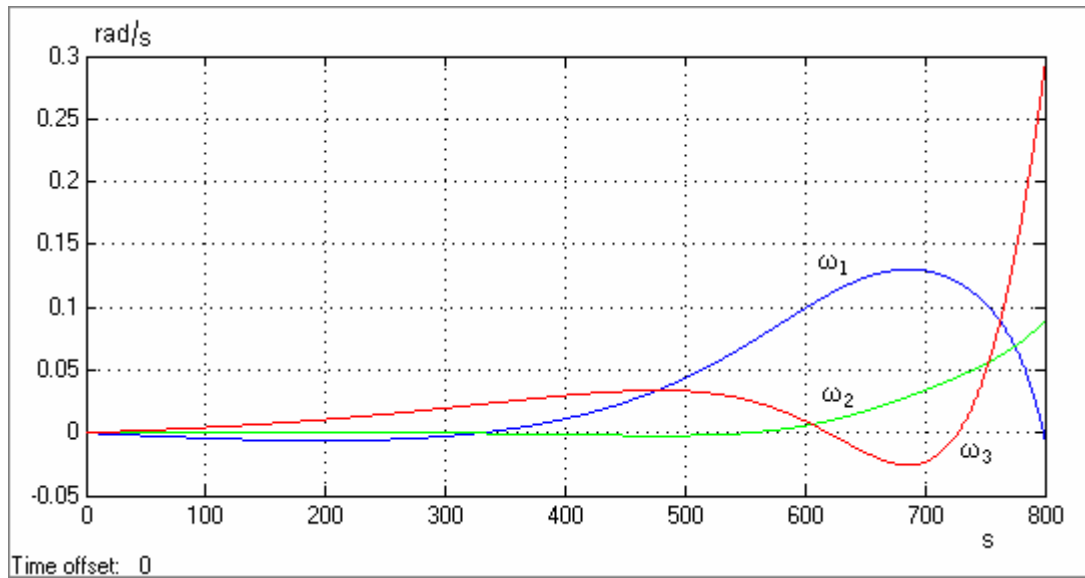


Figure A2.4 Time responses of angular velocities $\omega_1, \omega_2, \omega_3$ for large attitude errors of dynamic system.

A2.2 Linear Controllers with Pole Placement

A2.2.1 Small attitude angles simulations with passive linear controller for rigid spacecraft

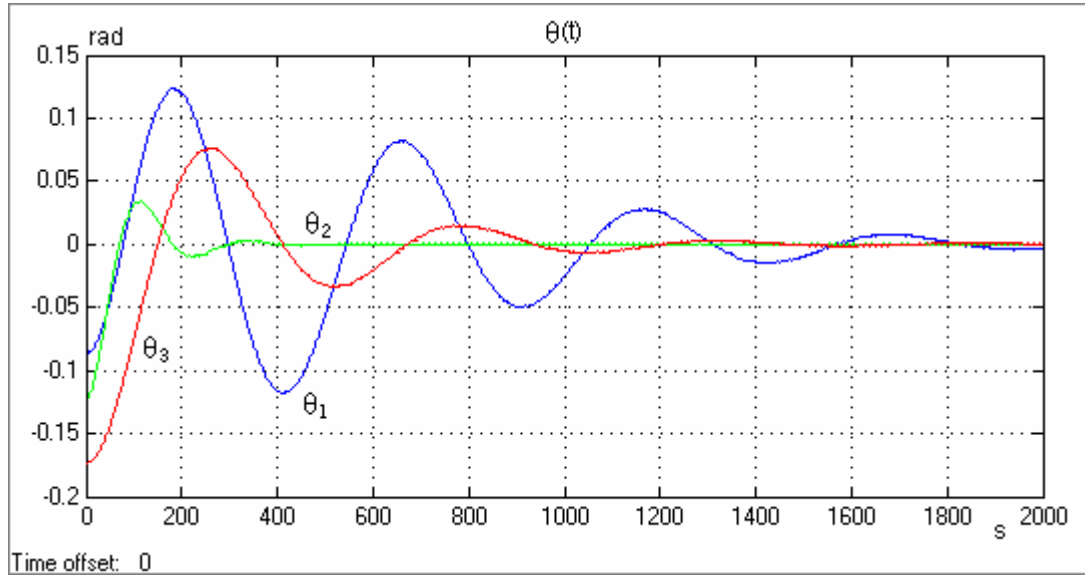


Figure A2.5 Time responses of attitude errors $\theta_1, \theta_2, \theta_3$ for small attitude angles orientation of passive linear controller.

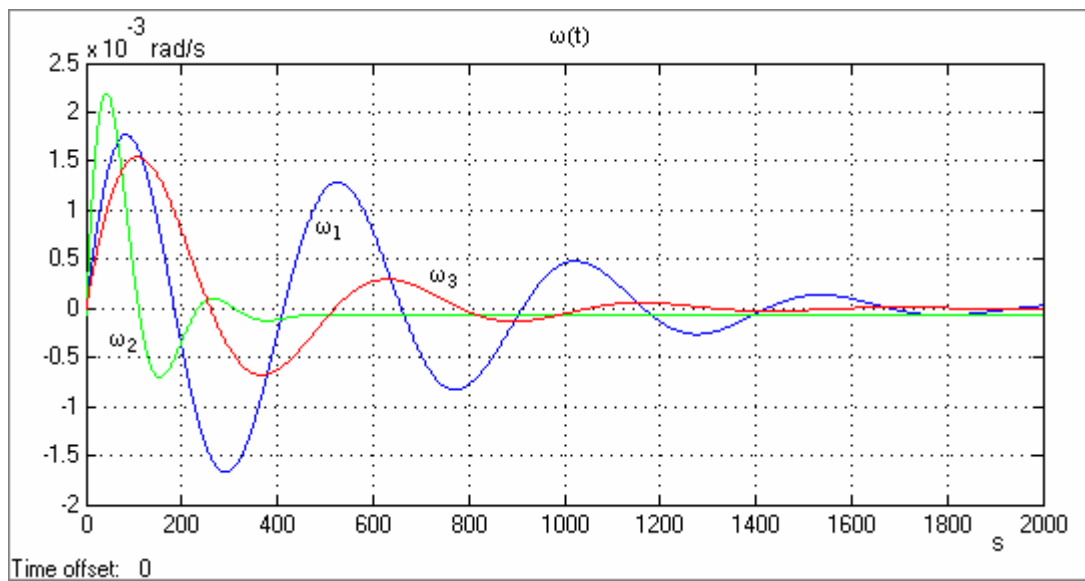


Figure A2.6 Time responses of angular velocities $\omega_1, \omega_2, \omega_3$ for small attitude angles orientation of passive linear controller.

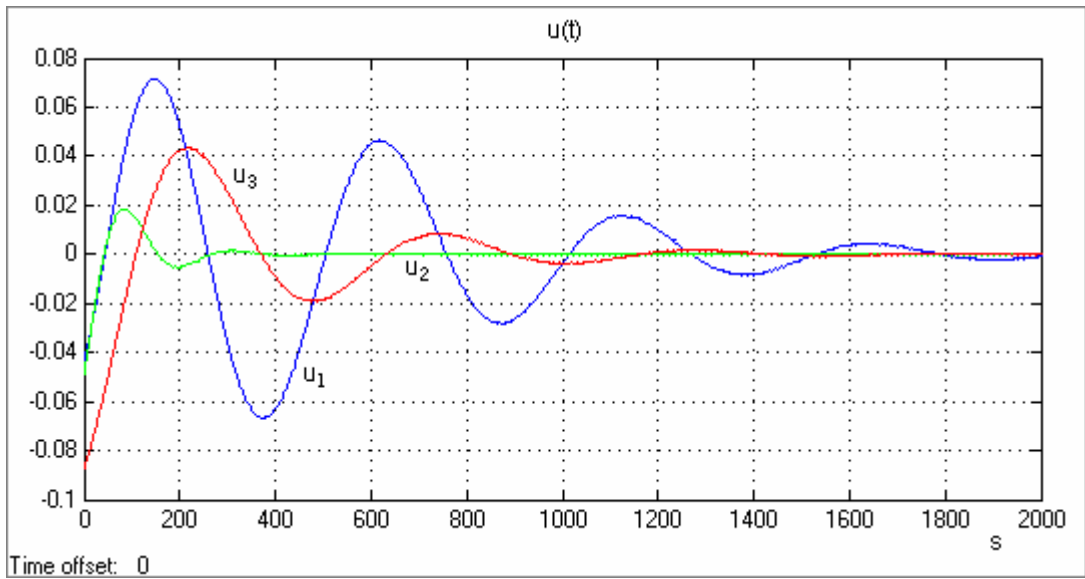


Figure A2.7 Time responses of control functions u_1, u_2, u_3 for small attitude angles orientation of passive linear controller.

A2.2.2 Small attitude angle simulations with combined linear controller for rigid spacecraft

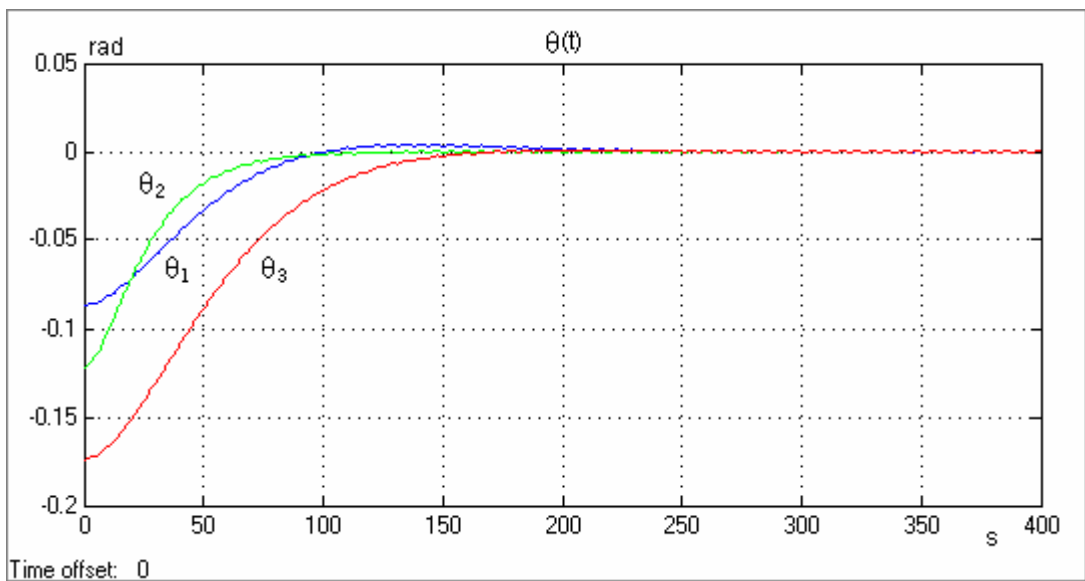


Figure A2.8 Time responses of attitude errors $\theta_1, \theta_2, \theta_3$ for small attitude angles orientation of combined linear controller.

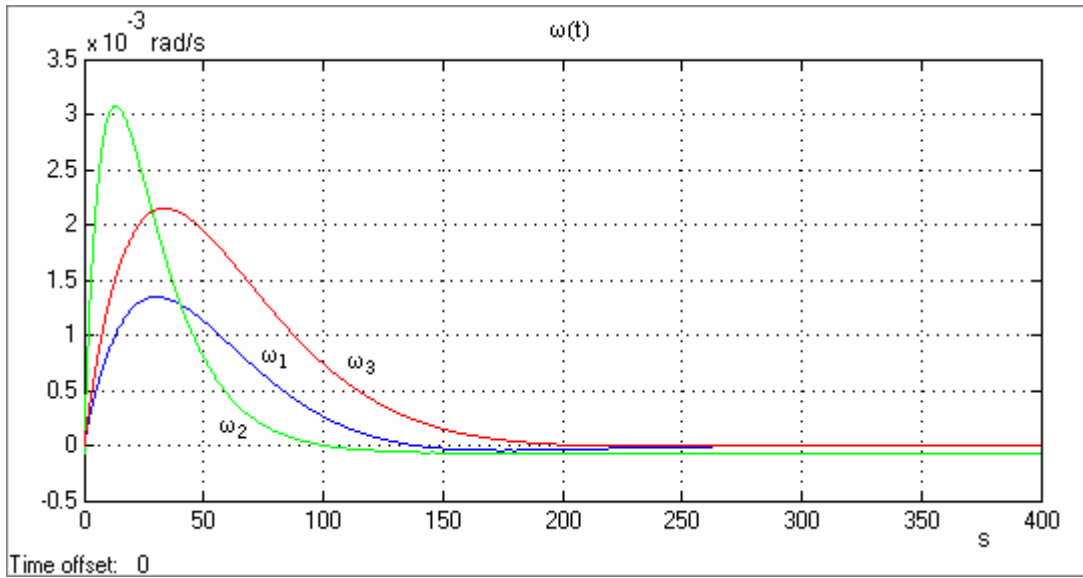


Figure A2.9 Time responses of angular velocities $\omega_1, \omega_2, \omega_3$ for small attitude angles orientation of combined linear controller.

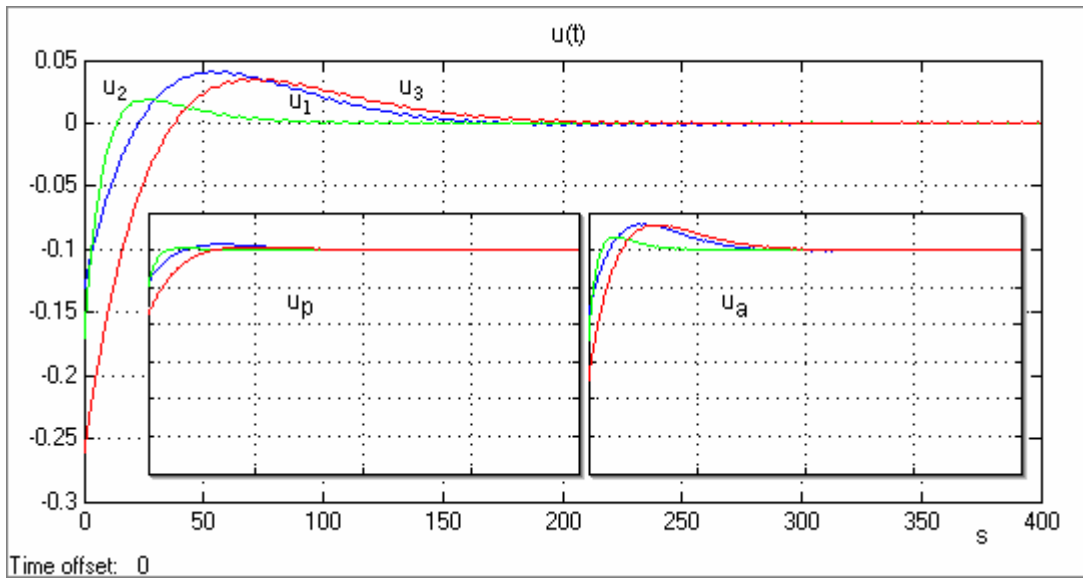


Figure A2.10 Time responses of control functions u_1, u_2, u_3 for small attitude angles orientation. Note that, two small inside-plots have same time scale and torque scale as $u(t)$. u_p and u_a plots represent the passive and active control functions, respectively, of combined linear controller.

A2.2.1 Large attitude angles simulations with passive linear controller for rigid spacecraft

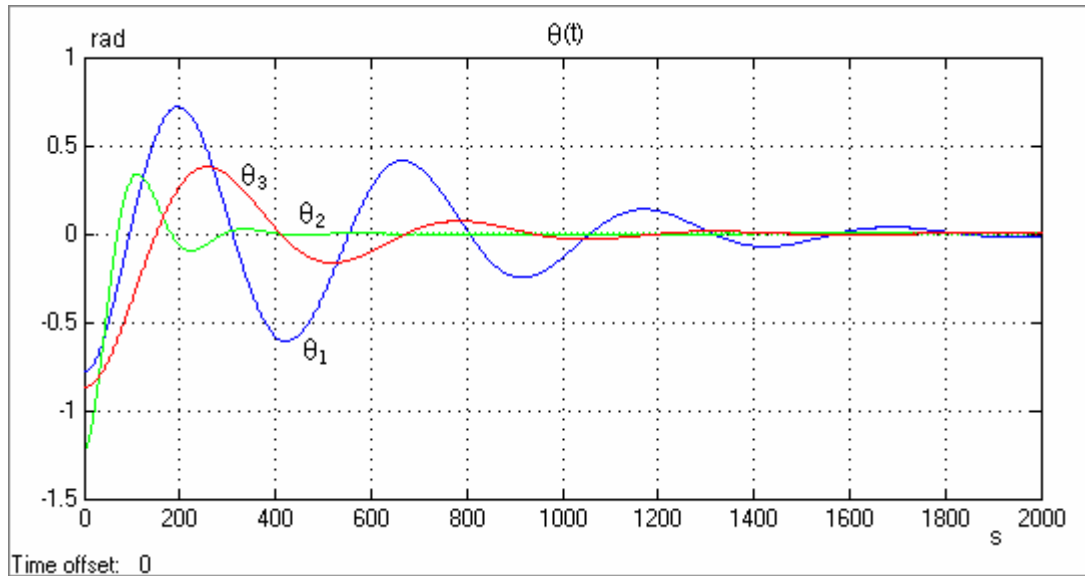


Figure A2.11 Time responses of attitude errors $\theta_1, \theta_2, \theta_3$ for large attitude angles orientation of passive linear controller.

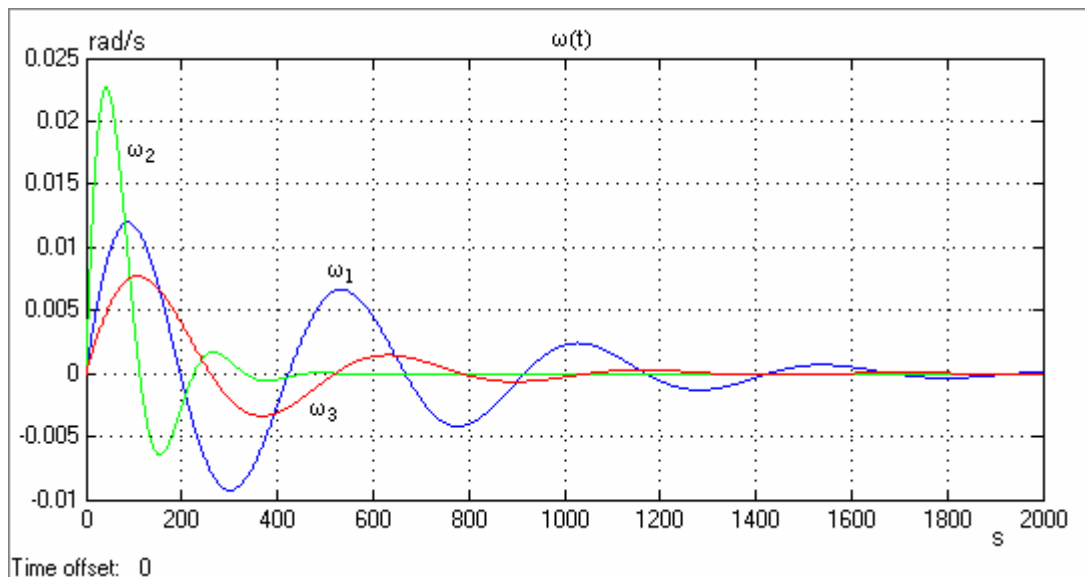


Figure A2.12 Time responses of angular velocities $\omega_1, \omega_2, \omega_3$ for large attitude angles orientation of passive linear controller.

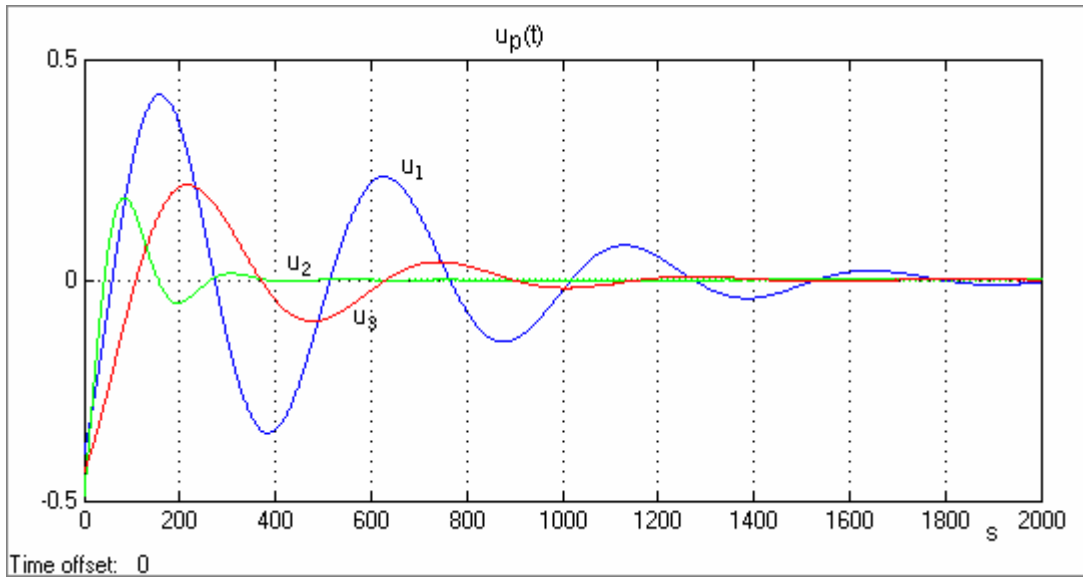


Figure A2.13 Time responses of control functions u_1, u_2, u_3 for large attitude angles orientation of passive linear controller.

A2.2.2 Large attitude angles simulations with combined linear controller for rigid spacecraft

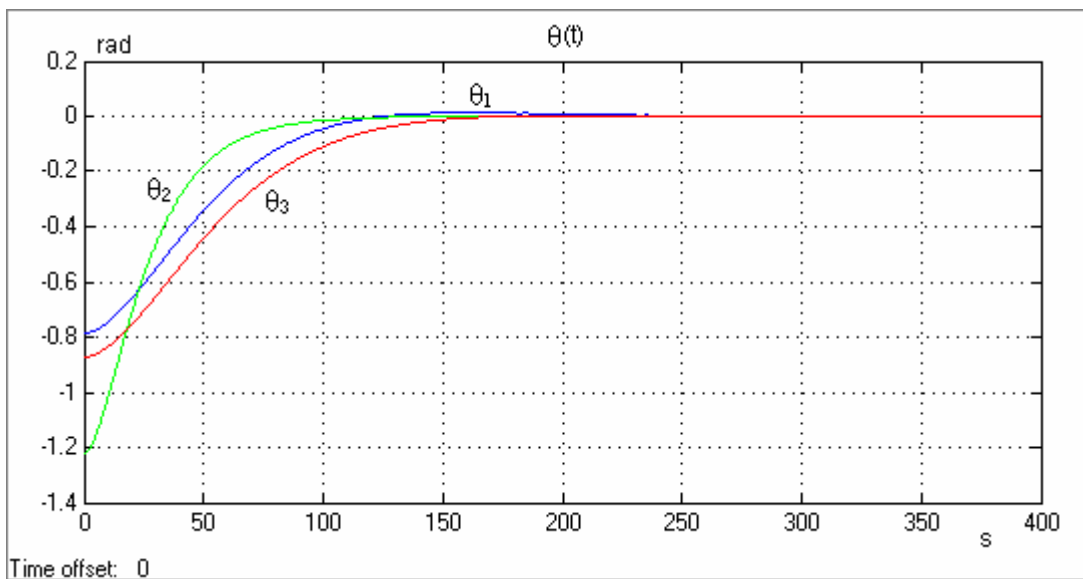


Figure A2.14 Time responses of attitude errors $\theta_1, \theta_2, \theta_3$ for large attitude angles orientation of combined linear controller.

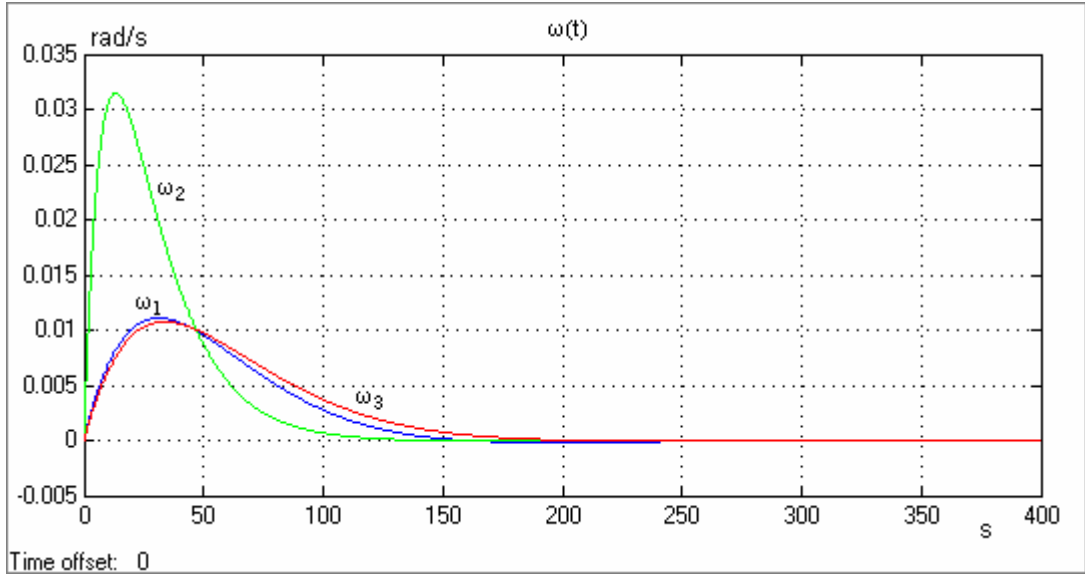


Figure A2.15 Time responses of angular velocities $\omega_1, \omega_2, \omega_3$ for large attitude angles orientation of combined linear controller.

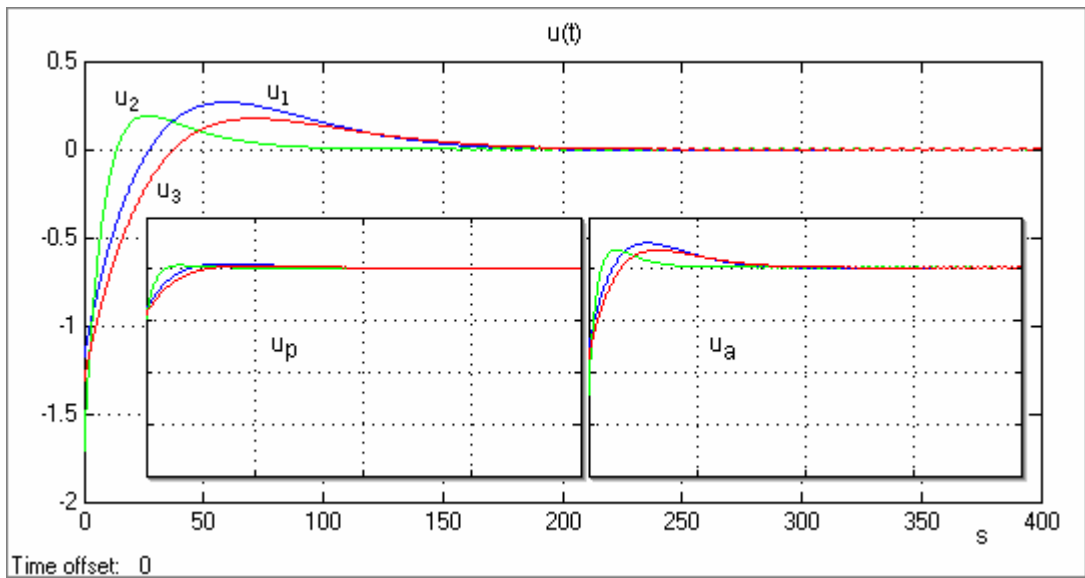


Figure A2.16 Time responses of combined control functions u_1, u_2, u_3 for large attitude angles orientation. Note that, two small inside-plots have same time scale and torque scale as $u(t)$. u_p and u_a plots represent the passive and active linear control functions, respectively, of combined linear controller.

A2.3 Sliding Mode Controllers

A2.3.1 Small attitude angles simulations with passive sliding mode controller for flexible spacecraft

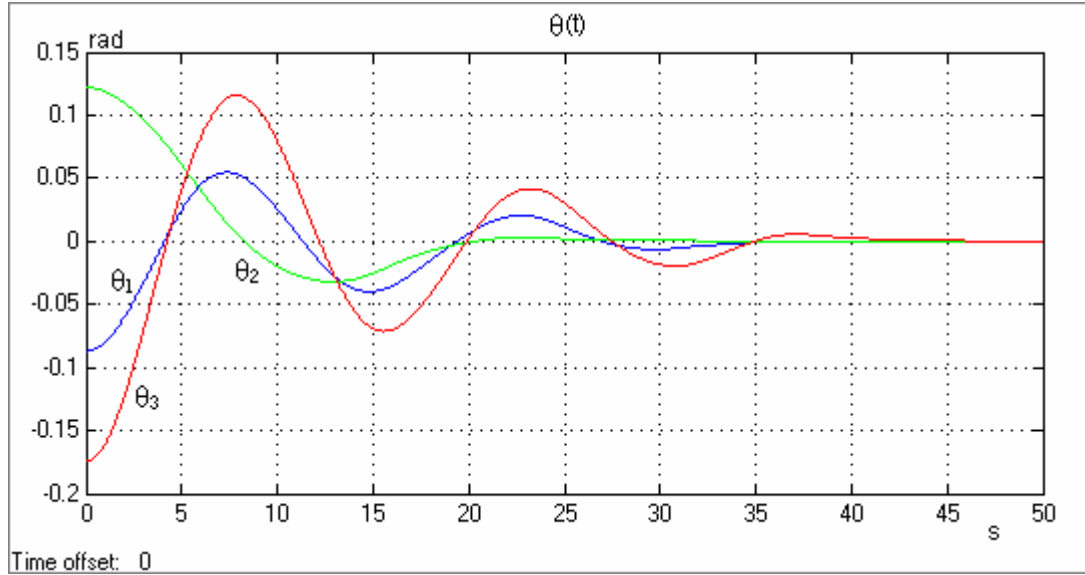


Figure A2.17 Time responses of attitude errors $\theta_1, \theta_2, \theta_3$ for small attitude angles orientation of passive sliding mode controller.

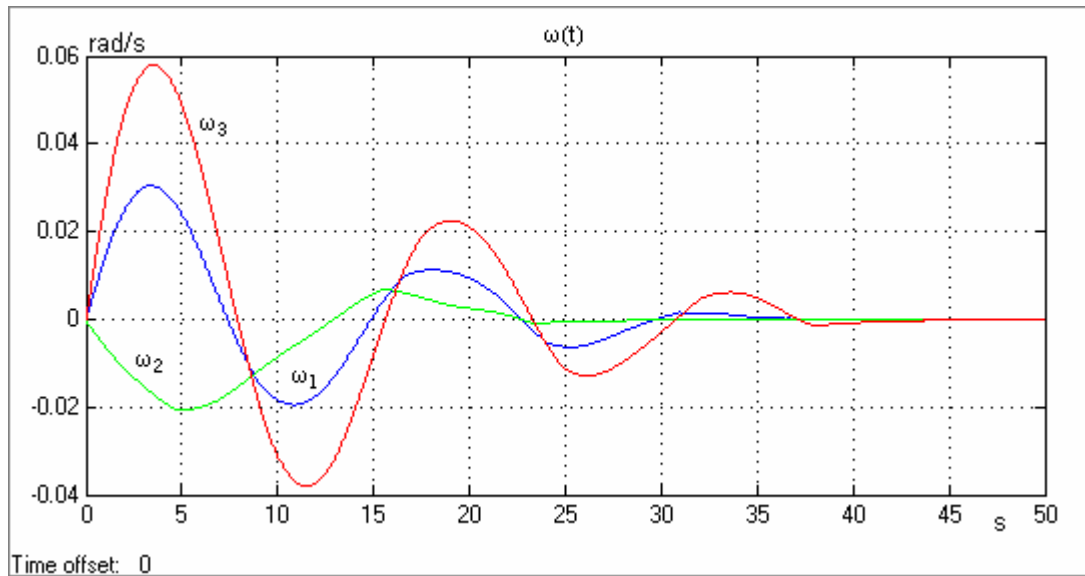


Figure A2.18 Time responses of angular velocities $\omega_1, \omega_2, \omega_3$ for small attitude angles orientation of passive sliding mode controller.

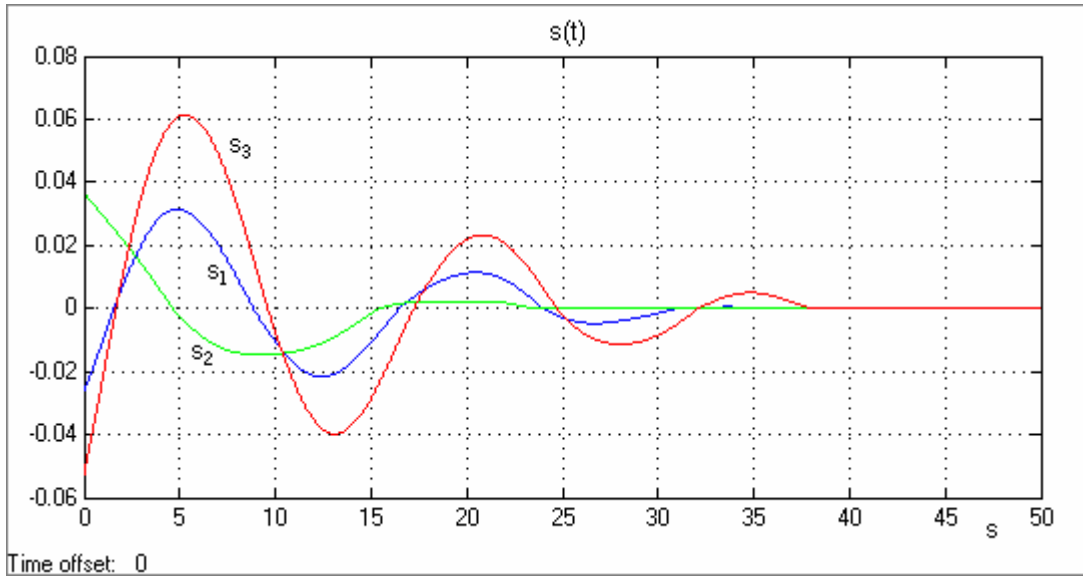


Figure A2.19 Time responses of sliding manifolds s_1, s_2, s_3 for small attitude angles orientation of passive sliding mode controller.

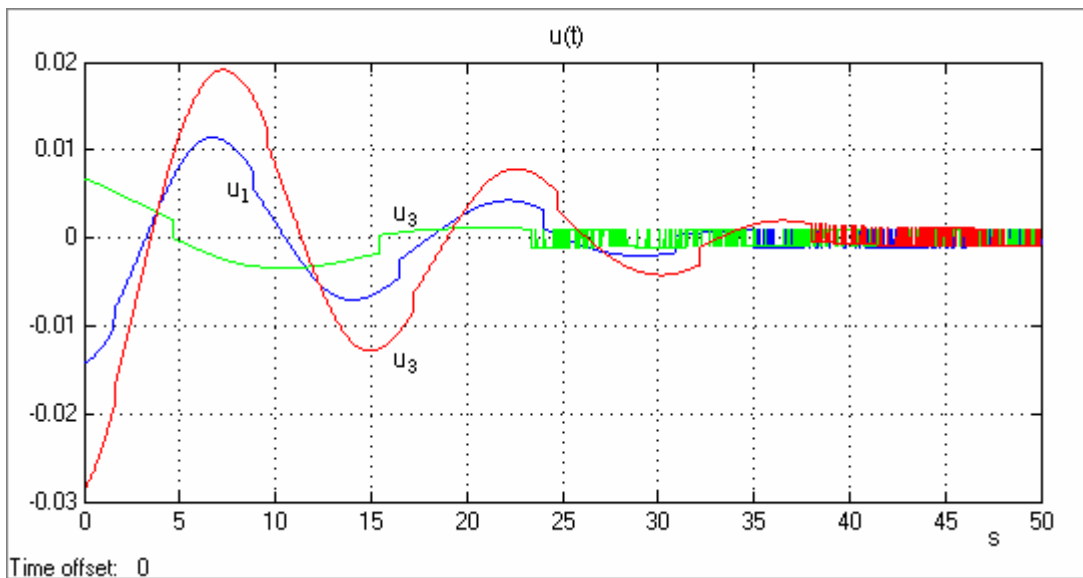


Figure A2.20 Time responses of control functions u_1, u_2, u_3 for small attitude angles orientation of passive sliding mode controller.

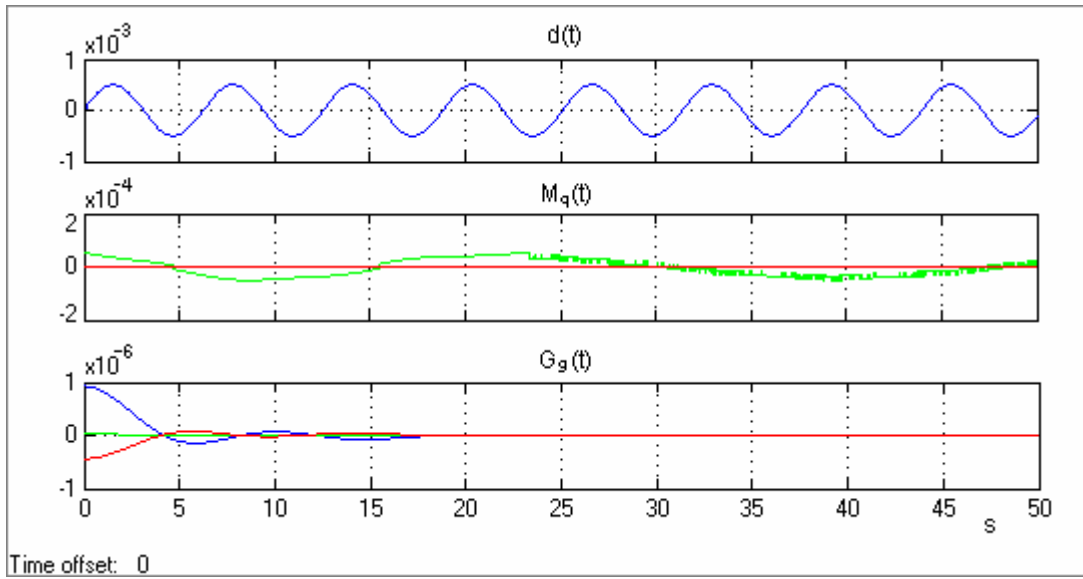


Figure A2.21 Three in one plot: gravity gradient $G_g(t)$, flexible membrane effects $M_q(t)$ and external disturbance effects such as sun pressure $d(t)$ for small attitude angles orientation for passive sliding mode controller.

A2.3.2 Small attitude angles simulations with combined sliding mode controller for flexible spacecraft

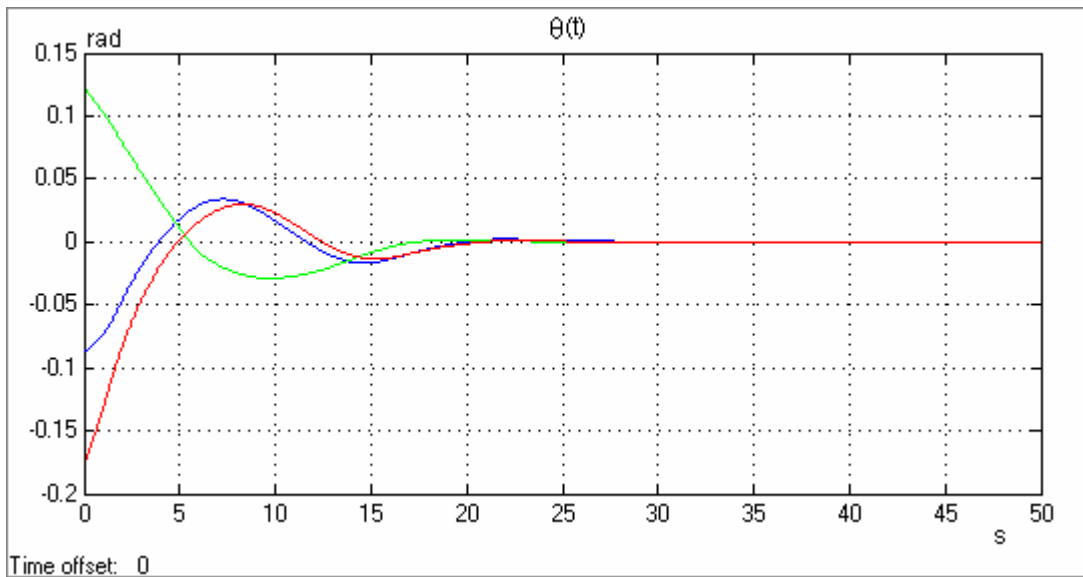


Figure A2.22 Time responses of attitude errors $\theta_1, \theta_2, \theta_3$ for small attitude angles orientation of combined sliding mode controller.

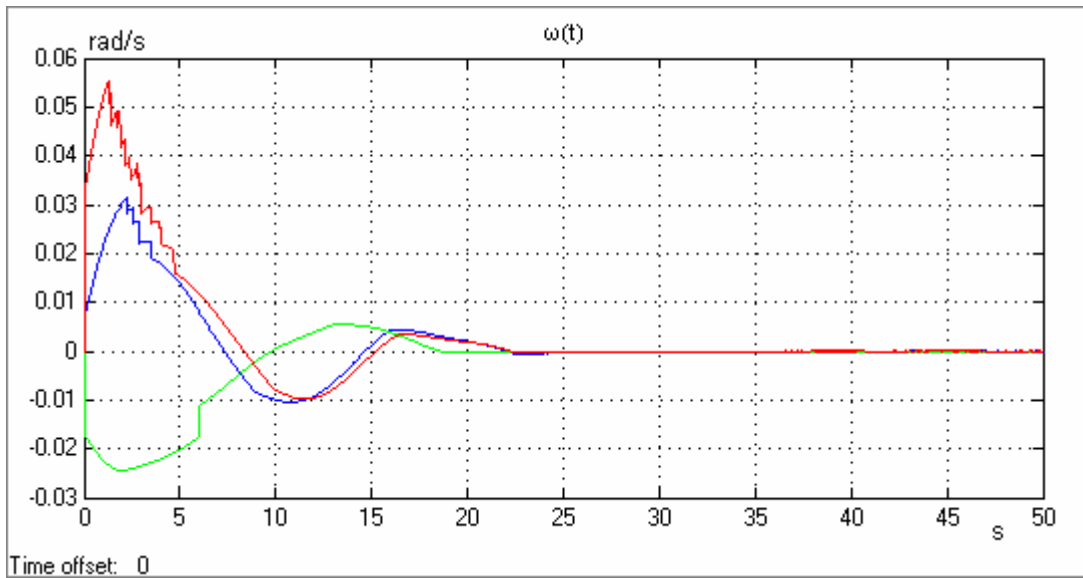


Figure A2.23 Time responses of angular velocities $\omega_1, \omega_2, \omega_3$ for small attitude angles orientation of combined sliding mode controller.

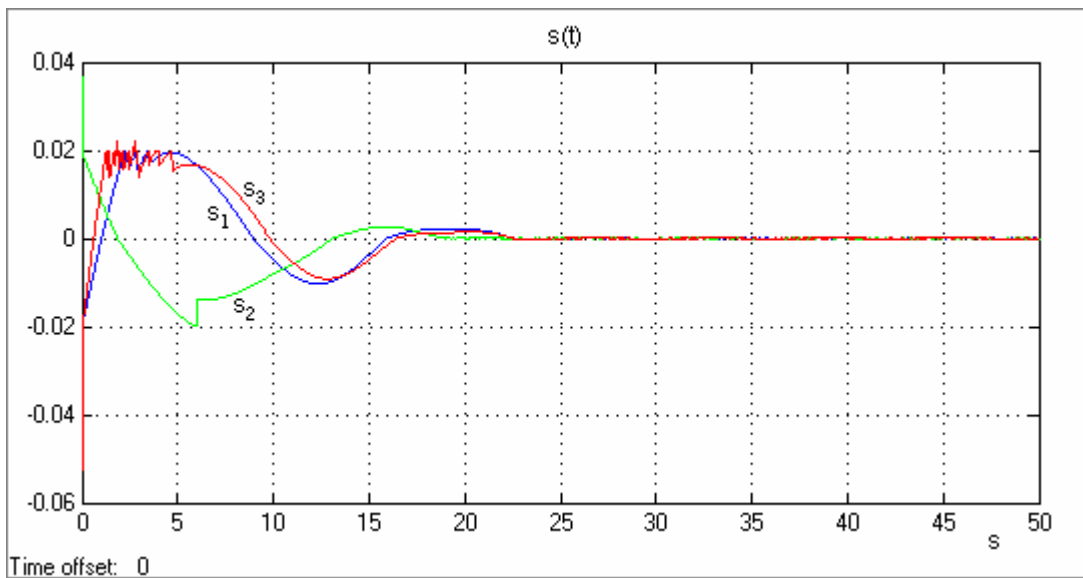


Figure A2.24 Time responses of sliding manifolds s_1, s_2, s_3 for small attitude angles orientation of combined sliding mode controller.

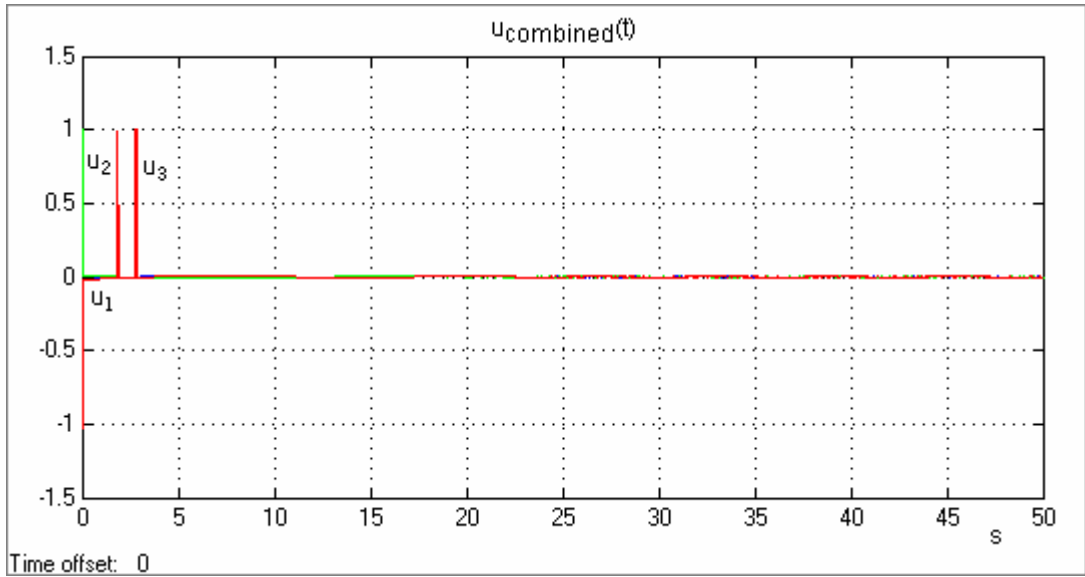


Figure A2.25 Time responses of combined control functions u_1, u_2, u_3 for small attitude angles orientation of combined sliding mode controller.

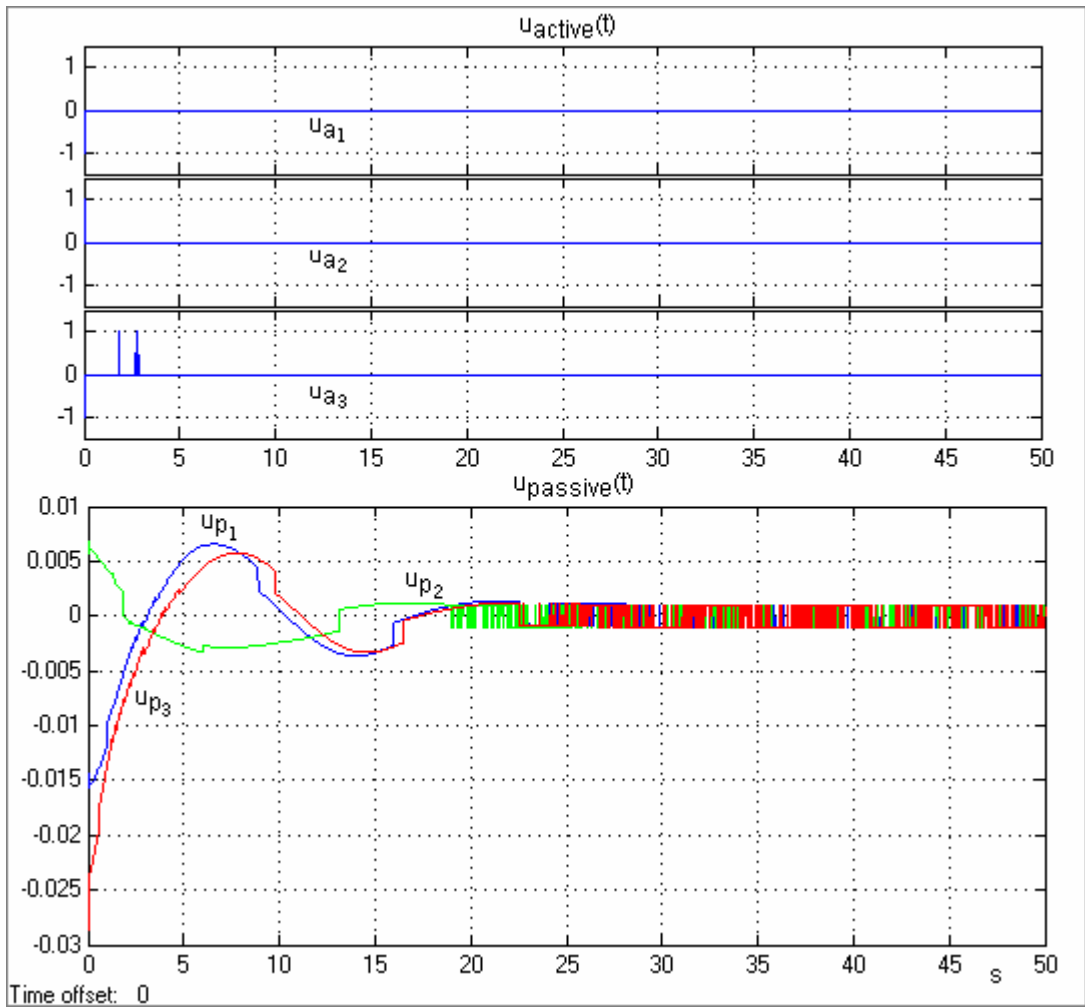


Figure A2.26 Time responses of active u_{1A}, u_{2A}, u_{3A} and passive u_{1P}, u_{2P}, u_{3P} control functions of combined sliding mode controller.

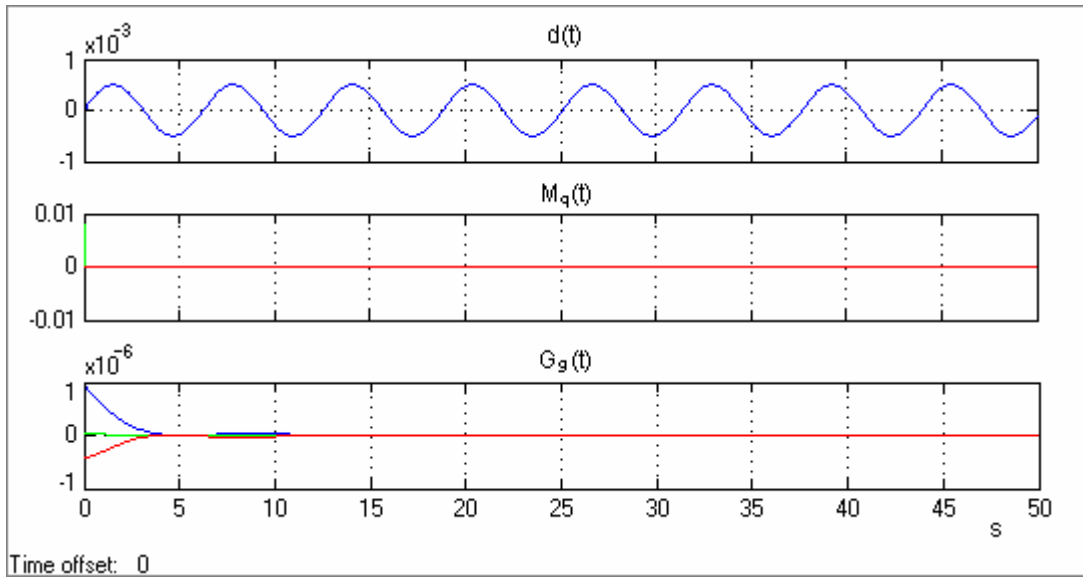


Figure A2.27 Three in one plot: gravity gradient $G_g(t)$, flexible membrane effects $M_q(t)$ and external disturbance effects such as sun pressure $d(t)$ for small attitude angles orientation for combined sliding mode controller.

A2.3.3 Large attitude angles simulations with passive sliding mode controller for flexible spacecraft

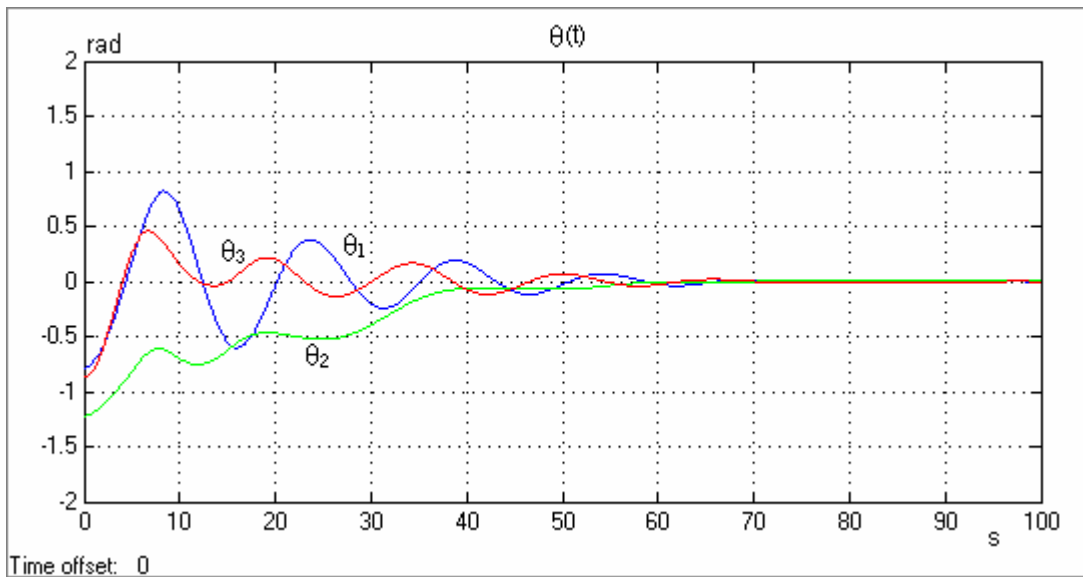


Figure A2.28 Time responses of attitude errors $\theta_1, \theta_2, \theta_3$ for large attitude angles orientation of passive sliding mode controller.

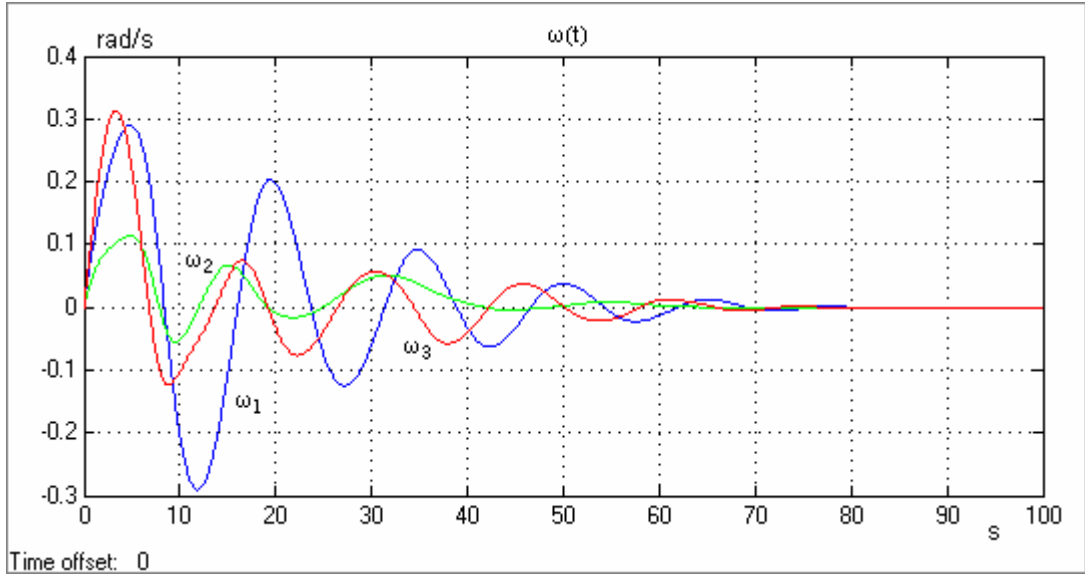


Figure A2.29 Time responses of angular velocities $\omega_1, \omega_2, \omega_3$ for large attitude angles orientation of passive sliding mode controller.

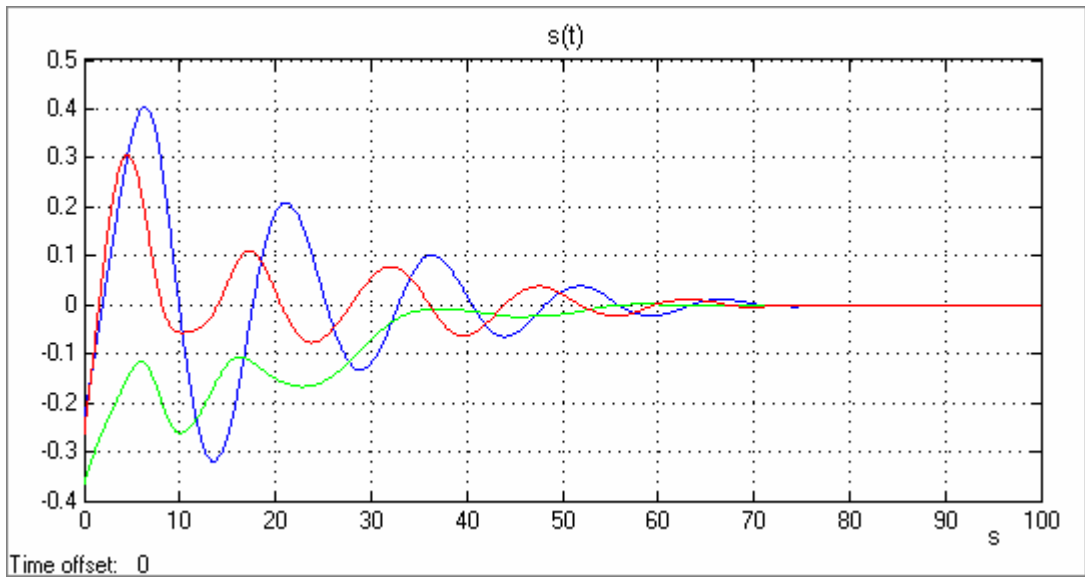


Figure A2.30 Time responses of sliding manifolds s_1, s_2, s_3 for large attitude angles orientation of passive sliding mode controller.

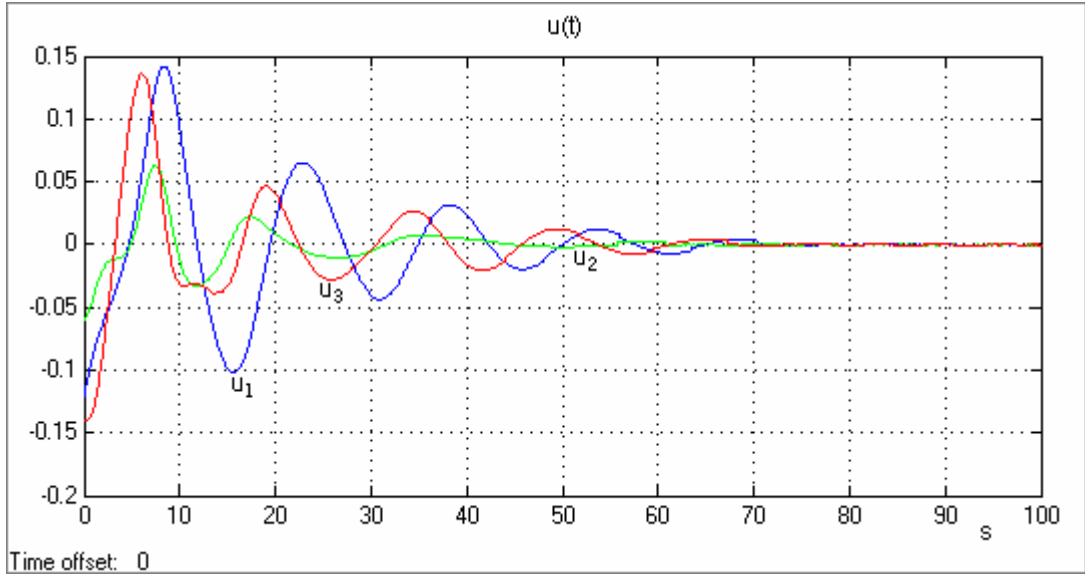


Figure A2.31 Time responses of control functions u_1, u_2, u_3 for large attitude angles orientation of passive sliding mode controller.

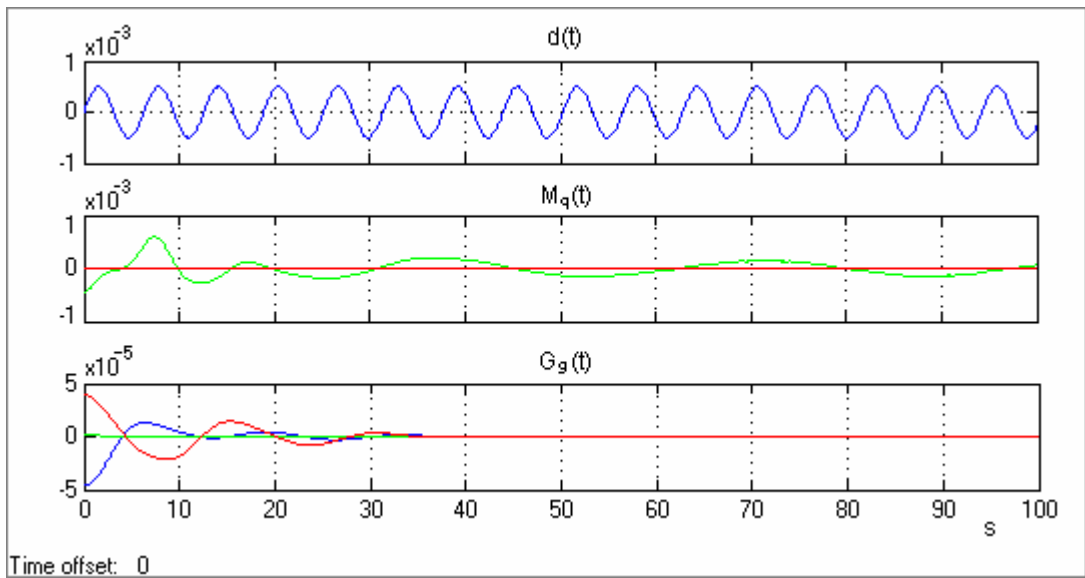


Figure A2.32 Three in one plot: gravity-gradient $G_g(t)$, flexible membrane effects $M_q(t)$ and external disturbance effects such as sun pressure $d(t)$ for large attitude angles orientation for passive sliding mode controller.

A2.3.4 Large attitude angle simulations with combined sliding mode controller for flexible spacecraft

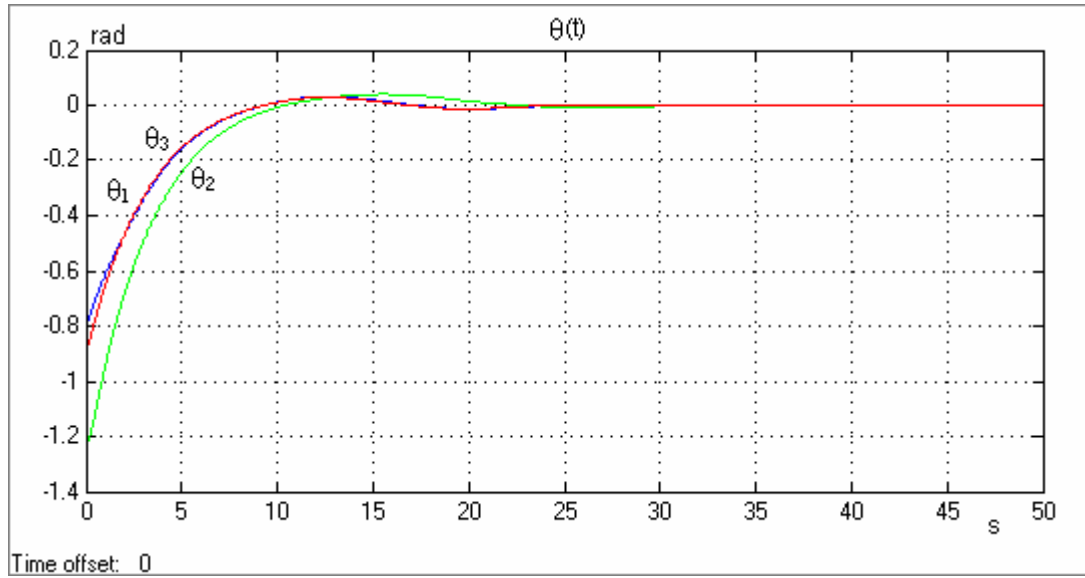


Figure A2.33 Time responses of attitude errors $\theta_1, \theta_2, \theta_3$ for large attitude angles orientation of combined sliding mode controller.

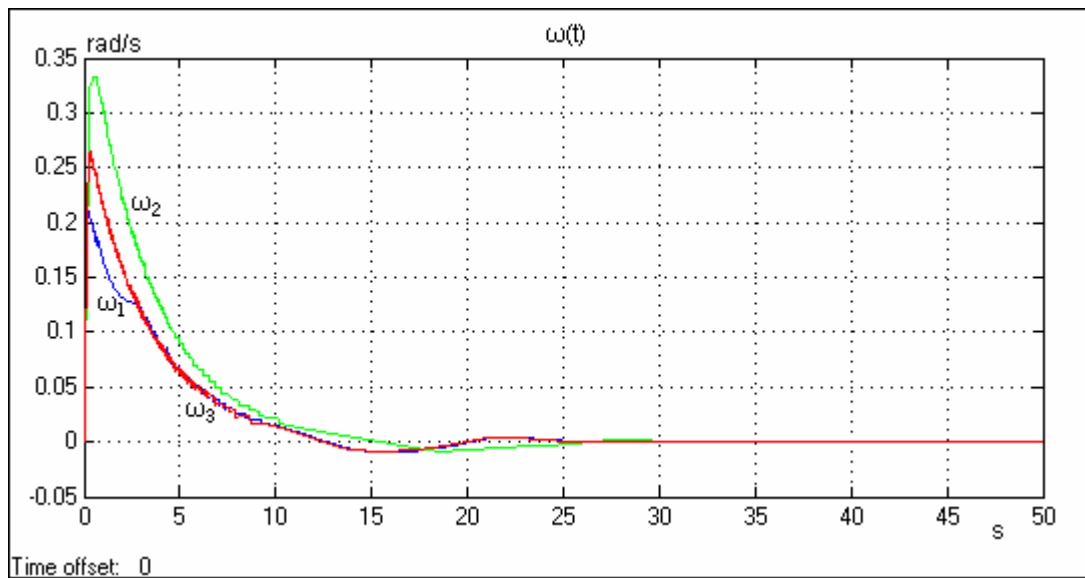


Figure A2.34 Time responses of angular velocities $\omega_1, \omega_2, \omega_3$ for large attitude angles orientation of combined sliding mode controller.

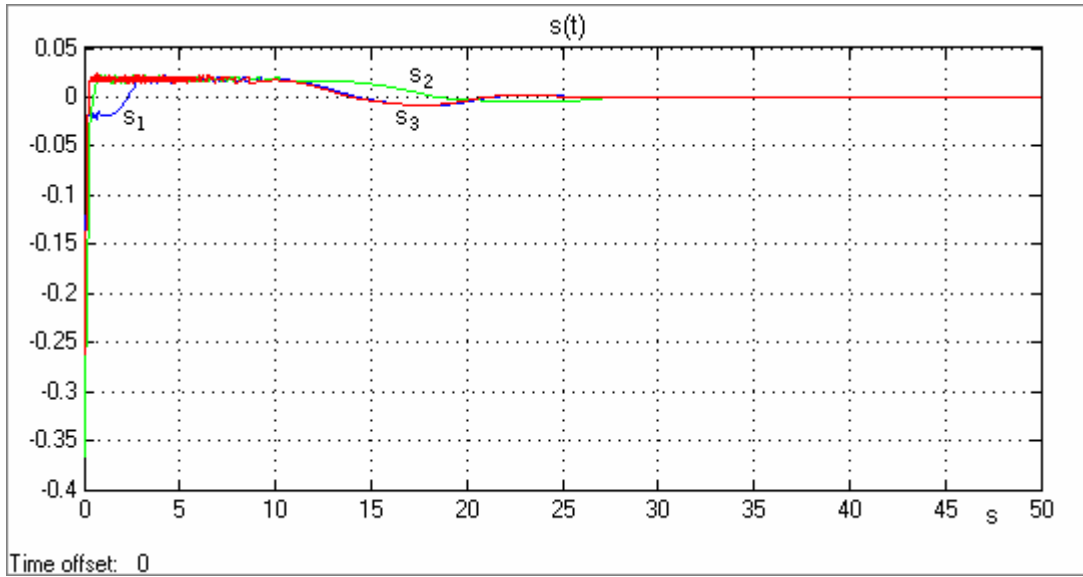


Figure A2.35 Time responses of sliding manifolds s_1, s_2, s_3 for large attitude angles orientation of combined sliding mode controller.

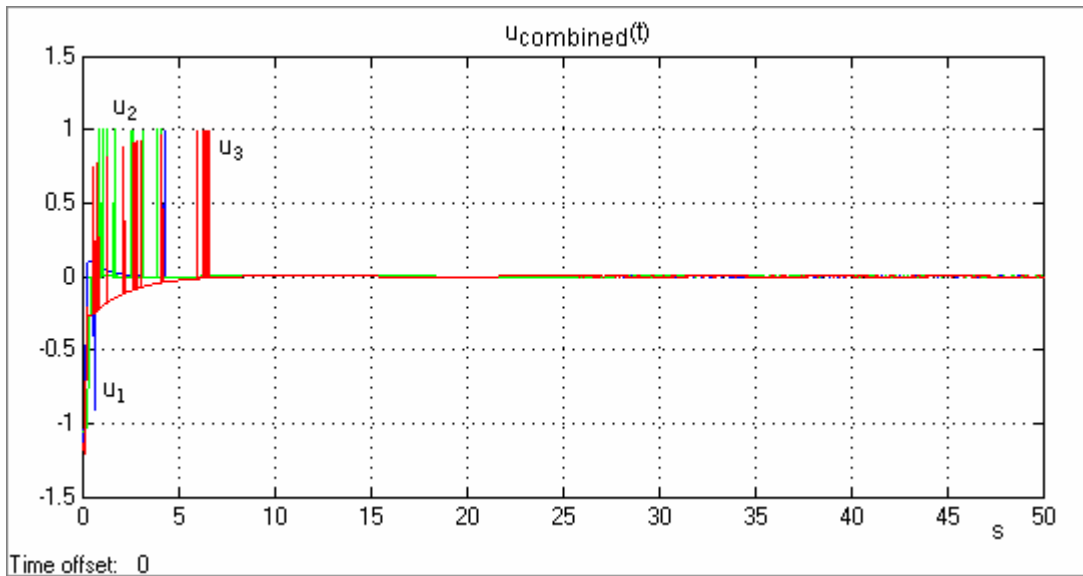


Figure A2.36 Time responses of combined control functions u_1, u_2, u_3 for large attitude angles orientation of combined sliding mode controller.

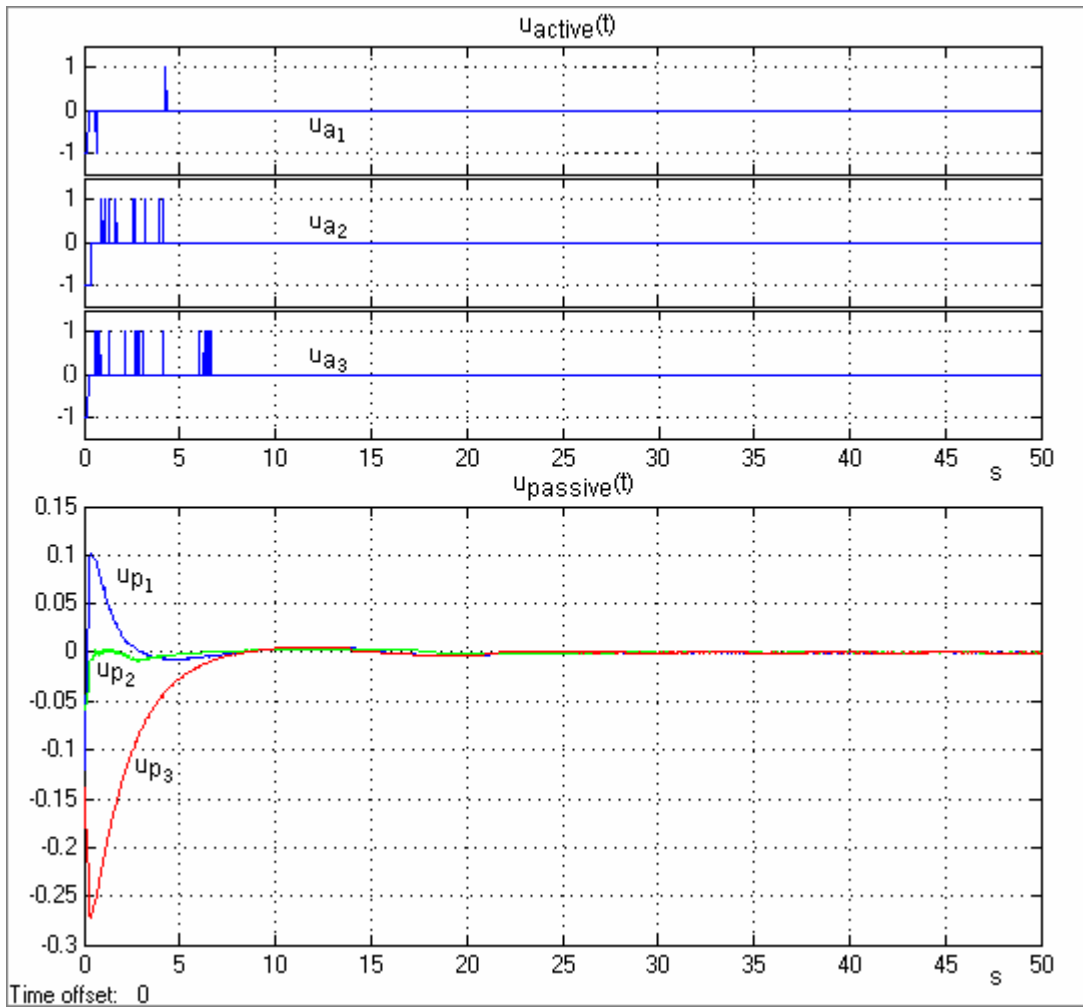


Figure A2.37 Time responses of active u_{1A}, u_{2A}, u_{3A} and passive u_{1P}, u_{2P}, u_{3P} control functions of combined sliding mode controller.

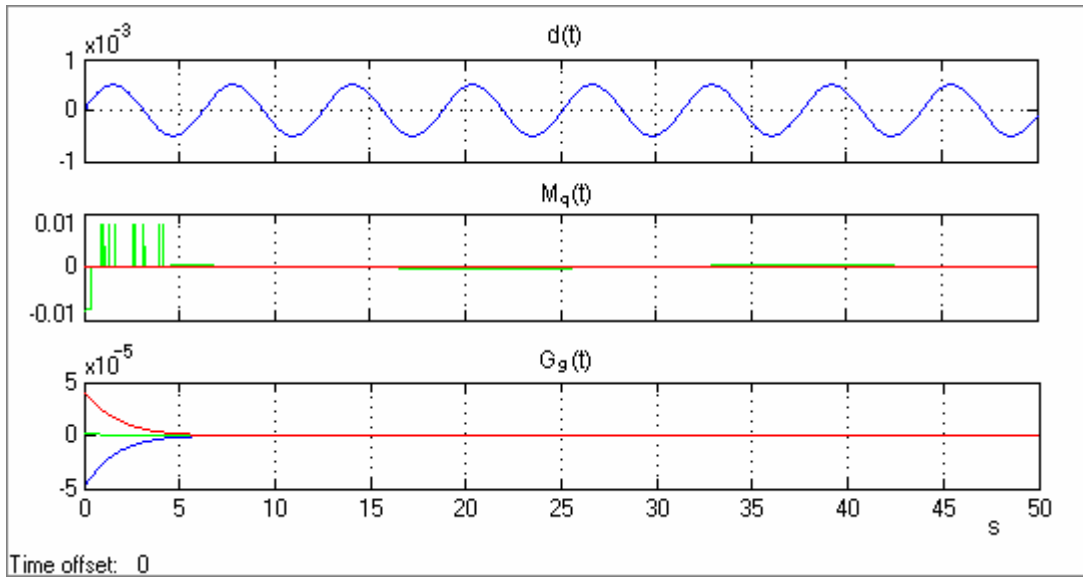


Figure A2.38 Three in one plot: gravity-gradient $G_g(t)$, flexible membrane effects $M_q(t)$ and external disturbance effects such as sun pressure $d(t)$ for large attitude angles orientation for combined sliding mode controller.

A2.3.5 Dynamic equation of sliding mode for small attitude angles

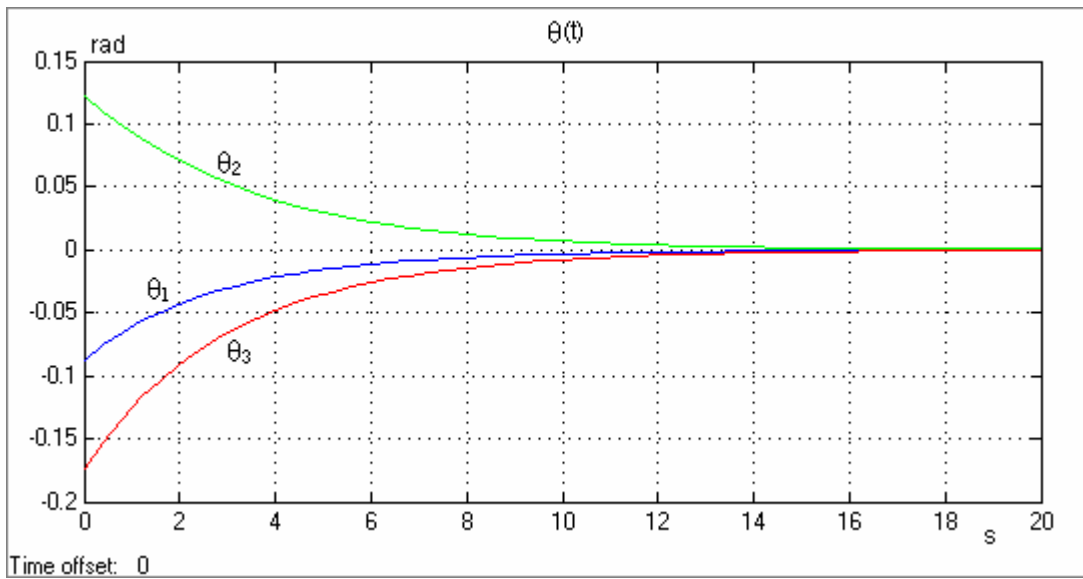


Figure A2.39 Time responses of dynamic Equation (4.9) for small attitude angles orientation.

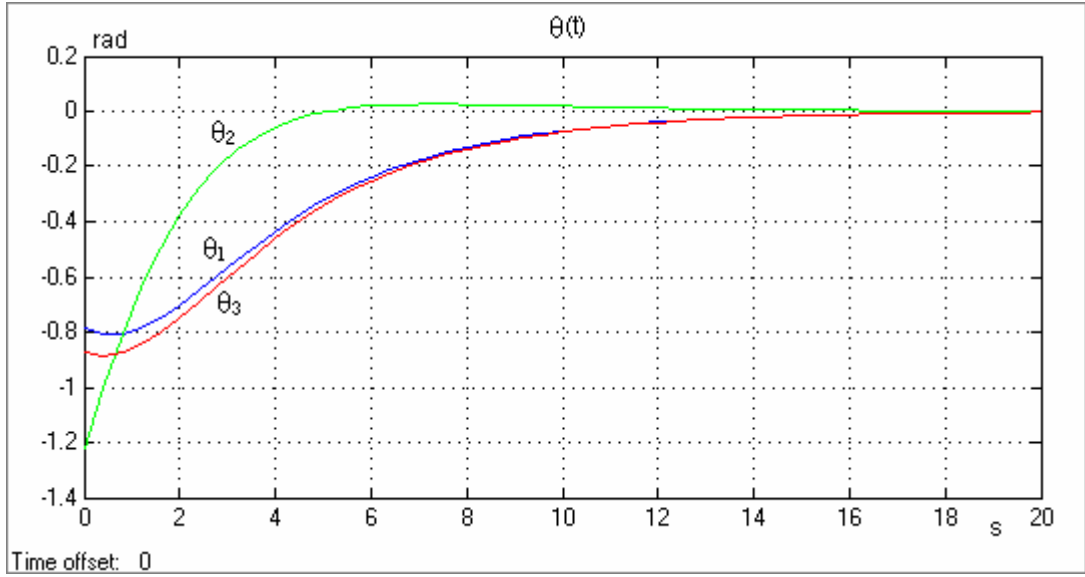


Figure A2.40 Time responses of dynamic Equation (4.9) for large attitude angles orientation.

Appendix 3. Source Codes for Matlab-Simulink Block Diagrams

A3.1 Dynamic System Initialization

The source code below is required for ‘dynamics.mdl’ Matlab-Simulink block diagram file in Appendix 1.1.

```
dynamic_system_ini.m

clear;
clc;

% spacecraft initialization
I11 = 3026; % kg.m2
I22 = 440; % kg.m2
I33 = 3164; % kg.m2
I21 = 0;
I12 = 0;
I13 = 0;
I31 = 0;
I23 = 0;
I32 = 0;
I = [I11 I12 I13; I21 I22 I23; I31 I32 I33];
k1 = (I22-I33)/I11;
k2 = (I11-I33)/I22;
k3 = (I11-I22)/I33;
n = (2*pi)/(23*3600 + 56*60 + 4.09054); % Real Day
H_0 = 0; % N.m.s
w_a = eye(3);
w_b = [0 0 -n; 0 0 0; n 0 0];
w_c = [0; -n; 0];

%flexibility
s_x2= 1.112^2; % rad/s
s_y2= 5.534^2; % rad/s
s_z2= 0.885^2; % rad/s
d_x = 35.865; % Vkg.m2
d_y = 2.532; % Vkg.m2
d_z = 35.372; % Vkg.m2
sq = sqrt(2);
Sig2= [1/s_x2 0 0; 0 1/s_y2 0; 0 0 1/s_z2];
Del = [1/(sq*d_x) 0 0; 0 1/(sq*d_y) 0; 0 0 1/(sq*d_z)];

% Initial attitude errors...
d1 = -5*(pi/180); % deg => rad
d2 = 7*(pi/180); % deg => rad
d3 = -10*(pi/180); % deg => rad
```

A3.2 Linear Controllers and System Initialization

The source code below is required for ‘linear.mdl’ Matlab-Simulink block diagram file in Appendix 1.2.

```
linear_control_ini.m

clear;
clc;

% spacecraft initialization
I11 = 3026;
I22 = 440;
I33 = 3164;
I21 = 0;
I12 = 0;
I13 = 0;
I31 = 0;
I23 = 0;
```

```

I32 = 0;
I = [I11 I12 I13; I21 I22 I23; I31 I32 I33];
k1 = (I22-I33)/I11;
k2 = (I11-I33)/I22;
k3 = (I11-I22)/I33;
d1 = 2.5;
d2 = 2;
d3 = 2.5;
H_0 = 0;
n = (2*pi)/(23*3600 + 56*60 + 4.09054); % Real Day

% Linear Model and Pole Placement
A = [0 1 0 0 0 0; -4*n^2*k1-(n*H_0)/I11 0 0 0 -n*(1-k1)+(H_0/I11) 0;
      0 0 0 1 0 0; 0 0 -3*n^2*k2 0 0 0;
      0 0 0 0 0 1; 0 -n*(k3+1)+(H_0/I33) 0 0 -n^2*k3-(n*H_0)/I33 0];
Ba = [0 0 0; d1/I11 0 0; 0 0 0; 0 d2/I22 0; 0 0 0; 0 0 d3/I33];
Bp = [0 0 0; 1/I11 0 0; 0 0 0; 0 1/I22 0; 0 0 0; 0 0 1/I33];
C = [1 0 0 0 0 0; 0 0 1 0 0 0; 0 0 0 0 1 0];
gTa = [1 60 0 0 0 0; 0 0 1 30 0 0; 0 0 0 0 1 60];
gTp = [.1 20 0 0 0 0; 0 0 .1 10 0 0; 0 0 0 0 .1 20];

% Disturbance and attitude errors
Dt = [1 0 1 0 1 0]';
d = [-45*pi/180; 0; -70*pi/180; 0; -50*pi/180; 0];

```

A3.3 Some Linear Controllers Functions

A3.3.1 Stability check of pole placed linear systems

The source code below computes the eigenvalues of the linearized system, and active, passive and combined linear controllers, respectively.

linear_stability.m

```

% stability check for pole placed system
lamdaA = eig(A)
lamda_a = eig(A-Bp*gTp)
lamda_p = eig(A-Ba*gTa)
lamda_c = eig(A-Ba*gTa-Bp*gTp)

```

A3.4 Sliding Mode Controllers and System Initialization

The source code below is required for 'sliding_mode.mdl' Matlab-Simulink block diagram file in Appendix 1.3.

sliding_mode_ini.m

```

clear;
clc;

% spacecraft initialization
I11 = 3026;
I22 = 440;
I33 = 3164;
I21 = 0;
I12 = 0;
I13 = 0;
I31 = 0;
I23 = 0;
I32 = 0;
I = [I11 I12 I13; I21 I22 I23; I31 I32 I33];
k1 = (I22-I33)/I11;
k2 = (I11-I33)/I22;
k3 = (I11-I22)/I33;
n = (2*pi)/(23*3600 + 56*60 + 4.09054); % Real Day
H_0 = 0.02*sqrt(I11*I33); % N.m.s - Lamda = 0.02 nutation frequency, rad/s

```

```

% flexibility
s_x2= 1.112^2;
s_y2= 5.534^2;
s_z2= 0.885^2;
d_x = 35.865;
d_y = 2.532;
d_z = 35.372;
sq = sqrt(2);
Sig2= [1/s_x2 0 0; 0 1/s_y2 0; 0 0 1/s_z2];
Del = [1/(sq*d_x) 0 0; 0 1/(sq*d_y) 0; 0 0 1/(sq*d_z)];

% Main system
S_a = [0 0 -n*(1-k1)+(H_0/I11); 0 0 0; -n*(k3+1)+(H_0/I33) 0 0];
S_b = [-4*n^2*k1-(n*H_0)/I11 0 0; 0 -3*n^2*k2 0; 0 0 -n^2*k3-(n*H_0)/I33];
w_a = eye(3);
w_b = [0 0 -n; 0 0 0; n 0 0];
w_c = [0; -n; 0];
gg1 = [0 0 0; 0 0 -1; 0 1 0];
gg2 = [0 0 1; 0 0 0; -1 0 0];
gg3 = [0 -1 0; 1 0 0; 0 0 0];
dwdt_a = eye(3);
dwdt_b = [0 0 -n; 0 0 0; n 0 0];

% Reaction wheel system
R_a = [-1/I11 0 0; 0 -1/I22 0; 0 0 -1/I33];
R_b = [0 0 n/I11; 0 n/I22 0; -n/I33 0 0];

% Kontrol => sari 1, pembe 2, mavi 3;
K_1 = [.01 0 0; 0 .01 0; 0 0 .01]; % RW
K_0 = [.1 0 0; 0 .1 0; 0 0 .1]; % RW
K_T = [1 0 0; 0 1 0; 0 0 1]; % THRS

% sliding manifold design...
k = 0.3;
L = [k 0 0; 0 k 0; 0 0 k]; % theta component
L1 = [1 0 0; 0 1 0; 0 0 1]; % w component

% Initial attitude errors -> *** large angle
d1 = -45*(pi/180); % deg => rad
d2 = -70*(pi/180); % deg => rad
d3 = -50*(pi/180); % deg => rad

```

The source code below is required for ‘sliding_manifold.mdl’ Matlab-Simulink block diagram file in Appendix 1.3.

Sliding_manifold_ini.m

```

% DYNAMICS' VALUES
k = 0.3;
n = (2*pi)/(23*3600 + 56*60 + 4.09054); % Real Day
eff_1 = [0 0 0; 0 0 0; 0 0 n];
eff_2 = [0 0 0; 0 0 0; 0 0 1];
eff_3 = [0 1 0; -1 0 0; 0 0 0];

% Initial attitude errors -> * small angle
theta_e1 = -5*pi/180; % deg => rad
theta_e2 = 7*pi/180; % deg => rad
theta_e3 = -10*pi/180; % deg => rad

```

A3.5 Some Sliding Mode Controllers Functions

A3.5.1 Selection of sliding boundary layer

Note that, ‘sliding_mode_ini.m’ file has to be executed before the source code below run.

`sliding_boundary.m`

```
% selecting max s0
w_ini = abs([0; 0; 0]);
theta_ini = abs([d1; d2; d3]);
N1 = K_T(1,1);
N2 = K_T(2,2);
N3 = K_T(3,3);
N = [N1; N2; N3]; % always positive number
s_initial = w_ini + k*theta_ini;
s_0max = N.*(s_initial)
```

A3.5.2 Calculating parameter ℓ

The source code below calculates vector ℓ in Section 4.1

`sliding_man_l.m`

```
% selecting l
l = 0.5*[-1 1 -1; -1 1 1; 1 1 1]*[k; k; k]
```

Appendix 4. Sensors and Control Elements

A4.1 Sensors

A4.1.1 Earth sensor [IRES-NE, InfraRed Earth Sensor]



Operating Modes

- Earth Acquisition mode (Wide Scan)
- Earth Pointing mode (Narrow Scan)
- Chord Mode (single beam crossing)

Performances

- 14-16.25 μm wavelength operating band
- Earth acquisition mode between 15,300 and 53,000 km altitude
- Operational capability up to 140,000 km altitude
- Operational range at GEO
 - *Pointing mode linear range: $\pm 5.5^\circ$ pitch; $\pm 2.5^\circ$ roll
 - *Acquisition mode linear range: $\pm 11^\circ$ pitch; $\pm 2.5^\circ$ roll
 - *Chord mode linear range: $\pm 23^\circ$ pitch; $\pm 14^\circ$ roll
 - *Acquisition mode sign range: $\pm 22^\circ$ pitch; $\pm 13^\circ$ roll
- 10 Hz output data rate
- Accuracy
 - * <0.05 deg random error (3 σ)
 - * <0.02 deg bias error

Data Interfaces

- Digital Serial Interface 32 bit or MIL-STD 1553B or MACS-Bus available

Mechanical Interfaces

- 150.8x165.7x178 mm size
- <2.3 kg mass

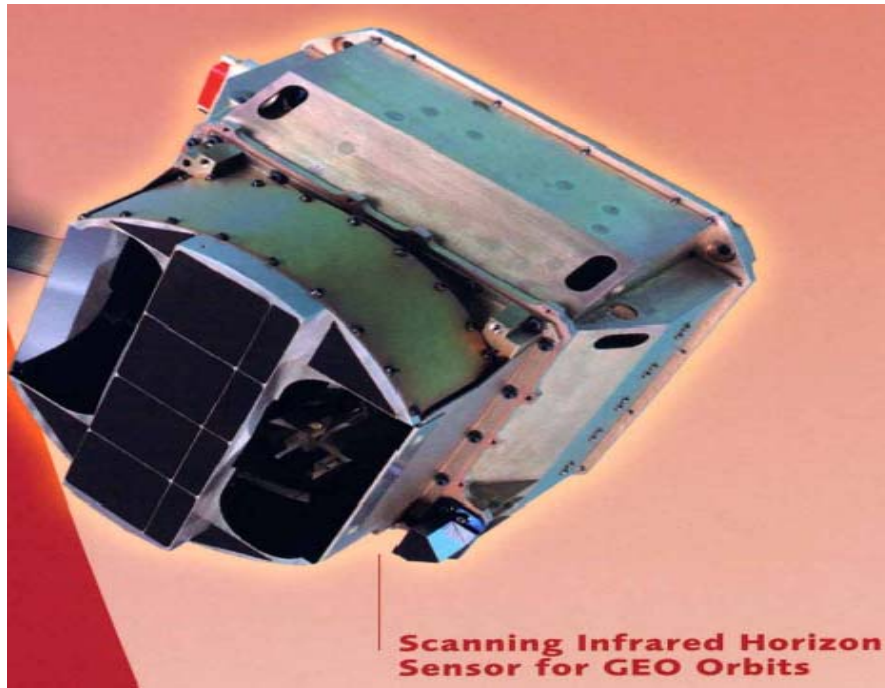
Electrical Interfaces

- 24 to 50 V unregulated Power Bus
- $<4 \div 5$ W power consumption depending on data interface

Environmental Conditions

- -30°C to $+55^\circ\text{C}$ operational temperature
- -40°C to $+60^\circ\text{C}$ storage temperature
- Ambient and space vacuum pressure
- Vibration levels
 - *Sine: 20 g peak
 - *Random: 18 g rms
 - *Shock: 2000g from 3 to 10 kHz
- > 15 years lifetime in GEO

A4.1.2 Earth sensor [STD -15], (www.sodem.fr)



PERFORMANCES

- Altitude range: 15 000 - 140 000 km
- Operating depointing range:
 - Nominal:
Pitch range : ± 12 deg (Roll = 0) - Roll range : ± 2.9 deg (Pitch = 0)
 - Extended:
Pitch range : ± 15.6 deg (Roll = 0) - Roll range : ± 14.5 deg (Pitch = 0)
- Output data rate: 1.25 Hz
- Accuracy budget: 3σ
 - bias: 0.035 deg
 - typical noise: 0.015 deg.

ENVIRONMENTAL CHARACTERISTICS

- Operating temperature : -25 deg C, +55 deg C
- Storage temperature : -40 deg C, +60 deg C
 - Vibration : 20 - 2 000 Hz :
- Z axis: 16.9 g.rms - X, Y axis: 13.2 g.rms

MECHANICAL INTERFACES

- Operating temperature : -25 deg C, +55 deg C
- Height: 168 mm - width: 206.5 mm - length: 206.5mm
 - Mass : 3.4 kg

ELECTRICAL INTERFACES

- Typical consumption : 7.5 W
- Power supply : 20 to 55 Volts
- Output data: 1553 protocole

RELIABILITY

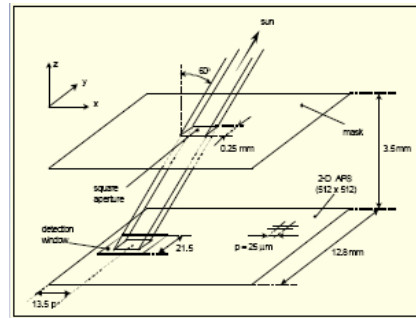
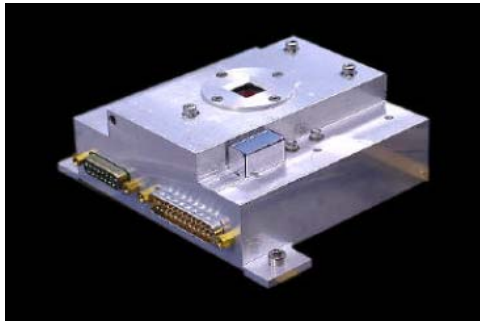
< 1 095 Fits

LIFE-SPAN

15 years in GEO orbit.,

Scanning Format

A4.1.3 APS-based sun sensor [STD -15], (www.sodern.fr)



PERFORMANCE

Altitude range : up to 50 AU
Field Of View : 120°X120° or more
Output data rate : up to 400Hz
Accuracy budget :
Bias error = 0.02° at 2σ (with calibration)
Random error (3σ) = 0.01° @ 400 Hz.

ENVIRONMENTAL CHARACTERISTICS

Operating T° : -50°C to +80°C
Vibration : Typical ARIANE 5 environment

MECHANICAL INTERFACE

Mass : < 0.30 kg
Width X Length X Height : 130 X 120 X 45 mm

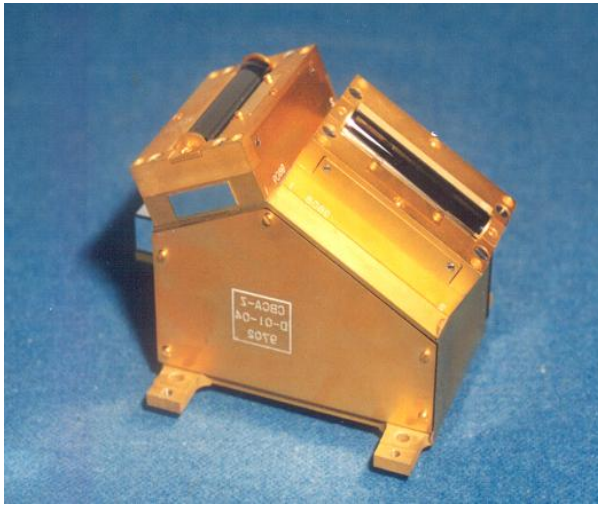
ELECTRICAL INTERFACE

Typical consumption : 1W
Power supply : from 6V to 12V
(option : 20V to 100V)
Output data : RS422 8 or 16 bits serial link
Temperature detection

RELIABILITY : 255 Fits

LIFE SPAN : > 15 years (GEO)

A4.1.4 Digital sun sensor [DSS2]



SPECIFICATIONS

FOV: $\pm 64^\circ \times \pm 60^\circ$

Accuracy: $0.05^\circ (0^\circ - \pm 32^\circ)$

$0.1^\circ (\pm 32^\circ - \pm 64^\circ)$

Resolution: 28"

Optic head mass: 350g

Optic head size: 86×50×30

Operating temperature: $-20^\circ\text{C} \sim +50^\circ\text{C}$

Output: 16bits digital

Power dissipation: 0.5W

Lifetime: 15 years (in geostationary orbit)

A4.2 Control Elements

A4.2.1 Reaction wheels [BBM/RW] (<http://www.deldix.de>)

Ball Bearing Momentum and Reaction Wheels (Standard Products)

TELDIX is the sole commercial manufacturer of ball bearing momentum and reaction wheels in Germany and leading manufacturer in Europe.

TELDIX Ball Bearing Momentum and Reaction Wheels are the ultimate choice for advanced satellite stabilization.

Reference Projects

European Satellite Programs:

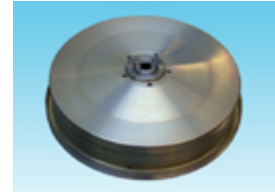
Abrixas, Artemis, Astra-2B, -1K,
Beppo-SAX,
Demeter, DFS,
ECS, ESSAIM, Eurasiasat 1, Europe*Star, EUROSTAR 2000+,
EUROSTAR 3000
Eutelsat II, Eutelsat W,
GE-1E/Sirius-2,
FBM,
Hispasat 1A, 1B, 1C, Hot Bird,
Inspector, ISO, Italsat,
MARECS, MAROTS, Mars Express, Microscope,
OTS,
Parasol, Picard, Proba, Proteus/Jason,
ROSAT,
SAR-Lupe, Skynet 4, Spacebus, Stentor, Symphonie A/B,
TDF-1, TDF-2, Telecom-1, Telecom II, TELE-X,
TUBSAT-B, Turksat 1, TV-SAT, TV-SAT-2

International Satellite Programs:

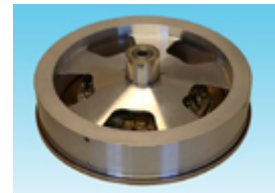
Agila 2, Amos, Apple, Aqua (PM-1), Arabsat II, Arabsat III, AsiaStar, Aura (Chemistry),
Beidou 1A, 1B, BSat 2a, 2b,
Chandra (CXO), Chinasat 8, 22,
DFH3, DFH4,
Echostar VI, ETS-V,
FBM,
GE 5, GOES,
Inmarsat II, Insat-1D, Insat-2, Insat-3, Intelsat V, Intelsat VII, IRAS, iSKY (KaStar)
KaistSat, KitSat 3,
METSAT, MOS-1, MS-T5, MT Sat,
Nahuel, NATO IV, Nilestar, N-Star, NSS-6 (K-TV)
OmegaSat, Orbcomm, Orion 1, Orion 2,
PanAmSat 6, 7, 8, Pioneer, Planet-A,
SBIRS Low, Sinosat, Sirius 1-3, Sky-1, Sky-2, ST-1, Step 4, Superbird,
Telstar 5, Telstar 6-12, Tempo, Thaicom,
Worldstar

Currently **556** wheels installed in **226** launched satellites representing **2074** years of accumulated in orbit operation.

(as of July 2004)



Momentum and Reaction Wheel RSI 12 4-12 Nms with integrated Wheel Drive Electronics



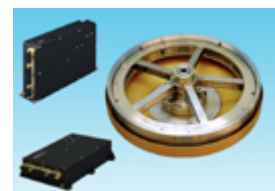
Momentum and Reaction Wheel RSI 45 14-45 Nms with integrated Wheel Drive Electronics



Momentum and Reaction Wheel RSI 68 14-68 Nms with integrated Wheel Drive Electronics

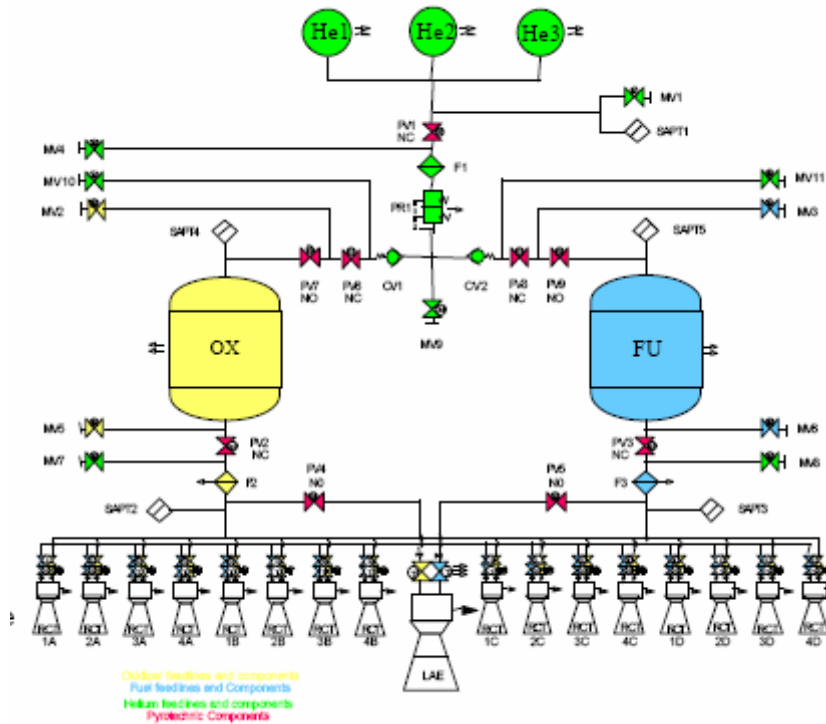


High Torque Momentum & Reaction Wheel HT-RSI 14-68 Nms with integrated Wheel Drive Electronics




Momentum and Reaction Wheel RDR 68 14-68 Nms with external Wheel Drive Electronics

A4.2.2 Thrusters (<http://www.space.eads.net>)




22 N Bipropellant Thruster Model S22 - 02



[click to enlarge](#)

Characteristics	
Propellant:	MON / MMH
Thrust vac:	22 N
Power:	31 kW 42 hp
Isp vac:	290 sec
Chamber press:	9 bar
Overall length:	212 mm
Nozzle dia:	55 mm
Mass:	650 g


10 N Bipropellant Thruster Model S10



Characteristics	
Propellant:	MON / MMH
Thrust vac:	10 N
Power:	14 kW 19 hp
Isp vac:	286 sec
Chamber press:	7 bar
Overall length:	138 mm
Nozzle dia:	37 mm
Mass:	350g

[Heritage](#)

4 N Bipropellant Thruster Model S4



Characteristics	
Propellant:	MON / MMH
Thrust vac:	4 N
Power:	6 kW 8 hp
Isp vac:	284.9 sec
Chamber press:	4 bar
Overall length:	115 mm
Nozzle dia:	30 mm
Mass:	290 g



Integration of 400 N apogee engine and heat shield to thrust frame.

BIOGRAPHY

Erkan Abdulhamitbilal was born in Balchik, Varna, Bulgaria in 1977. He was graduated from Astronautical Engineering department of Istanbul Technical University in 2002. He started his graduate education in ITU in Institute of Science and Technology, Aeronautical and Astronautical Engineering program in 2002.